Improving The Electrochemical Behaviors of Sacrificial Aluminium Anode by Various Method

A Thesis submitted to Gujarat Technological University

for the Award of

Doctor of Philosophy

in

Metallurgy Engineering

by

Kyada Tushal Kalubhai

Enrollment No. 219999921004

under supervision of

Dr. Indravadan B. Dave (Supervisor)

GUJARAT TECHNOLOGICAL UNIVERSITY,

AHMEDABAD

AUGUST 2026

Improving The Electrochemical Behaviors of Sacrificial Aluminium Anode by Various Method

A Thesis submitted to Gujarat Technological University

for the Award of

Doctor of Philosophy

in

Metallurgy Engineering

by

Kyada Tushal Kalubhai

Enrollment No. 219999921004

under supervision of

Dr. Indravadan B. Dave (Supervisor)

GUJARAT TECHNOLOGICAL UNIVERSITY,

AHMEDABAD

AUGUST 2026

DECLARATION

I declare that the thesis entitled **Improving The Electrochemical Behaviors of Sacrificial Aluminium Anode by Various Method** submitted by me for the degree of Doctor of Philosophy is the record of research work carried out by me during the period from **2021** to **2026** under the supervision of **Dr. Indravadan B. Dave** and this has not formed the basis for the award of any degree, diploma, associateship, fellowship, titles in this or any other University or other institution of higher learning.

I further declare that the material obtained from other sources has been duly acknowledged in the thesis. I shall be solely responsible for any plagiarism or other irregularities, if noticed in the thesis.

Signature of the Research Scholar:  Date: 03/08/2026

Name of Research Scholar: **Kyada Tushal Kalubhai**

Place: Ahmedabad

CERTIFICATE

I certify that the work incorporated in the thesis **Improving The Electrochemical Behaviors of Sacrificial Aluminium Anode by Various Method** submitted by **Kyada Tushal Kalubhai** was carried out by the candidate under my supervision/guidance. To the best of my knowledge: (i) the candidate has not submitted the same research work to any other institution for any degree/diploma, Associateship, Fellowship or other similar titles (ii) the thesis submitted is a record of original research work done by the Research Scholar during the period of study under my supervision, and (iii) the thesis represents independent research work on the part of the Research Scholar.

Signature of the Research Supervisor: …… Date: 03/08/2026

Name of Supervisor: **Dr. Indravadan B. Dave**

Signature of the Research Co-Supervisor: **NIL** Date: ……..

Name of Co-Supervisor:

Place: Ahmedabad

Course-work Completion Certificate

This is to certify that **Kyada Tushal Kalubhai** enrollment no. **219999921004** is enrolled for PhD program in the branch **Metallurgy Engineering** of Gujarat Technological University, Ahmedabad.

1.1.1.1.1 (Please tick the relevant option(s))

☐ He has been exempted from the course-work (successfully completed during M.Phil Course)

☐ He has been exempted from Research Methodology Course only (successfully completed during M.Phil Course)

☑ He has successfully completed the PhD course work for the partial requirement for the award of PhD Degree. His/ Her performance in the course work is as follows-

Grade Obtained in Research Methodology [PHD2001]	Grade Obtained in Research and Publication Ethics [PHD2002]	Grade Obtained in Self-Study Course/ Contact Program [PHD2003]
BB	AB	AB

Supervisor's Sign

Dr. Indravadan B. Dave

Originality Report Certificate

It is certified that PhD Thesis titled **Improving The Electrochemical Behaviors of Sacrificial Aluminium Anode by Various Method** by **Kyada Tushal Kalubhai** has been examined by us. We undertake the following:

a. Thesis has significant new work / knowledge as compared already published or are under consideration to be published elsewhere. No sentence, equation, diagram, table, paragraph or section has been copied verbatim from previous work unless it is placed under quotation marks and duly referenced.

b. The work presented is original and own work of the author (i.e. there is no plagiarism). No ideas, processes, results or words of others have been presented as Author own work.

c. There is no fabrication of data or results which have been compiled / analyzed.

d. There is no falsification by manipulating research materials, equipment or processes, or changing or omitting data or results such that the research is not accurately represented in the research record.

e. The thesis has been checked using **Turnitin Plagiarism Detection Software** (copy of originality report attached) and found within limits as per GTU Plagiarism Policy and instructions issued from time to time (i.e. permitted similarity index <=10%).

Signature of the Research Scholar:  Date: 03/08/2026

Name of the Research Scholar: **Kyada Tushal Kalubhai**

Signature of the Research Supervisor:  Date: 03/08/2026

Name of the Research Supervisor: **Dr. Indravadan B. Dave**

Place: Ahmedabad

Tushal Kyada

Tushal Kyada_PhD-Thesis_47896

Tushal Kyada_PhD-Thesis_47896

PHD Thesis

Gujarat Technological University

Document Details

Submission ID
trn:oid:::1:3475204334

Submission Date
Feb 7, 2026, 3:16 PM GMT+5:30

Download Date
Feb 7, 2026, 3:21 PM GMT+5:30

File Name
Tushal_Kyada_Thesis_7.2.2026.docx

File Size
37.4 MB

167 Pages

38,275 Words

237,528 Characters

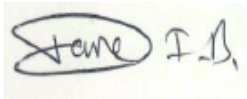

turnitin Page 1 of 176 - Cover Page Submission ID trn:oid:::1:3475204334

9% Overall Similarity

The combined total of all matches, including overlapping sources, for each database.

Filtered from the Report

- Bibliography
- Small Matches (less than 9 words)
- Submitted works

Exclusions

- 1 Excluded Source
- 2 Excluded Matches

Match Groups

- 293 Not Cited or Quoted 9%
  Matches with neither in-text citation nor quotation marks
- 4 Missing Quotations 0%
  Matches that are still very similar to source material
- 7 Missing Citation 0%
  Matches that have quotation marks, but no in-text citation
- 0 Cited and Quoted 0%
  Matches with in-text citation present, but no quotation marks

Top Sources

6% Internet sources
6% Publications
0% Submitted works (Student Papers)

Integrity Flags

0 Integrity Flags for Review

Our system's algorithms look deeply at a document for any inconsistencies that would set it apart from a normal submission. If we notice something strange, we flag it for you to review.

A Flag is not necessarily an indicator of a problem. However, we'd recommend you focus your attention there for further review.

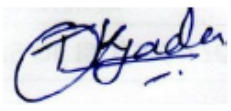

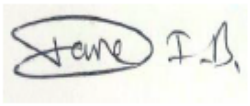

Match Groups

- 293 Not Cited or Quoted 9%
  Matches with neither in-text citation nor quotation marks
- 4 Missing Quotations 0%
  Matches that are still very similar to source material
- 7 Missing Citation 0%
  Matches that have quotation marks, but no in-text citation
- 0 Cited and Quoted 0%
  Matches with in-text citation present, but no quotation marks

Top Sources

- 6% Internet sources
- 6% Publications
- 0% Submitted works (Student Papers)

Top Sources

The sources with the highest number of matches within the submission. Overlapping sources will not be displayed.

1	Internet	msu-new-2023-ec2-ubuntu-unzip.s3.ap-south-1.amazonaws.com 3%
2	Internet	link.springer.com <1%
3	Internet	dokumen.pub <1%
4	Internet	backend.orbit.dtu.dk <1%
5	Internet	constellation.uqac.ca <1%
6	Publication	"ICAA13 Pittsburgh", Springer Science and Business Media LLC, 2016 <1%
7	Publication	"Light Metals 2022", Springer Science and Business Media LLC, 2022 <1%
8	Publication	Patel, Sonam Mukeshkumar. "Study the Effect of "Mn" in Magnesium & Magnesiu... <1%
9	Publication	Srikanta Moharana, Bibhuti B. Sahu, Suresh Sagadevan, "Nanocarbon to Polymer-... <1%
10	Publication	Yoshiki Oshida. "Magnesium Materials", Walter de Gruyter GmbH, 2021

11	Publication	
"Light Metals 2019", Springer Nature, 2019		<1%
12	Publication	
Mohammad Jamalpour, Reza Alizadeh. "Effects of heat treatment and Y addition ...		<1%
13	Publication	
"High Performance Structural Materials", Springer Nature, 2018		<1%
14	Internet	
www.researchgate.net		<1%
15	Internet	
pubs.rsc.org		<1%
16	Publication	
"TMS 2020 149th Annual Meeting & Exhibition Supplemental Proceedings", Spring...		<1%
17	Internet	
worldwidescience.org		<1%
18	Publication	
"Magnesium Technology 2011", Springer Science and Business Media LLC, 2016		<1%
19	Publication	
Kenneth E. Bannister. "Lubripedia - A 1001 Concise Illustrated Encyclopedia Refer...		<1%
20	Publication	
Bo Wei, Shuai Pan, Guizhen Liao, Asad Ali, Shuangbao Wang. "Sc-containing hiera...		<1%
21	Publication	
Liying Cui, Kun Liu, X.-Grant Chen. "Recent advances in cost-effective aluminum a...		<1%
22	Internet	
amsdottorato.unibo.it		<1%
23	Publication	
Saif Haider Kayani, Heon-Young Ha, oo Son, Jung-Moo		
24	Internet	
pure.manchester.ac.uk		<1%

Ph.D. Thesis Non-Exclusive License to

GUJARAT TECHNOLOGICAL UNIVERSITY

In consideration of being a Research Scholar at Gujarat Technological University, and in the interests of the facilitation of research at the University and elsewhere, I, **KyadaTushal Kalubhai** having Enrollment No. **219999921004** hereby grant a non-exclusive, royalty free and perpetual license to the University on the following terms:

a. The University is permitted to archive, reproduce and distribute my thesis, in whole or in part, and/or my abstract, in whole or in part (referred to collectively as the "Work") anywhere in the world, for non-commercial purposes, in all forms of media;
b. The University is permitted to authorize, sub-lease, sub-contract or procure any of the acts mentioned in paragraph (a);
c. The University is authorized to submit the Work at any National / International Library, under the authority of their "Thesis Non-Exclusive License";
d. The Universal Copyright Notice (©) shall appear on all copies made under the authority of this license;
e. I undertake to submit my thesis, through my University, to any Library and Archives. Any abstract submitted with the thesis will be considered to form part of the thesis.
f. I represent that my thesis is my original work, does not infringe any rights of others, including privacy rights, and that I have the right to make the grant conferred by this non-exclusive license.
g. If third party copyrighted material was included in my thesis for which, under the terms of the Copyright Act, written permission from the copyright owners is required, I have obtained such permission from the copyright owners to do the acts mentioned in paragraph (a) above for the full term of copyright protection.
h. I understand that the responsibility for the matter as mentioned in the paragraph (g) rests with the authors / me solely. In no case shall GTU have any liability for any acts / omissions / errors / copyright infringement from the publication of the said thesis or otherwise.
i. I retain copyright ownership and moral rights in my thesis, and may deal with the copyright in my thesis, in any way consistent with rights granted by me to my University in this non-exclusive license.
j. GTU logo shall not be used /printed in the book (in any manner whatsoever) being published or any promotional or marketing materials or any such similar documents.

k. The following statement shall be included appropriately and displayed prominently in the book or any material being published anywhere: “The content of the published work is part of the thesis submitted in partial fulfilment for the award of the degree of Ph.D. in Metallurgy Engineering of the Gujarat Technological University”.

l. I further promise to inform any person to whom I may hereafter assign or license my copyright in my thesis of the rights granted by me to my University in this nonexclusive license. I shall keep GTU indemnified from any and all claims from the Publisher(s) or any third parties at all times resulting or arising from the publishing or use or intended use of the book / such similar document or its contents.

I am aware of and agree to accept the conditions and regulations of Ph.D. including all policy matters related to authorship and plagiarism.

Date: 03/08/2026

Place: Ahmedabad

Signature of the Research Scholar

Recommendation of the Research Supervisor: Recommended for Submission

Recommendation of the Co-Research Supervisor: NIL

Signature of the Research Supervisor

Thesis Approval Form

The viva-voce of the PhD Thesis submitted by Kyada Tushal Kalubhai (Enrollment No. 219999921004) entitled **Improving The Electrochemical Behaviors of Sacrificial Aluminium Anode by Various Method** was conducted on Monday,03/08/2026 at Gujarat Technological University.

☑ The performance of the candidate was satisfactory. We recommend that he be awarded the PhD degree.

☐ Any further modifications in research work recommended by the panel after 3 months from the date of first viva-voce upon request of the Supervisor or request of Independent Research Scholar after which viva-voce can be re-conducted by the same panel again.

(briefly specify the modifications suggested by the panel)

☐ The performance of the candidate was unsatisfactory. We recommend that he should not be awarded the PhD degree.

(The panel must give justifications for rejecting the research work)

Dr. Indravadan B. Dave

Name and Signature of Supervisor with Seal

Dr. Nirav Jamnapara

---

1) (External Examiner 1) Name and Signature

Dr. Vivek D. Kalyankar

---

2) (External Examiner 2) Name and Signature

ABSTRACT

Aluminum-based alloys are extensively used as sacrificial anodes in marine cathodic protection systems owing to their high electrochemical activity, favorable current efficiency and low density. Among these, Al-Mg alloys are particularly attractive because of their robust resistance to passivation in chloride-rich seawater. Despite their broad utilization, the combined effect of silicon additions and thermal processing on the microstructural evolution, mechanical response and electrochemical performance of Al–Mg alloys remains inadequately understood. In this work, the synergistic effects of silicon content (1.5–6 wt.%) and T6 heat treatment on the properties of Al-6.5Mg-xSi alloys were systematically investigated.

Microstructural characterization using optical microscopy as well as scanning electron microscopy and X-ray diffraction revealed that increasing silicon content significantly alters the morphology and distribution of the Mg_2Si phase. With higher silicon additions, the Mg_2Si phase evolves from coarse, flake-like particles into a finer, interconnected Chinese-script eutectic structure. These microstructural modifications contribute to a progressive increase in hardness through the formation of strengthening intermetallic phases.

Electrochemical characterization was performed in a 3.5 wt.% NaCl environment to assess the stability of the investigated alloys. Long-term corrosion rates were determined via weight loss measurements and corrosion kinetics were analyzed using potentiodynamic polarization techniques. Anode performance was assessed in accordance with the DNV-RP-B401 standard.

The results indicate that silicon additions enhance depassivation behavior and shift the operating potential toward more electronegative values, which is desirable for sacrificial anode applications. However, silicon contents exceeding 1.5 wt.% were found to increase corrosion susceptibility due to intensified micro-galvanic interactions between the α-Al matrix and intermetallic phases. The application of T6 heat treatment effectively mitigates this drawback by dissolving coarse as-cast constituents and promoting the precipitation of fine, uniformly distributed Mg_2Si particles. This treatment also alters the corrosion mode from localized pitting to more uniform dissolution, a critical requirement for stable and predictable anode consumption.

The present investigation demonstrates that a balanced combination of silicon content and heat treatment is critical for achieving stable electrochemical behavior and prolonged service life in Al-Mg-Si sacrificial anodes. These insights contribute to a deeper understanding of composition-microstructure-corrosion relationships relevant to marine cathodic protection systems.

ACKNOWLEDGEMENT

First and foremost, I express my profound gratitude to Almighty God for bestowing upon me the strength, wisdom, perseverance, and guidance required to complete this doctoral research. His divine grace has been a constant source of inspiration throughout this academic journey.

I would like to express my sincere gratitude to my research supervisor, Dr. Indravadan B. Dave, for his invaluable guidance, constant encouragement, and unwavering support throughout the course of this research. His profound academic insight, constructive criticism, and continuous motivation played a decisive role in shaping both the direction and the quality of this work.

I extend my heartfelt appreciation to the members of my Doctoral Progress Committee (DPC), Dr. K. Santhy and Dr. Vandana J. Rao, for their constructive feedback, insightful suggestions, and dedicated efforts toward the advancement of my research. Their scholarly inputs and periodic evaluations significantly strengthened the technical depth and clarity of this work.

I am deeply grateful to Dr. Sonam M. Patel, Lecturer, Dr. S. & S. S. Ghandhy College of Engineering & Technology, Surat, for her dedicated guidance and mentorship as my co-guide. She provided consistent support at every stage of this research, from experimental planning and execution to data interpretation and thesis preparation. Her availability, patience, and insightful suggestions were instrumental in overcoming research challenges and successfully completing this doctoral work. Her contribution is sincerely and respectfully acknowledged.

I sincrely acknowledge Riddant Aluminium Pvt. Ltd., Sachin, Surat, for supplying high-purity silicon required for alloy development. I am also thankful to Addhya Engineering, Vadodara, for carrying out timely chemical analysis of the developed anodes.

I would like to thank Mr. Gyanesh, Olympus, for providing access to the digital microscope facilities for metallographic analysis. I also express my sincere gratitude to Dr. Vandana J. Rao for facilitating and supporting the X-ray diffraction (XRD) analysis at The Maharaja Sayajirao University of Baroda.

My sincere appreciation is extended to Dr. Alphonsa Joseph, Scientific Officer-H, FCIPT, Institute for Plasma Research (IPR), Gandhinagar, for granting permission and providing

facilities to carry out potentiodynamic polarization studies. Her support and technical guidance are gratefully acknowledged.

I would like to thank Mr. Vivek Singh, PhD Scholar, IIT Gandhinagar, for his assistance in SEM–EDS analysis at IIT Gandhinagar. I am also grateful to Mr. Mohit Sharma, PhD Scholar, IIT Roorkee, for his support in SEM/EDS characterization at IIT Roorkee.

I sincerely acknowledge Mr. Amit Patel, Owner, Metalab Analytical Solution and Shakti Anodes Pvt. Ltd., for facilitating sacrificial anode efficiency measurements at their laboratory. I also thank Mr. Suraj Dabekar for his assistance in carrying out potentiodynamic tests at The Maharaja Sayajirao University of Baroda.

Finally, I express my deepest gratitude to my family, especially my wife, for her unconditional love, patience, encouragement, and unwavering moral support throughout this demanding journey. Her constant faith in me has been my greatest source of strength and motivation. This work would not have been possible without her understanding, sacrifices, and continuous encouragement.

I also sincerely acknowledge the support and cooperation extended by my colleagues of the Department of Metallurgy and the management of Dr. S. & S. S. Ghandhy College of Engineering & Technology, Surat, for providing the necessary facilities and granting permission to carry out this research. Their encouragement and institutional support played an important role in the successful completion of this work.

Kyada Tushal Kalubhai

Research scholar, Gujrat Technological University,
Ahmedabad, Gujarat.

TABLE OF CONTENT

TABLE OF CONTENT……..…xvi

LIST OF ABBREVIATIONS……..…xx

LIST OF SYMBOLS……xxii

LIST OF FIGURES……xxiii

LIST OF TABLES……xxvi

CHAPTER 1 INTRODUCTION……1

1.1 Overview 1

1.2 Background 1

1.3 Economic Impact of Corrosion and Prevention Strategies 3

1.3.1 Pipeline Transportation & Corrosion Control 4

1.3.2 Corrosion Costs in the United States 4

1.3.3 Industrial Efforts to Combat Corrosion 6

1.4 Strategies for Corrosion Mitigation 6

1.4.1 Protective Coatings 6

1.4.2 Corrosion-Resistant Alloys 7

1.4.3 Corrosion Inhibitors 7

1.4.4 Environmental Control 8

1.4.5 Proper Design and Material Selection 8

1.4.6 Proper Design 8

1.4.7 Selection of Corrosion-Resistant Materials 9

1.4.8 Cathodic Protection 9

1.4.8.1 Impressed Current Cathodic Protection (ICCP) 9

1.4.8.2 Sacrificial Anode Cathodic Protection (SACP) 10

1.5 Motivations 13

1.6 Objective 14

1.7 Scope 14

1.8 Thesis Organization 15

CHAPTER 2 LITERATURE REVIEW……17

2.1 Overview 17

2.2 Utilization of Aluminum as a Sacrificial Anode 17
2.3 Electrochemical Properties of Aluminum and its Alloys 19
2.3.1 Key Electrochemical Characteristics Affecting Anode Performance 19
2.4 Challenges and Performance Considerations 23
2.4.1 Passivation of pure aluminium 23
2.4.2 Depassivation of Pure Aluminium 24
2.5 Methods to Improve the Electrochemical Behavior of Aluminum Anodes 25
2.5.1 Alloying 25
2.5.2 Heat Treatments 30
2.5.3 Cold Working 33
2.6 6XXX Series Aluminum Alloy 37
2.6.1 Al-Mg-Si Phase Diagram 38
2.6.2 Electrochemical Behaviour of Mg_2Si 39
2.6.3 Morphology of Mg_2Si 41
2.7 Effect of Mg in Al-Mg-Si alloy 43
2.8 Effect of Si in Al-Mg-Si alloy 45
2.9 Heat Treatment of Al-Mg-Si alloy 48
2.9.1 Precipitation Sequence During Aging of Al-Mg-Si Alloy 48
2.10 Literature Related to Past Work 52
2.11 Research Gap 53
CHAPTER 3 EXPERIMENTAL WORK 55
3.1 Overview 55
3.2 Materials and Methods 55
3.2.1 Raw Materials 55
3.2.2 Casting of Al-Mg-Si Alloys 56
3.2.3 Alloying Materials and Charge Determination 58
3.3 Experimental Procedure 59
3.3.1 Die Casting of Designed Alloy 59
3.3.2 Heat Treatment of Developed Alloys 61
3.4 Chemical Analysis 63
3.5 Hardness Evaluation 64
3.6 Microstructural Analysis and Phase Analysis 65
3.7 Corrosion Behavior Study 67

3.7.1 Standard weight loss method..... 68
3.7.2 Potentiodynamic Polarization Study..... 69
3.8 Examination of Corrosion-Induced Surface Degradation..... 70
3.9 Assessment of Anode Performance..... 71
3.9.1 Preparation of Electrolyte and Equipment..... 71
3.10 Summary..... 73
CHAPTER 4 RESULTS & DISCUSSION……75
4.1 Introduction..... 75
4.2 Effect of Silicon Addition on the Composition of Aluminum Alloys..... 75
4.3 Effect of Silicon Addition on the Microstructure of Aluminum Alloys..... 76
4.3.1 Microstructural Evolution of As-Cast Al-Mg-Si Alloys..... 76
4.3.2 Phase Volume Fraction Analysis..... 80
4.3.3 X-ray Diffraction (XRD) Analysis..... 82
4.3.4 Morphology of Mg_2Si..... 85
4.3.5 Microstructural Evolution of Heat Treated Al-Mg-Si Alloys..... 87
4.4 Effect of Silicon Addition on the Hardness of Aluminum Alloys..... 92
4.5 Corrosion..... 95
4.5.1 Corrosion study by Weight Method-As Cast..... 95
4.5.2 Corrosion Study by Weight Loss Method – Heat Treated Condition (T6)..... 101
4.5.3 Potentiodynamic Polarization Test..... 105
4.5.4 As-Cast Condition..... 106
4.5.5 Effect of Heat Treatment (T6 Condition)..... 107
4.5.6 Microstructure-Electrochemical Correlation..... 108
4.5.7 Corrosion Mechanism in Al–Mg–Si Alloys..... 110
4.6 Anode Performance Measurement..... 114
4.6.1 Evaluation of Anode Capacity and Consumption Rate..... 117
4.6.2 Influence of Heat Treatment on Anode Performance..... 119
4.6.3 Correlation with Microstructure and Potentiodynamic Polarization Behavior..... 120
4.6.4 Surface Examination after Anode Performance Testing..... 121
4.7 Summary..... 123
CHAPTER 5 MAJOR CONTRIBUTIONS AND HYPOTHESIS DEVELOPED…….124
5.1 Introduction..... 124
5.2 Research Contributions..... 124

5.3 Hypothesis Development 127
5.3.1 Basis for Hypothesis Formulation 127
5.3.2 Hypothesis H1: Influence of Silicon Content on Mg_2Si Morphology and Corrosion Initiation 129
5.3.3 Hypothesis H2: Role of Mg_2Si Continuity in Micro-Galvanic Corrosion 130
5.3.4 Hypothesis H3: Non-Linear Relationship Between Silicon Content and Anode Performance 130
5.3.5 Hypothesis H4: Heat Treatment Enhances Anodic Activity but Reduces Anode Efficiency at High Silicon Levels 131
5.3.6 Hypothesis H5: Uniform Anodic Dissolution Governs Long-Term Anode Efficiency 132
5.3.7 Hypothesis H6: Coupled Microstructure–Electrochemical Performance Relationship 132
5.4 Summary 133
CHAPTER 6 CONCLUSIONS AND SCOPE FOR FUTURE WORK 134
6.1 Conclusions 134
6.2 Future Scope of The Study 135
6.2.1 Effect of Cold Working on Microstructure–Electrochemical Coupling 135
6.2.2 Combined Effects of Cold Working and Heat Treatment 136
6.2.3 Interaction Between Cold Work and Mg_2Si Morphology 136
6.2.4 Advanced Electrochemical and Modeling Approaches 136
6.2.5 Three-Dimensional Corrosion Evolution and Cross-Sectional Characterization 136
6.2.6 Time-Dependent Electrochemical Transformation of Mg_2Si 137
REFERENCES 138
LIST OF PUBLICATIONS 150
PUBLISHED PAPER-1 151
PUBLISHED PAPER-2 152
PUBLISHED PAPER-3 153
PUBLISHED PAPER-4 154
PUBLISHED PAPER-5 155

LIST OF ABBREVIATIONS

Abbreviation	Full Form
Al	Aluminium
Mg	Magnesium
Mn	Manganese
Fe	Iron
Cu	Copper
Si	Silicon
Mg_2Si	Magnesium Silicide
α-Al	Alpha Aluminium Phase
β″	Beta Double-Prime Precipitate
CP	Cathodic Protection
SACP	Sacrificial Anode Cathodic Protection
ICCP	Impressed Current Cathodic Protection
CP (Purity)	Commercial Purity
HP	High Purity
DC	Die Casting
SEM	Scanning Electron Microscopy
EDS	Energy-Dispersive Spectroscopy
OES	Optical Emission Spectroscopy
XRD	X-Ray Diffraction
OM	Optical Microscopy
MPY	Mils Per Year
NaCl	Sodium Chloride
OCP	Open Circuit Potential
E_{corr}	Corrosion Potential
I_{corr}	Corrosion Current Density
SHE	Standard Hydrogen Electrode
SCE	Saturated Calomel Electrode
EMF	Electromotive Force

IGC	Intergranular Corrosion
PBR	Pilling-Bedworth Ratio
IGC	Intergranular Corrosion
MMO	Mixed Metal Oxide
wt.%	Weight Percent
A·h/kg	Ampere-hour per kilogram
kg/A·year	Kilogram per Ampere-year
SEM/EDS	Scanning Electron Microscopy with EDS
Al–Mg–Si	Aluminium–Magnesium–Silicon Alloy System
NACE	National Association of Corrosion Engineers

LIST OF SYMBOLS

Symbol	Description
et al.	*Et alia* (and others)
°C	Degree Celsius (Centigrade)
α	Alpha phase
β″	Beta double-prime precipitate
kg	Kilogram
g	Gram
mg	Milligram
M	Mass
D	Density
d	Diameter
l	Length
mm	Millimetre
μm	Micrometre (Micron)
cm	Centimetre
%	Percentage
s	Second
wt.%	Weight percentage
at.%	Atomic percentage
θ	Theta
HV	Vickers hardness
A	Ampere
h	Hour
A·h/kg	Ampere-hour per kilogram
kg/A·year	Kilogram per ampere-year
*E*corr	Corrosion potential
*I*corr	Corrosion current density
OCP	Open circuit potential
MPY	Mils per year
NaCl	Sodium chloride
μA/cm²	Microampere per square centimetre
mV	Millivolt
ρ	Density
σ	Stress
Δ	Change / difference
t	Time
T	Temperature
pH	Measure of acidity/alkalinity

LIST OF FIGURES

Figure 1.1 Basic corrosion Cell. 2
Figure 1.2 Illustrates the various forms of corrosion. 3
Figure 1.3 Annual Corrosion Cost Breakdown by Sector Categories ($137.9 Billion).[6] 4
Figure 1.4 Application of paint as coating. 7
Figure 1.5 Schematic set up of Impressed Current Cathodic Protection. 9
Figure 1.6 Schematic set up of sacrificial anode Cathodic Protection of pipeline. 10
Figure 2.1 Aluminum sacrificial anodes. 17
Figure 2.2 Application of sacrificial anodes in various industry. 19
Figure 2.3 Aluminium- Magnesium Silicide Phase Diagram. [85] 38
Figure 2.4 Potentiodynamic Scanning Curves Of Individual A(Al), Si And Mg_2Si In 3.5% Nacl Solution At The Beginning.[92] 40
Figure 2.5 Difference Morphology of Mg_2Si Phase.[92] 41
Figure 2.6 Calculated equilibrium phase diagrams of Al–Mg–Si alloys with varying Mg content.[101] 43
Figure 2.7 Effect of Mg on Morphology of Mg_2Si. [101] 44
Figure 2.8 Effect of Mg on mechanical properties of Al-Mg-Si alloy. [101] 45
Figure 2.9 Calculated equilibrium phase diagrams of Al–Mg–Si alloys with varying Si content.[101] 46
Figure 2.10 Effect of Mg on Morphology of Mg_2Si. [101] 46
Figure 2.11 Effect of Mg on mechanical properties of Al-Mg-Si alloy. [101] 47
Figure 3.1 (a) Aluminium wire, (b) Magnesium ingot, and (c) Silicon lump. 56
Figure 3.2 Electric Resistance Furnace at Dr. S & S. S. Ghandhy College of Engineering & Technology, Surat. 57
Figure 3.3 Metallic die. 57
Figure 3.4 Die Cast Al-Mg-Si Alloy. 59
Figure 3.5 Procedure for development of Al-Mg-Si alloy casting. 60
Figure 3.6 Detailed testing Plane for the experimental study. 61
Figure 3.7 Muffle furnace at Dr. S & S. S. Ghandhy College of Engineering & Technology, Surat. 62
Figure 3.8 Optical Emission Spectroscopy. 63

Figure 3.9 Brinell Hardness tester at Dr.S &S.S.Ghandhy College of Engg. & Tech., Surat. 64
Figure 3.10 Experimental set up for Microscopy, SEM and XRD analysis. 66
Figure 3.11 Experimental set up for standard weight loss method..... 68
Figure 3.12 Experimental setup for potentiodynamic polarization. 69
Figure 3.13 Experimental set up: MS vessel fill with electrolyte and specimen. 71
Figure 3.14 Experimental Set up for anode performance measurement as per DNV RP B401 ... 72
Figure 4.1 Microstructure of Al-6.5 %Mg alloys with varying Si content: (a) Al-6.5 %Mg, (b) Al-6.5 %Mg-1.5 %Si, (c) Al-6.5 %Mg-3 %Si, (d) Al-6.5 %Mg-4.5 %Si, and (e) Al-6.5 %Mg-6 %Si at 1000 X magnification, showing the evolution of Mg_2Si phases with increasing Si. 77
Figure 4.2 SEM images with marked analysis location (Spots) and corresponding EDS spectrum, confirming the presence of the phase Al_3Mg_2 and Mg_2Si. (a) Al-6.5Mg (b) Al-6.5Mg-1.5%Si (c) Al-6.5Mg-3%Si (d) Al-6.5Mg-4.5%Si and (e) Al-6.5Mg-6%Si alloys. 79
Figure 4.3 Volume fraction of α-Al and Mg_2Si phases in Al–6.5 %Mg alloys with varying Si content. 81
Figure 4.4 X-ray diffraction (XRD) patterns of the developed Al-6.5Mg-xSi alloys, showing the presence of α-Al, Mg_2Si, and Al_3Mg_2 phases. 82
Figure 4.5 Morphology of Mg_2Si particles in Al–6.5 %Mg alloys with different Si contents: (a) 1.5 %Si, (b) 3 %Si, (c) 4.5 %Si, and (d) 6 %Si at 3620 X magnification. 86
Figure 4.6 Microstructure of Al-6.5%Mg-xSi alloys in the T6 heat-treated condition showing the evolution of Mg_2Si precipitates: (a-d) at 500x and (a1-d1) at 1000x magnification. (a, a1) Al-6.5%Mg-1.5%Si, (b, b1) Al-6.5%Mg-3%Si, (c, c1) Al-6.5%Mg-4.5%Si, and (d, d1) Al-6.5%Mg-6%Si alloys. 88
Figure 4.7 Microstructures of Al–6.5Mg–xSi alloys in as-cast (a–c) and heat treated (a1–c1) conditions for 1.5%, 3%, and 6% Si at 1000× magnification. 89
Figure 4.8 SEM micrographs and corresponding EDS spectra confirming the presence of the Mg_2Si phase in T6 heat-treated alloys: (a) Al-6.5Mg–4.5%Si and (b) Al–6.5Mg–6%Si. 91
Figure 4.9 X-ray diffraction (XRD) patterns of the developed Al-6.5Mg-xSi alloys, showing the presence of α-Al, Mg_2Si phases. 92
Figure 4.10 Effect of Si addition and heat treatment on hardness of Al-6.5% Mg alloys. 93
Figure 4.11 Microstructure of Al-6.5 %Mg-1.5 %Si alloy at 100 X magnification, highlighting the dendritic α-Al matrix. 94
Figure 4.12 Comparison of hardness in as cast and heat treated condition. 95

Figure 4.13 Variation of corrosion rates over time for Al-6.5 %Mg alloys with different Si contents measured using the standard weight loss method in 3.5 % NaCl solution. 96
Figure 4.14 Surface morphologies of Al–6.5Mg–xSi alloys in the as-cast condition after weekly exposure to the corrosive medium. 98
Figure 4.15 Surface morphology and pit dimension measurements of Al–6.5 %Mg–xSi alloys after 6 weeks of exposure to 3.5 % NaCl solution. 100
Figure 4.16 Corrosion rate variation of T6 heat-treated Al-6.5%Mg-xSi alloys with different Si contents in 3.5 %NaCl solution. 102
Figure 4.17 Surface morphologies of Al–6.5Mg–xSi alloys in the heat treated condition after weekly exposure to the corrosive medium. 104
Figure 4.18 Potentiodynamic polarization curves of the developed Al-6.5Mg-xSi alloys in 3.5 % NaCl solution (As-Cast). 105
Figure 4.19 SEM images of Al-Mg-Si alloys after potentiodynamic polarization testing, showing corrosion morphology. 107
Figure 4.20 Potentiodynamic polarization curves of the developed Al-6.5Mg-xSi alloys in 3.5 % NaCl solution (T6 Heat treated). 108
Figure 4.21 Schematic illustration of the corrosion mechanism in Al-Mg-Si alloys exposed to chloride solution. The yellow line marks initial anodic sites that later become cathodic regions (red line). Representative SEM images support the proposed mechanism. [173]..... 110
Figure 4.22 EDS point analysis of different particles in Al-Mg-Si alloys after potentiodynamic polarization testing, identifying elemental composition..... 111
Figure 4.23 Comparison of consumption rate and anode capacity for "as-cast" and “heat treated” Al-6.5Mg-xSi alloys with varying silicon content. 118
Figure 4.24 Surface morphology of Al-6.5Mg-xSi sacrificial anode specimens after Anode performance measurement in both as-cast and T6 heat treated conditions. 122
Figure 5.1 Graphical abstract illustrating the hypothesis development framework for Al–6.5Mg–xSi sacrificial anode alloys, highlighting the influence of silicon content on Mg_2Si morphology, micro-galvanic interactions, electrochemical response, and resulting anode efficiency..... 128

LIST OF TABLES

Table 1.1 Summary of Corrosion-Related Costs by Sector in the U.S. Economy [6] 5
Table 2.1 Electromotive Force (EMF) Series - Standard Electrode Potential [27] 20
Table 2.2 Galvanic Series in Seawater. [4] 21
Table 2.3 Summary of the Effects of Alloying Elements on Aluminium Alloys 25
Table 2.4 Effect of Alloying Elements on the Performance of Aluminum Sacrificial Anodes 28
Table 2.5 summarizing the effects of various heat treatments on different aluminum alloys 31
Table 2.6 Summary of Research on the Effects of Cold Working on Aluminum Alloy 36
Table 2.7 Corrosion parameters of α(Al), Mg_2Si and Si in 3.5% NaCl Solution at the beginning [93] 40
Table 2.8 Overview of precipitate phases in the Al-Mg-Si system 49
Table 2.9 Comparative Analysis of Heat Treatment Parameters and Their Effects on Al-Mg-Si Alloy properties. 50
Table 3.1 Chemical composition of raw materials 55
Table 3.2 Summery of Designed Alloy 58
Table 3.3 Heat Treatment Parameters 62
Table 4.1 Chemical composition of Al–6.5%Mg alloys with varying Si additions (wt.%) determined by OES. 75
Table 4.2 Phase volume fraction and corresponding standard deviation of α-Al and Mg_2Si phases obtained from optical microscopy for Al–6.5Mg–xSi alloys. 80
Table 4.3 XRD peak positions (2θ), interplanar spacings (d), and Miller indices of α-Al matrix and secondary intermetallic phases (Mg_2Si and Al_3Mg_2) detected in Al–6.5Mg–xSi alloys. 83
Table 4.4 XRD peak positions (2θ), interplanar spacings (d), and Miller indices of α-Al matrix and intermetallic phase Mg_2Si detected in Al–6.5Mg–xSi alloys in as heat treated condition. 91
Table 4.5 Brinell hardness values of pure Al, Al-6.5%Mg, and Al-6.5%Mg-Si alloys in as-cast and heat-treated conditions. 92
Table 4.6 Weekly weight loss measurements (1–8 weeks) obtained from the standard weight loss method for Al–6.5Mg–xSi sacrificial anodes. 96
Table 4.7 Weekly corrosion rate (MPY) of Al-6.5%Mg-xSi alloys in the heat-treated (T6) condition measured using the standard weight loss method over an 8-week exposure period. 102

Table 4.8 Electrochemical corrosion parameters *E*corr and *I*corr of Al-6.5Mg-xSi alloys in as-cast and Heat-treated conditions 105
Table 4.9 Relationship between Mg_2Si characteristics, hardness, and corrosion behavior of developed Al-6.5%Mg-Si alloys in as-cast condition. 113
Table 4.10 Experimental data and electrochemical performance parameters for as-cast and T6 heat treated Al-6.5Mg-Si sacrificial anodes 115
Table 5.1 Contribution–Hypothesis–Evidence Linkage for the Present Study 126

CHAPTER 1
INTRODUCTION

1.1 Overview

This chapter explores the concept of corrosion, its financial implications and various prevention techniques, including cathodic protection and the use of sacrificial anodes. A specific focus is placed on aluminum as a sacrificial anode, with a detailed discussion on its passivation and depassivation through processes such as heat treatment, and alloying. The chapter also outlines the motivation, objectives, and scope of the research, ending with an overview of the thesis structure.

1.2 Background

Corrosion is a naturally occurring process in which a refined metal undergoes chemical or electrochemical interactions with its environment, leading to gradual material degradation and transformation into more stable compounds such as oxides, hydroxides, or salts.[1] Electrochemical corrosion specifically refers to metal oxidation caused by oxidizing agents such as oxygen, hydrogen ions, or hydroxide ions, resulting in the formation of metal oxides or salts.[2]

Localized and uniform corrosion occurs due to diffusion-controlled reactions, primarily affecting exposed surfaces. While passivation and chromate conversion coatings are widely used techniques to reduce surface reactivity and enhance corrosion resistance [3], some corrosion mechanisms remain complex and unpredictable in their onset and progression.

Figure 1.1 illustrates schematic diagram of basic corrosion cell. In a corrosion cell, a localized anodic region forms on the metal surface, where oxidation occurs, releasing electrons into the metallic structure.[4] These electrons travel to a corresponding cathodic site, where they participate in the reduction of oxygen, facilitated by hydrogen ions (H^+) present in the environment.

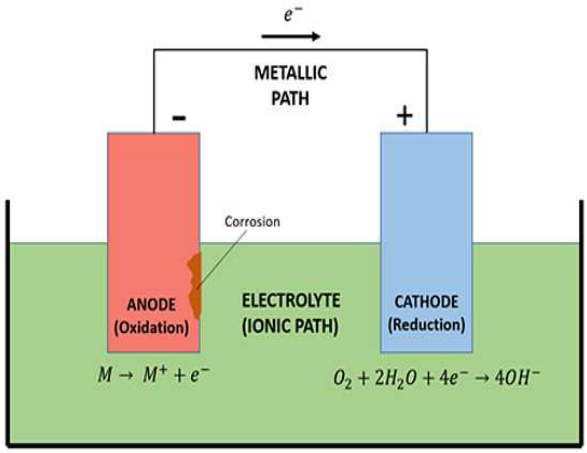

Figure 1.1 Basic corrosion Cell.

During corrosion process below reaction occurs[2];

- **Anodic Reaction (Oxidation at the Anode)**

At the anode, the metal undergoes oxidation, losing electrons and forming metal ions:

$$M \rightarrow Mn^{+} + ne^{-} \qquad \textit{Equation 1}$$

- **Cathodic Reaction (Reduction at the Cathode)**

The released electrons travel to the cathode, where they participate in the reduction of oxygen, facilitated by hydrogen ions

In acidic conditions (low pH):

$$O_2 + 4H^{+} + 4e^{-} \rightarrow 2H_2O \qquad \textit{Equation 2}$$

In neutral or alkaline conditions:

$$O_2 + 2H_2O + 4e^{-} \rightarrow 4OH^{-} \qquad \textit{Equation 3}$$

- **Electron Flow**

Electrons (e^{-}) move from the anode (where oxidation occurs) through the metallic path to the cathode (where reduction occurs). This movement of electrons drives the electrochemical reactions.

- **Electrolyte (Moisture/Atmospheric Conditions)**

The presence of moisture (H_2O) and dissolved gases like carbon dioxide (CO_2) leads to the formation of carbonic acid:

$$CO_2 + H_2O \rightarrow H_2CO_3 \qquad \textit{Equation 4}$$

Understanding different corrosion mechanisms is crucial for reducing maintenance costs, extending the lifespan of metallic structures, and ensuring operational safety in engineering applications. Figure 1.2 illustrates the various forms of corrosion, which often overlap in real-world scenarios, include [1]:

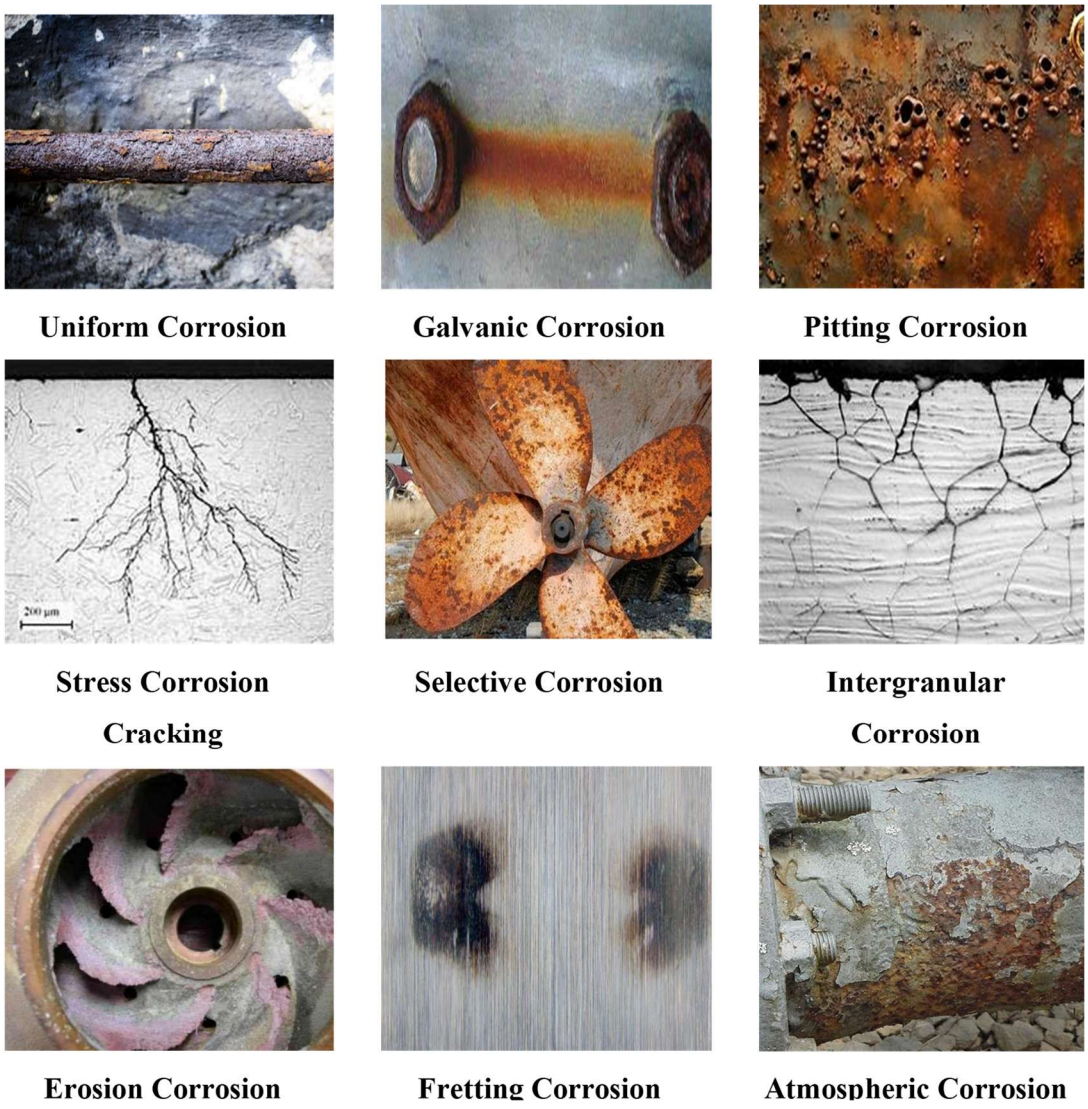

Figure 1.2 Illustrates the various forms of corrosion.

1.3 Economic Impact of Corrosion and Prevention Strategies

Corrosion remains a significant economic challenge worldwide, causing financial losses across industries. Estimates suggest that globally, corrosion-related expenses account for nearly 3.4% of the world's GDP, totaling approximately $2.5 trillion annually. In India, corrosion-related losses are estimated to be around 2-3% of the national GDP each year, amounting to roughly ₹2 lakh

crore.[5] Implementing effective corrosion prevention measures could help reduce these losses by 15-35% annually.

1.3.1 Pipeline Transportation & Corrosion Control

Pipelines, both offshore and underground, serve as an essential mode of transportation for hydrocarbons and other materials. Engineers India Limited (EIL) recommends their use due to efficiency and cost-effectiveness. According to the Ministry of Petroleum and Natural Gas, India has approximately 15,000 km of operational pipelines, with corrosion responsible for 22% of pipeline failures. Cathodic protection is the primary method used to mitigate pipeline corrosion, extending their lifespan and reducing maintenance costs.

1.3.2 Corrosion Costs in the United States

Corrosion has also been a topic of extensive research in the United States. A 2002 study by the Federal Highway Administration estimated that corrosion costs represented 3.1% of the U.S. GDP, amounting to approximately $276 billion per year. Over time, inflation and aging infrastructure have likely increased these costs[6].

In this research, the U.S. economy was segmented into five main categories comprising 26 individual sectors. Corrosion-related expenses were estimated for each sector, and when aggregated, the annual cost for the industries analyzed amounted to $137.9 billion. Figure 1.3 displays how these expenses are distributed among the five categories. Since the study did not cover every industry, the overall economic impact of corrosion on the U.S. economy is expected to be higher than $137.9 billion. [6]

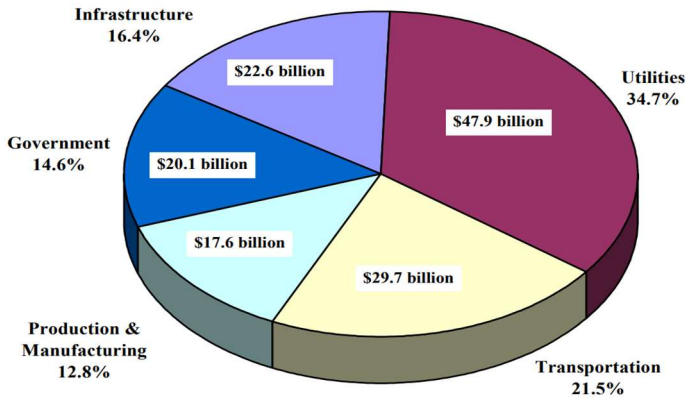

Figure 1.3 Annual Corrosion Cost Breakdown by Sector Categories ($137.9 Billion).[6]

Breakdown of this sector corrosion cost is as per Table 1.1. The data highlights how different industries, including infrastructure, production & manufacturing, transportation, and utilities, are impacted by corrosion-related expenses. Notably, utilities incur the highest cost ($47.9 billion), followed by transportation ($29.7 billion), and infrastructure ($22.6 billion).

Table 1.1 Summary of Corrosion-Related Costs by Sector in the U.S. Economy [6]

Sector	Sum of Value (Billion $)
Infrastructure	**22.6**
Gas & Liquid Transmission Pipelines	7
Hazardous Materials Storage	7
Highway Bridges	8.3
Waterways & Ports	0.3
Production & Manufacturing	**12.8**
Chemical, Petrochemical, and Pharmaceutical	1.7
Oil & Gas Exploration and Production	1.4
Petroleum Refining	3.7
Pulp and Paper	6
Transportation	**29.7**
Aircraft	2.2
Hazardous Materials Transport	0.9
Motor Vehicles	23.4
Railroad Cars	0.5
Ships	2.7
Utilities	**47.9**
Drinking Water & Sewer Systems	36
Electrical Utilities	6.9
Gas Distribution	5

1.3.3 Industrial Efforts to Combat Corrosion

Among various industries, the automotive sector has made the most significant progress in corrosion prevention. This has been achieved through the use of coated metals, stainless steel, advanced finishes, and material innovations that enhance durability while reducing corrosion-related expenses. Studies indicate that improved practices have helped eliminate about 35% of avoidable corrosion costs in the automotive industry.

The pipeline, aircraft, and shipbuilding industries have also adopted better materials and protective technologies, resulting in reduced repair and maintenance costs. However, despite advancements, the overall financial impact of corrosion remains high.

1.4 Strategies for Corrosion Mitigation

Although industries have made notable improvements, corrosion still imposes a substantial financial burden. Continued research, the adoption of corrosion-resistant materials and the application of advanced protective technologies are essential to further reduce costs and enhance infrastructure durability worldwide.

Preventing corrosion requires a multifaceted approach that includes the use of protective coatings, corrosion-resistant alloys, cathodic protection, corrosion inhibitors, proper design and material selection, environmental control and regular maintenance. Implementing these methods can significantly reduce the economic impact of corrosion, extend the lifespan of materials, and ensure safety across various industries.

1.4.1 Protective Coatings

Protective coatings are one of the most widely used methods to prevent corrosion. They act as a barrier between the metal and the corrosive environment.

Organic Coatings: These include paints, varnishes, and lacquers. They provide a physical barrier and can be enhanced with corrosion inhibitors. According to the U.S. Department of Commerce Census Bureau, the total annual cost for organic coatings in the U.S. was estimated at $108.6 billion in 1998.[6]

Figure 1.4 Application of paint as coating

Metallic Coatings: Techniques like galvanizing, where a layer of zinc is applied to steel, are common. Hot-dip galvanizing and electroplating are effective methods for providing sacrificial protection. The market for metallizing and galvanizing in the U.S. was estimated at $1.4 billion in 1998.[6]

1.4.2 Corrosion-Resistant Alloys

Alloying is a well-established technique for improving the corrosion resistance of metals by introducing specific elements into their structure. Incorporating elements such as chromium, nickel, and molybdenum into base metals like iron or steel enhances their ability to resist degradation in corrosive environments. A notable example is stainless steel, which contains at least 10.5% chromium. This chromium reacts with oxygen to form a thin, stable, and self-repairing chromium oxide layer (Cr_2O_3) on the surface. This passive layer acts as a protective barrier, inhibiting further oxidation and corrosion of the metal beneath. The performance of this protective layer depends on factors such as the alloy's composition, environmental conditions, and the stability of the oxide film.[7,8]

1.4.3 Corrosion Inhibitors

Corrosion inhibitors are chemical compounds that, when added in small concentrations to a corrosive environment, significantly reduce the rate of metal degradation. These inhibitors function by forming a protective barrier on the metal surface, altering the electrochemical reactions

that cause corrosion.[1] Their application is widespread in industries such as oil and gas, water treatment, power generation, and manufacturing.

1.4.4 Environmental Control

Environmental control is a proactive approach to corrosion prevention that involves modifying the conditions of the surrounding environment to reduce the likelihood of corrosion. This method focuses on controlling factors such as temperature, humidity, pH, and the presence of corrosive agents like oxygen, chlorides, or sulfur compounds. For instance, in industrial settings, dehumidifiers can be used to lower moisture levels, thereby minimizing the risk of electrochemical reactions that lead to corrosion. Similarly, controlling the pH of a solution to maintain a neutral or slightly alkaline environment can significantly reduce the corrosion rate of metals. Another common practice is the use of inhibitors, which are chemical additives that interact with the metal surface or the environment to slow down or prevent corrosion.[1]

1.4.5 Proper Design and Material Selection

Proper design and material selection play a critical role in minimizing corrosion and extending the service life of structures, machinery, and components. By integrating corrosion-resistant materials and implementing smart design strategies, industries can significantly reduce maintenance costs and improve safety.

1.4.6 Proper Design

Effective corrosion prevention begins with designing components and structures that minimize exposure to corrosive elements. Key principles include[2]:

a. Avoiding Crevices and Trapped Moisture
b. Reducing Galvanic Corrosion Risks
c. Ensuring Proper Coating Application
d. Optimizing Structural Design

1.4.7 Selection of Corrosion-Resistant Materials

Material selection is a key factor in corrosion prevention. Industries choose materials based on environmental conditions, operational requirements, and cost-effectiveness.[1]

1.4.8 Cathodic Protection

Cathodic protection (CP) is a proven electrochemical method used to prevent corrosion in metal structures, particularly those exposed to soil, water, and industrial environments. It works by converting the metal surface into a cathode through the application of an external current (Impressed Current Cathodic Protection - ICCP) or by using a sacrificial anode (Sacrificial Anode Cathodic Protection).[2] This method is extensively utilized in protecting pipelines, underground tanks, marine structures, and ship hulls from corrosion. CP is commonly applied in industries such as pipelines, marine vessels, underground storage tanks, and offshore structures. [1,2,8] There are two types of cathodic protection methods as explain below;

1.4.8.1 Impressed Current Cathodic Protection (ICCP)

ICCP uses an external DC power source to apply a protective current to the structure. Durable anodes such as graphite, platinum, or mixed metal oxides (MMO) are utilized, minimizing material consumption as shown in Figure 1.6[9], ICCP is highly effective in protecting large structures such as underground pipelines. To improve its efficiency, isolation kits are frequently used to divide pipelines into smaller sections and insulate the flanges at connection points, ensuring better corrosion prevention. [10]

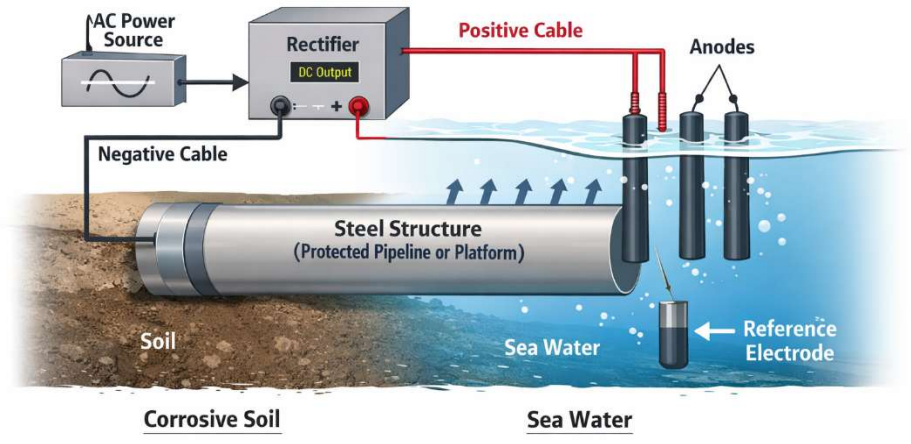

Figure 1.5 Schematic set up of Impressed Current Cathodic Protection.

1.4.8.2 Sacrificial Anode Cathodic Protection (SACP)

This method involves attaching more reactive metals like magnesium, zinc, or aluminium to the structure needing protection. These anodes corrode preferentially, shielding the main structure from deterioration. SACP is widely used in marine applications, buried pipelines, and offshore installations. This method is widely used in the oil and gas industry, where aluminium sacrificial anodes are installed on steel components to enhance corrosion resistance.[11] Hot-dip galvanization is another example, where steel is coated with zinc, forming a protective layer that sacrifices itself to shield the underlying metal from corrosion.

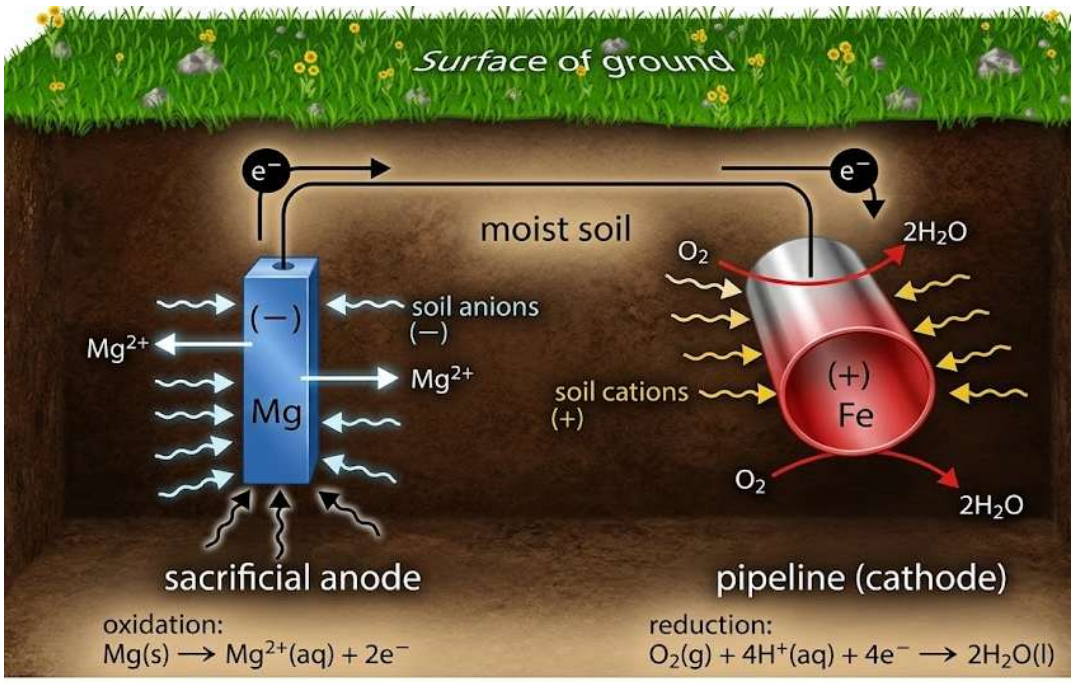

Figure 1.6 Schematic set up of sacrificial anode Cathodic Protection of pipeline.

In this system, the metal requiring protection functions as the cathode, while a more reactive metal or alloy with a higher electrochemical potential serves as the anode. Through a redox reaction, the anode oxidizes and gradually corrodes, while the cathode remains protected from deterioration. This process effectively shifts corrosion from the protected metal to the sacrificial anode.[2,12] The anode is connected to the structure using lead wires or cast-m straps, which can be secured through welding or mechanical fastening.

Commonly used sacrificial anode materials include aluminum (Al), magnesium (Mg), and zinc (Zn), each selected based on the specific environmental and operational conditions.[1,4]

a) Zinc (Zn) Anodes

Zinc anodes are widely used in seawater applications due to their stable electrochemical behavior and consistent output. These anodes provide reliable protection for ship hulls, offshore structures, and pipelines. A typical zinc anode composition includes[13]:

- Zinc (Zn): Balance
- Aluminum (Al): 0.4 – 0.6%
- Cadmium (Cd): 0.075 – 0.125%
- Iron (Fe): ≤ 0.005%
- Copper (Cu): ≤ 0.006%

b) Magnesium (Mg) Anodes

Magnesium anodes are ideal for environments with high electrical resistivity, such as soil and freshwater systems. These anodes generate a high driving voltage, making them effective for protecting buried pipelines and storage tanks.[14–16] A standard magnesium anode composition includes:

- Magnesium (Mg): Balance
- Manganese (Mn): 0.5 – 1.3%
- Aluminum (Al): ≤ 0.01%
- Zinc (Zn): < 0.01%
- Silicon (Si): < 0.1%
- Copper (Cu): ≤ 0.004%

c) Aluminum (Al) Anodes

Aluminum-based anodes are commonly used in marine applications due to their high efficiency and lightweight nature. They are alloyed with trace elements to enhance performance and longevity. A typical aluminum anode composition includes:

- Aluminum (Al): Balance
- Zinc (Zn): 4.0 – 6.5%
- Indium (In): 0.014 – 0.020%
- Silicon (Si): 0.08 – 0.21%
- Iron (Fe): ≤ 0.090%
- Copper (Cu): ≤ 0.005%

Sacrificial anodes offer several advantages

- **Easy Installation –** Sacrificial anodes can be installed without requiring an external power source, making them convenient for various applications[17]
- **Minimal Maintenance –** These anodes function passively and do not require continuous monitoring, reducing maintenance efforts [4]
- **Reliable Corrosion Protection –** As long as the anode remains active, it effectively protects the metal structure by corroding in place of the protected surface [18]
- **No Risk of Overprotection –** Unlike impressed current systems, sacrificial anodes naturally regulate the protection level, preventing damage due to excessive current[2]
- **Ideal for Remote Locations –** Since they operate independently of electricity, they are well-suited for isolated areas where power access is limited [1]
- **Cost-Effective for Small Structures –** Sacrificial anodes are economically viable for protecting smaller assets such as pipelines, water heaters, and ships[17]

Some of the drawback of Sacrificial anodes;

- **Finite Lifespan –** Once fully consumed, the anode must be replaced, leading to recurring costs[4]
- **Reduced Efficiency in High-Resistivity Environments –** In soils or water with high resistivity, sacrificial anodes may not provide adequate protection, requiring additional anodes [18]
- **Bulky and Heavy for Large Systems –** Larger infrastructure requires multiple anodes, increasing weight and space requirements [1]
- **Higher Costs for Extensive Applications –** For large-scale infrastructure, such as long pipelines or offshore platforms, impressed current cathodic protection (ICCP) systems are often more cost-efficient [2]
- **Frequent Replacement Needs –** Depending on environmental conditions, sacrificial anodes may degrade quickly, leading to repeated replacements and increased maintenance efforts [1]
- **Limited Adjustability –** Unlike ICCP systems, sacrificial anodes do not allow precise control of protection levels, making optimization difficult [17]

1.5 Motivations

Corrosion is a significant challenge across industries such as transportation, manufacturing, infrastructure, and utilities, leading to economic losses of nearly 3.5% of GDP (Rs. 2.0 lakh crore annually in India). However, effective corrosion protection measures can reduce these costs by 15-35%, extending the lifespan of structures and equipment. Cathodic and anodic protection systems require substantial investment. In 1998, corrosion protection hardware sales totaled $146 million, with sacrificial anodes accounting for $60 million. The annual cost of replacing sacrificial anodes in water heaters and related replacements reached $1.24 billion, bringing the total yearly expenditure on cathodic and anodic protection to $2.22 billion (NACE International, 1998).

Among corrosion control techniques, cathodic protection is widely recognized. The sacrificial anode method is preferred for its self-sufficiency, ease of installation, localized protection, and minimal interference with nearby structures. It is commonly used in marine engineering, oil and gas pipelines, underground storage tanks, and offshore structures.

Aluminum and its alloys serve as effective sacrificial anodes, especially in marine environments, protecting ships, offshore platforms, and submerged structures. However, aluminum naturally forms a passive oxide layer when exposed to oxygen, which limits its effectiveness over time. To overcome this, research focuses on modifying aluminum's composition and structure. Recent studies have reported conflicting conclusions regarding the influence of alloy composition, heat treatment, grain size, and microstructural characteristics on the electrochemical performance of aluminium sacrificial anodes. These inconsistencies are primarily attributed to differences in alloy chemistry, experimental methodologies, and testing conditions, highlighting the need for systematic investigations under controlled conditions to establish clear structure–property relationships.[19] One approach involves alloying aluminum with 6.5% magnesium and varying silicon content to disrupt passivation and improve electrochemical performance. Additionally, heat treatment methods have been investigated to modify the microstructure and secondary phases, enhancing electrochemical activity and improving aluminum's effectiveness as a sacrificial anode.

1.6 Objective

The present research is designed to address the identified research gaps and key challenges associated with aluminum-based sacrificial anodes. The electrochemical behavior of aluminum sacrificial anodes can be studied by adding magnesium and silicon with the following potential objectives.

1) To fabricate aluminum-based sacrificial anodes alloyed with magnesium and silicon, with particular emphasis on the formation and distribution of the Mg_2Si phase for enhanced anodic performance.
2) To examine the influence of heat treatment on the evolution and morphology of the Mg_2Si phase, and its role in modifying microstructural characteristics.
3) To evaluate the synergistic effects of alloying and heat treatment on the microstructure, mechanical hardness, and electrochemical behavior of the developed Al-Mg-Si alloys.

1.7 Scope

The primary aim of this research is to improve the performance of Aluminum-6.5% Magnesium sacrificial anodes through two approaches: alloying with silicon (Si) and heat treatment.

In the first approach, Si is incorporated into the Al-6.5% Mg alloy in varying concentrations (1.5%, 3%, 4.5%, and 6% by weight) to evaluate its recovery in the developed alloy. The hardness of the resulting alloy is compared with pure aluminum to assess the individual effects of magnesium and silicon on mechanical properties. To analyze the impact of Si addition on microstructure and electrochemical behavior, optical and scanning electron microscopy (SEM) is utilized for microstructural characterization. X-ray diffraction (XRD) is performed to identify phase formations, while the corrosion behavior of both Al-6.5% Mg and the Si-alloyed samples is studied using weight loss method and potentiodynamic testing. The corrosion potential of the developed alloys is evaluated to determine improvements resulting from Si addition.

The second approach focuses on the heat treatment of the developed alloy. The hardness and grain size of the heat-treated samples are measured and compared with the untreated alloy to assess the effects of heat treatment. Microstructural changes due to heat treatment are examined using optical

microscopy and SEM and their influence on corrosion behavior is analyzed using weight loss methods and potentiodynamic testing. The findings from these tests are compared to understand the impact of microstructural modifications on corrosion resistance.

Finally, a comprehensive analysis is conducted to draw conclusions based on the results obtained from both alloying and heat treatment, highlighting their effectiveness in enhancing the performance of Al-6.5% Mg sacrificial anodes.

1.8 Thesis Organization

Chapter 1 Introduces the concept of corrosion, its definition, and its economic impact. Various corrosion prevention strategies, including protective coatings, corrosion-resistant materials, cathodic protection, inhibitors, optimized design, material selection, and environmental control, are discussed. The role of aluminum as a sacrificial anode is explored, along with its passivation and depassivation behavior. Additionally, the effects of alloying, Heat treatment and Cold working on corrosion resistance are examined. The chapter concludes with an outline of the research motivations, objectives, scope, and thesis structure.

Chapter 2 reviews existing research on the corrosion of aluminum and its alloys. It covers fundamental corrosion mechanisms and different types of corrosion, such as pitting, intergranular corrosion, and stress corrosion cracking. The influence of alloy composition on corrosion resistance is analyzed, with a focus on elements such as magnesium, silicon, zinc, tin, titanium, lanthanum, silver, selenium, copper, zirconium, strontium, gallium, and bismuth. The impact of heat treatment on aluminum anodes is also discussed. Furthermore, research gaps in the field are identified to establish the need for further investigation.

Chapter 3 details the methodology used in the study, including information on raw materials, casting processes, charge calculations, and furnace operations. The preparation of test samples and experimental setup are described. It also covers chemical composition analysis, mechanical property evaluation. Specific attention is given to hardness testing and microstructural characterization using optical and scanning electron microscopy. Corrosion rate assessments, including potentiodynamic polarization studies and standard weight loss measurements, are

discussed. Finally, the examination of corroded samples through pit size measurement and SEM analysis is presented.

Chapter 4 presents the experimental results and discussion. It begins with the effect of silicon addition on the chemical composition and microstructure of Al–6.5%Mg alloys. Detailed microstructural characterization is carried out using optical microscopy, X-ray diffraction (XRD), and image analysis to evaluate phase formation, grain structure, phase volume fraction, Mg_2Si morphology, and the influence of T6 heat treatment. The chapter further examines the effect of silicon addition on hardness, corrosion behaviour through weight loss and potentiodynamic polarization studies, corrosion mechanisms, and the correlation between microstructure and electrochemical performance. Finally, the anodic performance of the developed alloys is evaluated in terms of anode capacity, consumption rate, efficiency, and post-test surface examination, with comparisons made between as-cast and heat-treated conditions.

Chapter 5 highlights the major contributions of the research and presents the hypotheses developed based on the experimental findings. It summarizes the significant scientific contributions of the study and proposes hypotheses describing the influence of silicon content, Mg_2Si morphology, heat treatment, and microstructure–electrochemical interactions on the corrosion behaviour and sacrificial anode performance of Al–6.5%Mg alloys.

Chapter 6 summarizes the major conclusions drawn from the experimental investigation. The chapter presents the key findings regarding the effects of silicon addition and T6 heat treatment on microstructure, hardness, corrosion behaviour, and sacrificial anode performance. It also outlines the scope for future research, including the influence of cold working, combined thermo-mechanical processing, advanced electrochemical characterization, modelling approaches, and three-dimensional corrosion studies for further enhancement of aluminum sacrificial anode alloys.

CHAPTER 2
LITERATURE REVIEW

2.1 Overview

This chapter provides a comprehensive review of the corrosion properties, mechanical behavior and microstructural characteristics of Aluminum-Magnesium-Silicon (Al-Mg-Si) alloys. The chapter discusses the basic phenomena of corrosion in Al-Mg-Si alloys, the types of corrosion they are susceptible to and the influence of alloy composition on their corrosion resistance. Additionally, the chapter reviews the effects of cold working, heat treatment and other processing techniques on the performance of Al-Mg-Si alloys, particularly in marine and industrial environments. The chapter concludes by identifying research gaps and summarizing the key findings from previous studies.

2.2 Utilization of Aluminum as a Sacrificial Anode

Aluminum is widely utilized as a sacrificial anode to protect carbon steel structures from corrosion, particularly in industrial, offshore and marine applications.[20,21] Its popularity is due to its excellent electrochemical properties, cost-effectiveness, and high efficiency in aggressive environments.[4] Figure 2.1 shows the aluminum sacrificial anodes. Aluminum anodes work by corroding preferentially to the protected metal, ensuring long-term structural integrity.

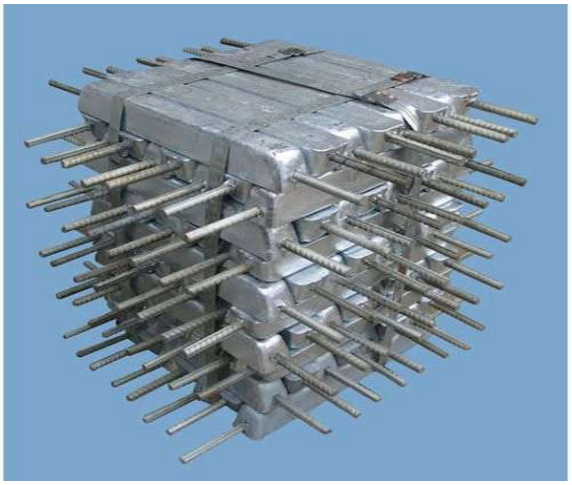

Figure 2.1 Aluminum sacrificial anodes

Aluminum anodes are manufactured in different forms, including cast, extruded, and welded types, each designed for specific applications.[22] Extruded anodes are created by forcing a combination of aluminum and alloying elements through an extrusion process, resulting in a uniform shape and high structural integrity. Cast anodes are produced by pouring molten aluminum into pre-designed molds, making them ideal for large-scale applications such as ships and offshore structures. Welded anodes involve bonding an aluminum plate onto a steel surface, providing strong adherence and effective corrosion protection. The selection of an anode type depends on factors such as structural dimensions, environmental exposure, and operational requirements. Extruded anodes are particularly effective for protecting smaller components, whereas cast anodes are preferred for large marine and industrial structures.

Aluminum is widely recognized for its corrosion-resistant properties and effectiveness as a sacrificial anode in cathodic protection systems. Its high electrochemical equivalent, excellent thermal and electrical conductivity, and cost-effectiveness make it a preferred choice for galvanic anode applications. [23] With a high anode capacity (2500 amp.hr/kg) and a low consumption rate (3.4 kg/amp.yr), aluminum provides long-lasting protection in seawater, freshwater, and brackish environments. Its moderate open circuit potential (-1.66V vs. SHE) ensures efficient corrosion prevention without excessive metal loss, while its density (2.70 gm/cc) contributes to its durability and stability in harsh conditions. These properties make aluminum an ideal choice for protecting marine structures, pipelines, and other corrosion-prone installations.

Furthermore, aluminum anodes are readily available, easy to manufacture and highly effective in chloride-rich environments, enhancing their suitability for safeguarding ship hulls, underwater pipelines, and offshore rigs. Their long service life and efficiency in both high and low resistive mediums further reinforce their importance in industrial applications. These are some common applications of corrosion prevention in different sectors

- **Marine Industry:** Used extensively to protect ship hulls, offshore platforms, and submerged metallic structures.
- **Oil & Gas Pipelines:** Effective for protecting submerged and underground pipelines in saline environments.

- **Storage Tanks and Heat Exchangers:** Commonly used in industrial water storage tanks and cooling systems to prevent internal corrosion.

Figure 2.2 Application of sacrificial anodes in various industry.

2.3 Electrochemical Properties of Aluminum and its Alloys

Pure aluminum exhibits unique electrochemical properties that make it a widely used material in corrosion protection and industrial applications. One of its most notable characteristics is its natural passivation, where aluminum spontaneously forms a thin, protective oxide layer (Al_2O_3) when exposed to oxygen. This oxide film enhances corrosion resistance by preventing further oxidation and significantly reducing aluminum's reactivity in neutral and mildly acidic environments.

The presence of impurities or exposure to chloride-rich environments can lead to pitting corrosion, which compromises the protective oxide layer and accelerates localized corrosion. In aggressive environments, aluminum alloys with elements like zinc, indium or gallium are often preferred as they help prevent passivation and improve the material's electrochemical performance in cathodic protection systems.[24,25]

2.3.1 Key Electrochemical Characteristics Affecting Anode Performance

The performance of aluminium-based sacrificial anodes is influenced by several electrochemical characteristics:

2.3.1.1 Electrode Potential

Electrode potential is a fundamental concept that dictates the direction and efficiency of electrochemical reactions. It is defined as the voltage difference between a given electrode and a standard reference electrode, typically the standard hydrogen electrode (SHE).[26] This potential reflects the tendency of a metal to either gain electrons (reduction) or lose electrons (oxidation).

Metals exhibit different electrochemical behaviors depending on their surrounding environment. Two important reference systems help us understand and predict metal reactivity and corrosion: the Electromotive Force (EMF) Series and the Galvanic Series. While both rank metals based on their tendency to gain or lose electrons, they serve different purposes in electrochemical and corrosion science.

The Electromotive Force (EMF) Series, also known as the electrochemical series, ranks metals according to their standard electrode potentials in aqueous solutions. The more negative the electrode potential, the greater the metal's tendency to lose electrons and undergo oxidation. As shown in Table 2.1, aluminum (Al) has a standard electrode potential of -1.66 V vs. SHE, placing it among highly reactive metals that readily corrode in most environments.[27]

Table 2.1 Electromotive Force (EMF) Series - Standard Electrode Potential [27]

Reaction	**Standard Electrode Potential (E°) vs. SHE (V)**
Fluorine ($F_2 + 2e^- \rightarrow 2F^-$)	+2.87 V
Gold ($Au^{3+} + 3e^- \rightarrow Au$)	+1.50 V
Chlorine ($Cl_2 + 2e^- \rightarrow 2Cl^-$)	+1.36 V
Oxygen ($O_2 + 4H^+ + 4e^- \rightarrow 2H_2O$)	+1.23 V
Silver ($Ag^+ + e^- \rightarrow Ag$)	+0.80 V
Copper ($Cu^{2+} + 2e^- \rightarrow Cu$)	+0.34 V
Hydrogen ($2H^+ + 2e^- \rightarrow H_2$) (Reference)	0.00 V
Lead ($Pb^{2+} + 2e^- \rightarrow Pb$)	-0.13 V

Iron ($Fe^{2+} + 2e^- \rightarrow Fe$)	-0.44 V
Zinc ($Zn^{2+} + 2e^- \rightarrow Zn$)	-0.76 V
Aluminum ($Al^{3+} + 3e^- \rightarrow Al$)	**-1.66 V**
Magnesium ($Mg^{2+} + 2e^- \rightarrow Mg$)	-2.37 V
Sodium ($Na^+ + e^- \rightarrow Na$)	-2.71 V
Potassium ($K^+ + e^- \rightarrow K$)	-2.92 V
Lithium ($Li^+ + e^- \rightarrow Li$)	-3.05 V

The significance of electrode potential in electrochemical reactions lies in its ability to predict the spontaneity of redox processes. A more negative electrode potential indicates a greater propensity for oxidation, making the material a suitable anode in cathodic protection systems. Conversely, a more positive potential suggests a tendency for reduction, characteristic of cathodic materials. Aluminum's position in the EMF series places it below many structural metals such as steel and copper, making it an excellent candidate for use as a sacrificial anode. However, in its pure form, aluminum develops a passive oxide layer (Al_2O_3) that limits its electrochemical activity and prevents it from being an effective sacrificial anode in many environments.[26]

In real conditions, especially in seawater, metals behave differently than predicted by the EMF Series. The Galvanic Series provides an empirical ranking of metals based on their observed corrosion tendencies in specific electrolytes, particularly chloride-rich environments like seawater. [4]

Table 2.2 Galvanic Series in Seawater. [4]

Metal/Alloy	**Galvanic Behavior**
Magnesium & Magnesium Alloys	**Most Anodic (Active)**
Zinc	
Aluminum Alloys (Al-Zn, Al-Mg-In sacrificial anodes)	
Aluminum (Pure)	
Mild Steel, Cast Iron	
Low Alloy Steels	
Lead	

Brasses (Copper-Zinc Alloys)	
Copper	
Bronzes (Copper-Tin Alloys)	
Nickel-Copper Alloys (Monel 400)	
Stainless Steel (Active, Non-passivated)	
Silver Solder	
Nickel & High-Nickel Alloys	
Titanium	
Graphite	
Platinum, Gold	**Most Cathodic (Noble)**

In the Galvanic Series as shown in Table 2.2, aluminum and its alloys exhibit different behavior depending on their composition. While pure aluminum is relatively corrosion-resistant due to its oxide film, aluminum-zinc alloys are engineered to be more active, making them ideal for use as sacrificial anodes in cathodic protection.[28] Although aluminum (-1.66V) is highly reactive in the EMF Series, in the Galvanic Series, its oxide film slows corrosion, making it behave less active than expected. In cathodic protection applications, aluminum and its alloys are often employed as sacrificial anodes due to their favorable electrochemical properties.

2.3.1.2 Current Efficiency

Current efficiency is a critical parameter in electrochemical applications, particularly in sacrificial anode performance and corrosion protection systems. It defines the effectiveness of a metal in converting electrical charge into actual material consumption during oxidation. In cathodic protection, higher current efficiency ensures that more of the anode's material is actively used to protect the structure, reducing waste and improving system longevity [28].

To optimize the current efficiency of aluminum sacrificial anodes, it is essential to minimize oxide film formation, which can hinder effective metal dissolution. The addition of alloying elements such as zinc and indium helps maintain continuous activation in seawater, ensuring better performance. Aluminum alloys are widely preferred for sacrificial anodes due to their engineered compositions, which enable a consistent dissolution rate and high efficiency. In contrast,

magnesium anodes, although providing a higher driving voltage, exhibit lower current efficiency due to rapid dissolution and hydrogen evolution. Zinc anodes, while effective, have a lower energy capacity per unit mass compared to aluminum, making them less suitable for long-term applications. Several factors influence the efficiency of aluminum alloys, including alloy composition, where elements like indium, tin, or zinc prevent passivation; electrolyte conditions, as higher chloride concentrations enhance aluminum activation; and anode design, where larger surface areas improve utilization.[29]

2.3.1.3 Corrosion Resistance

While sacrificial anodes are designed to corrode, their lifespan and effectiveness depend on controlled corrosion rates. The addition of elements such as indium and gallium helps in activating the aluminum surface, preventing the formation of a non-conductive oxide layer, and ensuring consistent anode performance.

2.4 Challenges and Performance Considerations

2.4.1 Passivation of pure aluminium

One of the primary challenges associated with aluminum sacrificial anodes is the formation of an oxide layer on the surface, which can lead to passivation and reduced effectiveness. Passivation is a widely used method to enhance the corrosion resistance of metals by forming a protective oxide layer on their surface. In the case of pure aluminum, passivation occurs naturally when the metal is exposed to air or moisture, resulting in the development of a thin, adherent aluminum oxide (Al_2O_3) layer. According to Pourbaix diagrams, aluminum oxide is a thermodynamically stable compound. The Pilling-Bedworth Ratio (PBR) for aluminum oxide is calculated to be 1.28, indicating that the oxide layer formed on the aluminum surface is denser than the underlying metal. This characteristic suggests that the oxide film provides a protective barrier, limiting further oxidation and influencing the corrosion behavior of aluminum. The formation and growth of the oxide layer on aluminum are influenced by various factors, including oxygen pressure, temperature, surface characteristics of the metal, and the presence of chemical elements within the alloy. These parameters determine the stability and protective nature of the oxide film, affecting the overall corrosion resistance and electrochemical behavior of aluminum in different

environments.[30] This oxide layer serves as a barrier, preventing further oxidation and shielding the underlying metal from aggressive environmental conditions.

Aluminum passivation is particularly significant in industries where corrosion resistance is crucial, such as aerospace, automotive, and marine applications. The passivation layer helps aluminum maintain its structural integrity and durability even in harsh environments. [31] Additionally, anodization is a controlled method of passivation that enhances the protective oxide layer by applying an electric current in an electrolytic bath. This process increases the thickness and uniformity of the oxide layer, further improving aluminum's resistance to wear and corrosion.

Despite its advantages, aluminum passivation has certain limitations. The oxide layer can degrade in highly acidic or alkaline environments, leading to localized corrosion such as pitting or crevice corrosion.

To mitigate passivation, it is essential to regulate key factors such as temperature, pH levels and the presence of specific ions in the electrolyte.[32] If the pH or temperature is too high, the oxide layer can become denser and more resistant to breakdown, reducing the anode's electrochemical activity. Similarly, the presence of certain ions, such as chlorides or sulfates, can influence the stability of the oxide film. Maintaining optimal electrolyte composition and controlling the surrounding environmental parameters can help prevent excessive passivation, ensuring the continued effectiveness of aluminum anodes.

2.4.2 Depassivation of Pure Aluminium

Depassivation involves the removal or disruption of the protective oxide layer on a metal surface, such as aluminum, to enhance its corrosion activity. The processes of passivation and depassivation in pure aluminum are critical factors that influence its effectiveness as a sacrificial anode in cathodic protection systems.[30] The ability of aluminum to form and break down its oxide layer directly impacts its electrochemical activity and overall performance in corrosion prevention. This process is particularly significant in applications like sacrificial anodes in cathodic protection systems, where aluminum's ability to corrode is utilized to protect other metals. Several techniques can achieve depassivation of aluminum and improve their electrochemical performance.

2.5 Methods to Improve the Electrochemical Behavior of Aluminum Anodes

2.5.1 Alloying

Specific chemical agents can dissolve or disrupt the oxide layer, effectively depassivation the surface. Alloying involves adding specific elements to aluminum to enhance its properties, including its corrosion resistance. For instance, incorporating manganese into aluminum increases strength through solution strengthening and improves strain hardening while not appreciably reducing ductility or corrosion resistance.

Similarly, adding magnesium to aluminum increases strength through solid solution strengthening and improves strain hardening ability. [33] These alloys are the highest-strength non-heat-treatable aluminum alloys and are therefore used extensively for structural applications.

Some alloying elements can decrease corrosion resistance. For example, the introduction of copper to aluminum can reduce ductility and corrosion resistance. Therefore, the selection of alloying elements must be carefully considered to balance the desired mechanical properties and corrosion resistance.

The impact of various alloying elements on aluminium alloys has been widely researched, particularly in relation to corrosion resistance, anode efficiency, microstructural modifications, and mechanical properties. When introduced in specific amounts, these elements significantly alter the alloy's structure, enhance its performance, and influence its electrochemical characteristics.

The Table 2.3 provides an overview of how different alloying elements affect aluminium alloys, as reported in various studies. It outlines their role in phase formation, grain structure refinement, corrosion behavior, and improvements in anode efficiency.

Table 2.3 Summary of the Effects of Alloying Elements on Aluminium Alloys.

Sr No.	Alloying Element	Effect of Alloying Element	Reference
1	Zinc (Zn)	Increases anode efficiency up to 86.59% at 6% Zn; forms β phase that enhances dissolution of Al matrix	[34],[35],[36] [37]

2	Tin (Sn)	Forms Sn globules that act as nucleation sites for corrosion, increasing anode efficiency to 98.65% at 0.1% Sn	[36][38]
3	Titanium (Ti)	Acts as a grain refiner, forms $TiAl_3$ phase, improves uniformity, reduces intergranular corrosion	[39]
4	Titanium (Ti) & Magnesium (Mg)	Forms $TiAl_3$ and $MgZn_2$ particles, increases galvanic corrosion, improves uniformity	[35],[36],[40]
5	Titanium (Ti) & Zirconium (Zr)	Acts as grain refiners, reduces segregation, improves uniformity and anode performance	[36]
6	Silicon (Si)	Forms fine-grain structure, reduces Zn segregation, improves corrosion uniformity	[41], [19], [20]
7	Lanthanum (La)	Forms Al_2LaZn_2 phases, inhibits grain growth, improves uniformity and dissolution of Al matrix	[25], [36]
8	Gallium (Ga) & Bismuth (Bi)	Reduces grain boundary precipitates, improves uniformity and dissolution [42]	[36]
9	Titanium (Ti) & Strontium (Sr)	Ti refines grain, Sr modifies Al structure, improves anode efficiency from 77% to 87%	[36] [43]
10	Silver (Ag)	Improves corrosion resistance, increases hardness and strength but reduces current capacity	[44]
11	Selenium (Se)	Forms inclusions improving metallography, increases anode efficiency to 90% at 0.5% Se	[45]

12	Gallium (Ga) & Zinc (Zn)	Reduces corrosion potential by 0.1-0.5V, improves anode efficiency	[46]
13	Tin (Sn) & Magnesium (Mg)	Sn shifts potential from -0.92V to -1.1V, Mg refines grain size from 150-200 μm to 70-100 μm	[47]
14	Copper (Cu)	Weakens oxide film, increases pit formation, decreases corrosion resistance	[47][48]

Several research studies indicate that alloying elements play a crucial role in enhancing the performance of aluminum anodes. This summary highlights key findings from various studies, focusing on how alloying additions influence the dissolution of the α-aluminum matrix in binary (Al-X, where X = Zn, Mg, Fe, Sn, Ti, etc.) and ternary (Al-X-Y, where X and Y = Zn, Mg,Si Fe, Sn, Ti, etc.) compounds to improve electrochemical efficiency. The investigation by Muazu A. and Yaro S. A. examines the effect of zinc addition (1-8 wt%) on aluminum's performance as a sacrificial anode in seawater. The findings reveal that increasing zinc content enhances anode efficiency, with the highest efficiency observed at 6% Zn. Pure aluminum exhibited an efficiency of 21.23%, while the Al-6%Zn alloy achieved 86.59%. This improvement is attributed to the formation of the β-phase, which facilitates the breakdown of the passive film, thereby enhancing the performance of the aluminum anode in seawater. [34] The study by S. Lameche-Djeghaba, et. al. explores the electrochemical behavior of pure aluminum and Al–5%Zn alloy in a 3% NaCl solution. The findings indicate that the Al–5%Zn alloy, when coupled with carbon steel, provides better protection compared to pure aluminum. Additionally, the study examines the effect of temperature on the electrochemical performance, highlighting the enhanced corrosion resistance of the alloy under varying condition. Yaya Zheng et.al examines the intergranular corrosion (IGC) of Al-Mg-Si alloys with varying silicon content. The findings reveal that IGC susceptibility is primarily influenced by the high electrochemical potential difference between MgSi particles and solute-depleted zones. Additionally, an excess of silicon increases IGC susceptibility due to the higher presence of MgSi precipitates along grain boundaries, which accelerates corrosion.[49]

Table 2.4 highlights the influence of various alloying elements and environmental conditions on the performance of aluminum sacrificial anodes, providing insights into optimizing their composition for enhanced corrosion protection.

Table 2.4 Effect of Alloying Elements on the Performance of Aluminum Sacrificial Anodes.

Alloy and Element Used	Analysis Environment	Observations	Reference
Al-Zn-Sn with MnO_2 incorporation	Seawater simulation	MnO_2 addition improved galvanic efficiency and promoted uniform corrosion.	Shibli & Binoj, 2009 [50]
Al-5% Zn-0.02% In with Ti and Zr additions	3 wt.% NaCl solution	Optimal Ti (0.03–0.05 wt.%) and Zr (0.05 wt.%) enhanced anode efficiency and current capacity.	Sina et al., (2006) [43]
Al-Bi-Ga-Pb-In and Al-Bi-Ga-Sn-In alloys	Seawater, freshwater, and soil environments	Al-Bi-Ga-Sn-In alloys exhibited better dissolution morphology; Bi content influenced corrosion rate and current efficiency.	Liu et al., 2024 [51]
Al-5% Zn-0.015% In-0.1% Si with Ti addition	NACE standard TM0190-2012 setup	Ti addition increased electrochemical capacity up to 2,747 Ah/kg.	Worasaen & Mungsantisuk, 2017 [52]
Al-Ga-In with varying Bi content	Electrochemical testing setups	Optimal Bi content shifted open-circuit	Liu et al., 2024 [53]

		potential negatively and promoted activation dissolution; excessive Bi led to uneven dissolution and reduced efficiency.	
Al with Ti and Sr additions	Electrochemical testing setups	Ti addition (0.03 wt.%) improved anode efficiency and current capacity; Sr effects were also evaluated.	M. Saremi.et.al 2004 [54]
Al alloys with Zn, Sn, Mg, Cu, Fe, and Si additions	Corrosion behavior analysis	Alloying elements significantly influenced morphology and corrosion behavior of aluminum alloys.	Ahmed M, et.al 2010[55]
Mg and Mg-Al 5% Zn metal-rich primers	0.6 M NaCl solution	Mg-Al 5% Zn primer maintained negative open-circuit potential	Korjenic A et.al 2024 [56]
Al-Zn-Mg (6 % to11%)	3.5 wt% NaCl solution	The formation of $Al_2Zn_3Mg_3$ has been observed, and with 8.5% Mg addition, there is a noTable enhancement in anode current capacity	Orozco et al.(2007) [57]

Al-Zn-In-Mg-Ti with Si (0.1%)	3.5 wt% NaCl	Formation of Mg_2Si is observed and fine grain formation leads to improved corrosion uniformity	Wen et al.(2011) [41]

The selection and precise composition of these elements directly influence the corrosion resistance, anode efficiency and microstructural modifications of aluminum alloys used in sacrificial applications.

2.5.2 Heat Treatments

Heat treatment plays a crucial role in modifying the mechanical properties of aluminum alloys for specific applications. Optimizing parameters such as solution temperature, quenching rate, and aging conditions is essential to achieving desired strength, toughness and corrosion resistance.

Applying heat can alter the oxide layer's structure or composition, leading to its breakdown and removal. For aluminum, this process can help reduce its reactivity and improve corrosion resistance by minimizing the oxide layer on its surface. One effective heat treatment method is annealing, where aluminum is heated to a specific temperature and maintained at that level for a set period.[48] This facilitates recrystallization, reducing internal defects and dislocations within the material, thereby enhancing its overall properties.[48]

Another widely used technique is solution heat treatment followed by quenching. In this method, aluminum is heated to a high temperature, allowing alloying elements and impurities to dissolve uniformly. [58] The material is then rapidly cooled by immersing it in water or oil, which helps refine its microstructure.[59] This process not only enhances mechanical properties but also contributes to reducing the oxide layer on the surface, ultimately improving corrosion resistance.

Aging promotes the controlled precipitation of secondary phases, which strengthen the alloy by hindering dislocation movement. Aging can be:

- **Natural Aging (T4 condition):** Alloy is stored at room temperature, allowing the slow formation of Guinier-Preston (GP) zones, which increase strength over time.

- **Artificial Aging (T6 condition):** Alloy is heated to **120–200°C** for a controlled time to accelerate the precipitation of strengthening phases such as Mg_2Si (in 6xxx alloys) or Al_2Cu (in 2xxx alloys).[60]
- **Overaging (T7 condition):** Extended aging at higher temperatures leads to coarser precipitates, reducing peak strength but improving stress corrosion resistance.[61]

The choice of heat treatment method depends on the intended application and the specific characteristics desired in the aluminum material. Proper selection and execution of these processes ensure that aluminum maintains its strength, durability, and corrosion-resistant properties in various industrial applications. [62]

The heat treatment process significantly influences the microstructure and properties of aluminum alloys by altering their strength, ductility, and corrosion resistance. Precipitation hardening enhances strength and hardness by refining the size and distribution of precipitates, making the alloy more resistant to deformation. However, overaging can reduce strength while improving fracture toughness and stress corrosion resistance, making the material more durable under prolonged use. Additionally, certain heat treatments, such as the T7 temper, enhance corrosion resistance by stabilizing precipitates and minimizing susceptibility to intergranular corrosion.[63] Table 2.5 comprehensive overview of how different aluminum alloys respond to specific heat treatment processes, highlighting the resulting effects on their properties

Table 2.5 summarizing the effects of various heat treatments on different aluminum alloys.

Alloy	Heat Treatment	Heat Treatment Parameters	Effect on Properties	Reference
6061 Aluminum Alloy	Solution Treatment + Aging (T6)	Solution treatment at 529°C for 1, 3, and 5 hours; aging at 160°C	Enhanced mechanical properties; variations in quenching media (water and oil) affect hardness and fatigue resistance	[64]
7050 Aluminum Alloy	Solution Heat Treatment	Varying temperatures and times	Grain growth behavior; microhardness reduction with prolonged time and elevated temperature	[65]
AlSi7Mg Alloy	T6 Heat Treatment	Solution treatment and artificial aging	Improved tensile strength, elongation, and hardness;	[66]

		with optimized parameters	optimization reduces treatment duration	
2024 Aluminum Alloy	Quenching and Aging	Quenching at 495°C; aging for five days	Corrosion behavior and mechanical properties influenced; microstructural changes observed	[63]
Al–10Si–Mg Alloy	Air-Cooling Heat Treatment	Specific parameters not detailed	Elimination of Mg_2Si skeletal phase; impact on mechanical properties	[67]
EN AC-AlSi11(Fe) Alloy	T6 Heat Treatment	Solution treatment and artificial aging with varying temperatures and times	Positive effect on mechanical properties; microstructural changes observed	[68]
TiB_2/2024Al Composites	T4 and T3 Heat Treatments	Specific parameters not detailed	Anisotropic behavior; T4 shows good isotropy of yield strength; texture components weakened	[69]
6061 Aluminum Alloy	Precipitation Hardening	Solution treatment followed by aging	Increased yield strength due to formation of fine precipitates	[70]
Al–Li (8090) Alloy	Solution Treatment + Aging (T6)	Solution treatment at 530°C, water quench, aging at 150°C for 16 hours	Enhanced strength due to δ' (Al_3Li) precipitates; reduced density	[71]
Al–Mn (3003) Alloy	Annealing (O Temper)	Heating to 415°C, followed by slow cooling	Improved ductility and formability; reduced strength	[71]
Al–Si–Cu (4032) Alloy	Solution Treatment + Aging (T6)	Solution treatment at 500°C, quenching, aging at 170°C for 10 hours	Increased hardness and wear resistance due to Si and Cu precipitates	[71]
Al–Mg (5083) Alloy	Stabilization Anneal	Heating to 345°C, holding for 2 hours, air cooling	Stress relief; improved dimensional stability; maintains corrosion resistance	[71]

Al–Zn–Mg–Cu (7050) Alloy	Solution Treatment + Aging (T76)	Solution treatment at 475°C, quenching, two-step aging at 120°C and 160°C	Balanced strength and stress corrosion cracking resistance	[71]
Al–Cu–Li (2195) Alloy	Solution Treatment + Aging (T8)	Solution treatment at 530°C, cold work, aging at 155°C for 36 hours	High strength-to-weight ratio; improved fatigue resistance	[71]

Research studies continue to explore novel heat treatment techniques to further enhance the performance of aluminum alloys, particularly for aerospace, automotive, and structural applications. Understanding the relationship between alloy composition, heat treatment, and resulting properties remains essential for advancing material performance and expanding the potential applications of aluminum alloys in modern industries.

2.5.3 Cold Working

Cold working, also known as cold deformation or work hardening, involves the plastic deformation of metals at temperatures below their recrystallization point. This process not only augments the mechanical properties of aluminum alloys but also significantly influences their electrochemical behavior. Understanding the relationship between cold working and the electrochemical properties of aluminum alloys is crucial for optimizing their performance in specific environments. Several methods of cold working are commonly used, including:

- **Rolling** – Reduces the thickness of aluminum sheets by passing them between rollers.
- **Drawing** – Used to produce wires and tubes by pulling aluminum through a die.
- **Pressing and Forging** – Deforms aluminum alloys into desired shapes using compressive force.
- **Shot Peening** – Improves fatigue strength and corrosion resistance by introducing compressive stress on the surface.

Cold working can enhance or deteriorate corrosion resistance, depending on factors such as alloy composition, degree of deformation, and exposure conditions. It is widely used for disrupting the passivation layer on pure aluminium by introducing a high density of dislocations within the material. These dislocations act as nucleation sites for the initiation and growth of oxide films. Since the formation of an oxide layer serves as a protective barrier against corrosion, breaking this layer is essential for depassivation.[72]

When aluminum undergoes cold working, its surface experiences structural modifications, making it rougher and more chemically active. This increased reactivity facilitates the formation of oxide films more easily. Consequently, cold working not only alters the material's mechanical properties but also plays a significant role in regulating its surface behavior for applications where controlled oxidation is required.[36]

Cold working influences the corrosion resistance of aluminum alloys through several key mechanisms:

1) **Microstructural Modifications:** Plastic deformation introduces dislocations, grain refinement, and residual stresses, all of which can alter corrosion behavior. Grain boundaries, in particular, may act as preferential sites for localized corrosion.[73]

2) **Precipitation of Secondary Phases:** Certain alloying elements, such as magnesium (Mg) and copper (Cu), can form secondary phases due to cold working. The precipitation of phases like β-Al_3Mg_2 along grain boundaries increases susceptibility to intergranular corrosion and stress corrosion cracking.[74]

3) **Texture Formation:** Cold working can reorient grains, leading to electrochemical anisotropy, which affects corrosion behavior depending on the alloy and exposure environment.[73]

The impact of cold working on the electrochemical properties of aluminum alloys has been widely studied, particularly in applications such as sacrificial anodes and aluminum-air batteries. Various researchers have explored different cold working techniques, including rolling, uniaxial compression, and thickness reduction, to enhance the corrosion resistance and electrochemical efficiency of aluminum-based materials.

Panagopoulos C. et al. conducted a study on the impact of cold rolling on the electrochemical properties of 5083 aluminum alloy, which is widely utilized in marine and structural applications due to its excellent corrosion resistance. Their research investigated the effects of 7% and 15% cold rolling reductions in a 3.5% NaCl solution, revealing significant microstructural modifications. The cold rolling process resulted in grain refinement and an increase in secondary intermetallic phases. While these changes contributed to improved microhardness, they also facilitated the formation of galvanic cells between the aluminum matrix and intermetallic phases. This galvanic coupling, in turn, led to an increased susceptibility to localized corrosion, highlighting the trade-off between mechanical strengthening and corrosion resistance in cold-worked aluminum alloys.[75]

Mauro Quaresma Lobato et al. conducted a comparative study on aluminum alloys with zirconium (Zr) and magnesium (Mg) additions, focusing on the influence of cold working on their corrosion resistance. Their findings indicated that while cold working enhanced the alloy's mechanical strength, it also promoted the precipitation of the β-Al_3Mg_2 phase. The presence of this phase at grain boundaries increased the material’s susceptibility to pitting and intergranular corrosion, demonstrating a trade-off between mechanical performance and electrochemical stability.[76]

Wafa Taktak et al. investigated the effects of cold working on the 5754-aluminum alloy, which is widely used in automotive body panels. Their study revealed that plastic deformation influenced both the microstructural evolution and ductile fracture behavior of the alloy. While it maintained good overall corrosion resistance, the increase in dislocation density due to cold working created localized sites more prone to corrosion. These findings highlight the complex interplay between mechanical processing and electrochemical stability in aluminum alloys.[77]

Y. P. Asmara et al. investigated the effect of cold working on the efficiency of aluminum sacrificial anodes, commonly used for corrosion protection of carbon steel structures. The study highlights that cold working enhanced the electrochemical performance of the anodes by increasing corrosion rates and shifting corrosion potentials to more negative values, which improved their sacrificial function. Microstructural analysis revealed that cold work introduced higher dislocation densities, reducing passive oxide layer formation and enhancing anodic dissolution.[78]

Cold working emerges as a valuable technique for enhancing the electrochemical performance of aluminum alloys, particularly in corrosion protection applications. By introducing microstructural

modifications such as grain refinement, increased dislocation density and the precipitation of secondary phases, cold working significantly influences the corrosion behavior of Al-Mg alloys.

Cold working generally enhances strength and refines grain structures, it may also introduce localized corrosion susceptibility due to increased dislocation density and secondary phase formation. The selection of appropriate cold working parameters, in combination with post-processing treatments like annealing or heat treatment, is crucial for optimizing the performance of aluminium alloys for specific applications.

Table 2.6 Summary of Research on the Effects of Cold Working on Aluminum Alloy.

Researcher(s)	**Alloy Type**	**Cold Working Parameters**	**Effect of Cold Working**
Norafif et.al.[79]	Pure Aluminum Anodes	Rolling-type cold working, increasing deformation levels	Enhanced anode performance due to refined microstructure and increased internal stress
Harchegani et al. [80]	AA1100, AA7050 Aluminum	Cold working compared to annealed state	Negative corrosion potential observed, lower corrosion current density, improved electrochemical and anti-corrosion behavior
Asmara et al. [78]	Aluminum Sacrificial Anode	Reduction of thickness by 20% and 40%	Increased corrosion performance with lower corrosion potential in 3% NaCl environment
Boroujeny et al. [81]	Al-Zn-In Alloy	10-40% uniaxial compression followed by semi-solid treatment at 635-660°C for 40 minutes	Refined microstructure, enhanced anodic efficiency with 30% deformation and heat treatment at 650°C

Mistry et al.[82]	Al-Mg Alloy	Forging as cold working process	Enhanced sacrificial anode efficiency due to refined grain structure
Taktak et al.[77]	5754 Aluminum Alloy	Cold rolling	Altered ductile fracture behavior and increased localized corrosion sites

2.6 6XXX Series Aluminum Alloy

The 6XXX series aluminum alloys, primarily composed of aluminum, magnesium (Mg), and silicon (Si), are widely recognized for their excellent strength, corrosion resistance, and weldability. These alloys are extensively used in automotive, aerospace, and structural applications due to their balanced mechanical and electrochemical properties.[28] The presence of magnesium and silicon leads to the formation of Mg_2Si precipitates, which play a crucial role in age hardening.[83] The precipitation of these strengthening phases enhances the alloy's strength through heat treatment, particularly in T6 temper conditions. Unlike the 5XXX series, which relies on solid solution strengthening, the 6XXX series benefits from precipitation hardening, making them highly suitable for structural and load-bearing applications. The ability to undergo precipitation hardening makes them highly desirable for applications requiring enhanced strength while maintaining good formability.

The corrosion resistance of 6XXX series alloys is generally high due to the presence of a stable oxide layer. However, intergranular corrosion can occur due to the precipitation of Mg_2Si at grain boundaries, particularly in chloride-containing environments. Researchers have found that aging treatments can optimize corrosion resistance by controlling the distribution and size of precipitates. [84] Furthermore, surface treatments such as anodizing and alloy modifications with elements like Zn and Sn have been explored to improve electrochemical stability.

Polmear et al. investigated the precipitation behavior of Mg_2Si phases in 6061 aluminum alloy and observed that artificial aging at optimal temperatures significantly improved hardness and tensile strength. The study also highlighted that excessive aging leads to over-precipitation, reducing mechanical performance due to the coarsening of Mg_2Si particles.[58] Additionally, it was found that proper aging conditions improve corrosion resistance by limiting the formation of anodic phases that could trigger localized corrosion.

2.6.1 Al-Mg-Si Phase Diagram

The composition of 6XXX series aluminum alloys plays a crucial role in determining their mechanical and electrochemical properties. Factors such as microstructure, grain size, precipitate distribution, and crystallographic orientation significantly influence their overall performance.[85] These alloys are primarily composed of magnesium (Mg) and silicon (Si), making them heat-treatable. The maximum solubility of Mg in the aluminum matrix reaches approximately 16.26 atomic weight percent at 450°C, while Si exhibits a maximum solubility of 1.59 atomic weight percent at 1080°C.[35]

When Mg and Si are present together, they form Mg_2Si precipitates, which are distributed along the grain boundaries, enhancing the alloy's mechanical strength and corrosion resistance.[86] The phase diagram of Al-Mg-Si alloys illustrates in Figure 2.3 shows the solubility limits of Mg and Si as a function of temperature, highlighting the formation of the Mg_2Si phase. The maximum solubility of Mg_2Si in aluminum is 1.85%, but it decreases with increasing temperature, impacting the precipitation-hardening behavior of the alloy. [85]

The Al-Mg-Si phase diagram is essential in understanding the solidification behavior, phase stability, and precipitation characteristics of aluminum alloys containing magnesium (Mg) and silicon (Si). This system is particularly significant for 6XXX series aluminum alloys, which rely on precipitation hardening to enhance mechanical strength and corrosion resistance. The interaction between these three elements determines the formation of key phases such as Mg_2Si, which influences the alloy's hardness, ductility, and thermal stability.

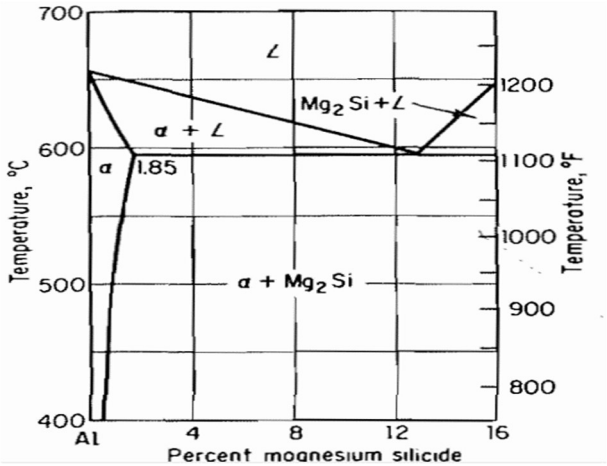

Figure 2.3 Aluminium- Magnesium Silicide Phase Diagram. [85]

The Al-Mg-Si phase diagram consists of several key phases that influence the properties of these alloys. The α-Al phase serves as the primary solid solution in which Mg and Si dissolve, contributing to solid solution strengthening.[58] The Mg_2Si phase acts as the main strengthening precipitate in 6XXX series alloys, forming during heat treatment to enhance hardness and strength through age hardening, with a maximum solubility of 1.85% at 450°C, decreasing as the temperature rises.[28] Additionally, the β phase exists as a metastable precursor to equilibrium Mg_2Si and plays a crucial role in strengthening T6 heat-treated aluminum alloys.[84] The Al_3Mg_2 intermetallic phase, which forms in high-magnesium alloys, can negatively impact corrosion resistance due to its tendency for selective dissolution.[87] Silicon-rich phases appear when excess Si is present, which may improve wear resistance but could reduce overall ductility.[88]

Increasing the magnesium (Mg) content in Al-Mg alloys from 5 to 10 mass% has been shown to improve sacrificial protection.[89] As the concentrations of both Mg and silicon (Si) rise, the anodic polarization curve shifts toward a more negative potential with a corresponding increase in current. This shift is attributed to the presence of Mg_2Si phase, which plays a key role in enhancing sacrificial protection. The effectiveness of this protection increases as the proportion of Mg and Si in the alloy grows[90]. Due to the low solubility of Si in Mg, most Si atoms react with Mg to form the Mg_2Si intermetallic compound through a diffusion-driven process.[91]

2.6.2 Electrochemical Behaviour of Mg_2Si

The Mg_2Si phase is composed of approximately 63.2% magnesium (Mg) and 36.8% silicon (Si) and crystallizes in a cubic structure with a lattice parameter ranging between 0.635 and 0.640 nm. This phase exhibits low solubility, has a density of 1.88 g/cm³, and melts at 1087°C. [85]

The potentiodynamic scanning curves and associated corrosion parameters for α-Al (aluminum matrix), Mg_2Si, and Si are presented in Figure 2.4 and Table 2.7. The results indicate that Mg_2Si has the most negative corrosion potential, while Si exhibits the most positive corrosion potential. Additionally, the corrosion current density of Mg_2Si is significantly higher compared to α-Al and Si, suggesting that Mg_2Si is more prone to corrosion in the initial stages of the process.[92]

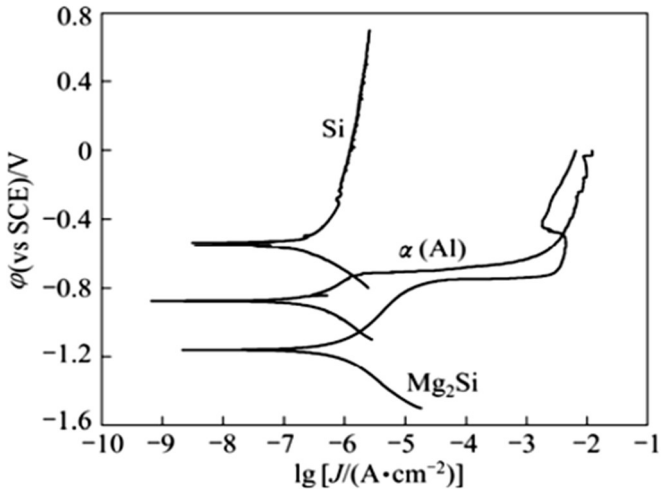

Figure 2.4 Potentiodynamic Scanning Curves of Individual A(Al), Si And Mg_2Si In 3.5% Nacl Solution At The Beginning.[92]

Similar findings were reported by Buchheit et al. where potentiodynamic polarization tests demonstrated that the corrosion potential of Mg_2Si is significantly reduced.[89][90] Investigations using Scanning Kelvin Probe Force Microscopy (SKPFM) revealed that the Volta potential of Mg_2Si particles is 100 to 180 mV lower than the surrounding aluminum matrix, indicating that Mg_2Si behaves anodically relative to aluminum.[93]These observations suggest that Mg_2Si particles serve as preferential anodic sites in corrosion reactions. [94]

Table 2.7 Corrosion parameters of α(Al), Mg_2Si and Si in 3.5% NaCl Solution at the beginning [93]

Phase	SCE (V)
α(Al)	-0.8761
Mg_2Si	-1.1598
Si	-0.5470

Birbilis et al. observed that the Mg_2Si phase exhibits a significantly lower potential compared to the 6XXX series aluminum matrix, which typically ranges from -0.72 V to -0.75 V vs. SCE.[95] Their research in a 0.1 mol/L NaCl solution also confirmed that Mg_2Si particles possess a significantly more negative corrosion potential compared to the aluminum matrix.

Furthermore, in regions with a high concentration of Mg_2Si particles, the open circuit potential (OCP) shifts to less negative values. This shift is attributed to the preferential dissolution of Mg from Mg_2Si in chloride environments, leading to the formation of SiO_2. As Mg dissolves, the

remaining particles become Si-enriched, making them more noble, which consequently shifts the OCP to a less negative value.[93]

2.6.3 Morphology of Mg_2Si

There are several different morphologies for the eutectic Mg_2Si in as-cast Al–Mg–Si alloys, as fig. 9. Various researchers reported typical morphologies such as lamellar, rod, crossed and rooftop-like, flake and curved. [[96] [97] [98] Figure 9, (a1) shows rod-like and intergranular lamellar Mg_2Si, (b1) shows lamellar Mg_2Si, (a2) shows flake like Mg_2Si while (b2) shows rod like[97] Mg_2Si morphology.

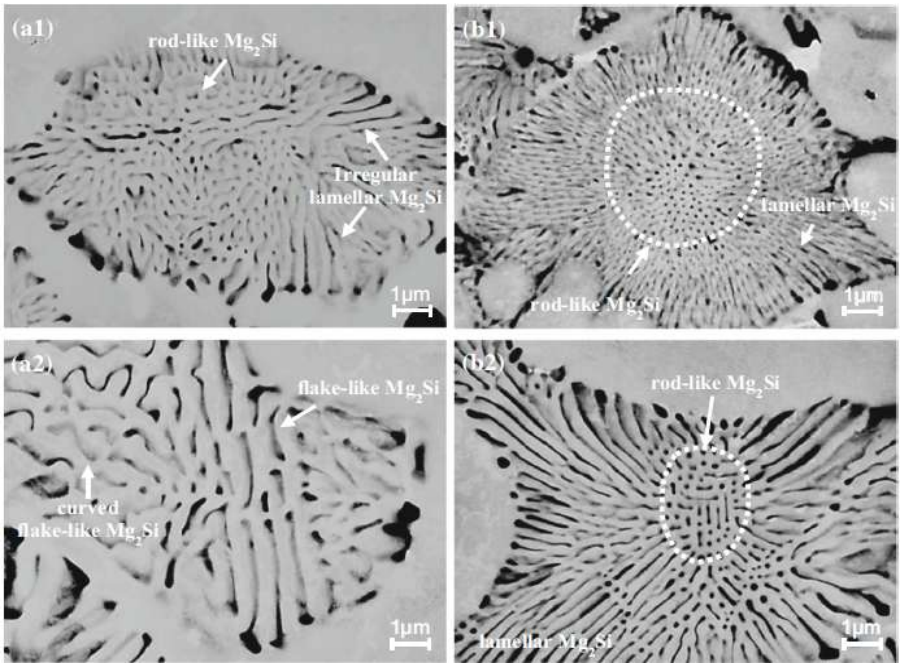

Figure 2.5 Difference Morphology of Mg_2Si Phase.[92]

Li C, et al. highlighted that the Mg_2Si phase in Al-Mg-Si alloys significantly influences their mechanical properties and performance.[99] This phase can take on different morphologies, which affect the alloy's strength, ductility, and toughness. The primary morphologies include coarse Chinese script structures, which tend to act as stress concentrators, leading to reduced ductility and toughness, and fine polygonal or spheroidal particles, which contribute to improved mechanical properties by enhancing both strength and ductility.

Zhang et al. (2022) emphasized that several factors influence the morphology of the Mg_2Si phase, with cooling rate being one of the most critical. A rapid cooling rate results in the formation of finer Mg_2Si particles, whereas slower cooling leads to coarser structures that are less desirable for mechanical performance. Liu et al. (2019) further explained that alloy composition plays a crucial role in shaping the Mg_2Si phase, and a well-balanced magnesium-to-silicon ratio promotes a more uniform dispersion of fine particles, leading to superior mechanical performance. Additionally, Ganesh M. et al. demonstrated that the addition of alloying elements such as strontium (Sr) modifies the morphology of the Mg_2Si phase.[100] Their study showed that Sr additions transform the Mg_2Si phase from a coarse Chinese script structure into a fine fibrous form, ultimately improving the alloy's mechanical properties.

Zhu X et al.reported that the morphology of Mg_2Si directly affects the mechanical behavior of Al-Mg-Si alloys.[101] Coarse Mg_2Si particles often serve as initiation sites for cracks, reducing the overall toughness and ductility of the alloy. In contrast, fine and uniformly distributed Mg_2Si particles act as effective barriers to dislocation movement without creating stress concentrations, thereby enhancing both strength and ductility. Therefore, controlling the morphology of the Mg_2Si phase through factors such as cooling rate, alloy composition, and modification with elements like Sr is essential for optimizing the properties of Al-Mg-Si alloys. A comprehensive understanding of these factors allows for the development of alloys with tailored mechanical properties to meet specific engineering requirements.

The morphology of Mg_2Si changes with the solidification rate, transitioning from a lamellar to a rod-like structure at higher cooling.[97] Li, et al. and Shimosaka et .al research indicates that the addition of certain alloying elements can also modify the morphology of the eutectic Mg_2Si phase.[102][103] Studies by Tebib and Farahany found that elements such as Sr and Bi altered the eutectic Mg_2Si structure from flake-like to fibrous, commonly referred to as "Chinese script-like" morphology.[104][105] Similarly, Li (2020) observed that an increase in Ni content transformed flake-like eutectic Mg_2Si into a rod-like structure.[99] Additionally, Nordin et.al discovered that the presence of Sb increased the irregularity of flake-like eutectic Mg_2Si, leading to the formation of a distinct divorced eutectic microstructure.[79]

2.7 Effect of Mg in Al-Mg-Si alloy

Magnesium (Mg) plays a crucial role in Al-Mg-Si alloys by influencing their microstructural characteristics and mechanical properties. According to Zhu et al, increasing Mg levels in these alloys affects the distribution of primary α-Al grains and Al-Mg_2Si eutectic phases, leading to a more uniform microstructure. A higher Mg concentration reduces the formation of coarse α-Al grains, which tend to accumulate in the center of cast samples, thereby decreasing microstructural inhomogeneity.[101] According to Zhu et al. (2018), increasing the Mg content in Al-Mg-Si alloys lowers the liquidus temperature, thereby suppressing the precipitation of coarse primary α-Al grains, which typically accumulate in the central region of the casting. This results in a more uniform microstructure, reducing inhomogeneity.

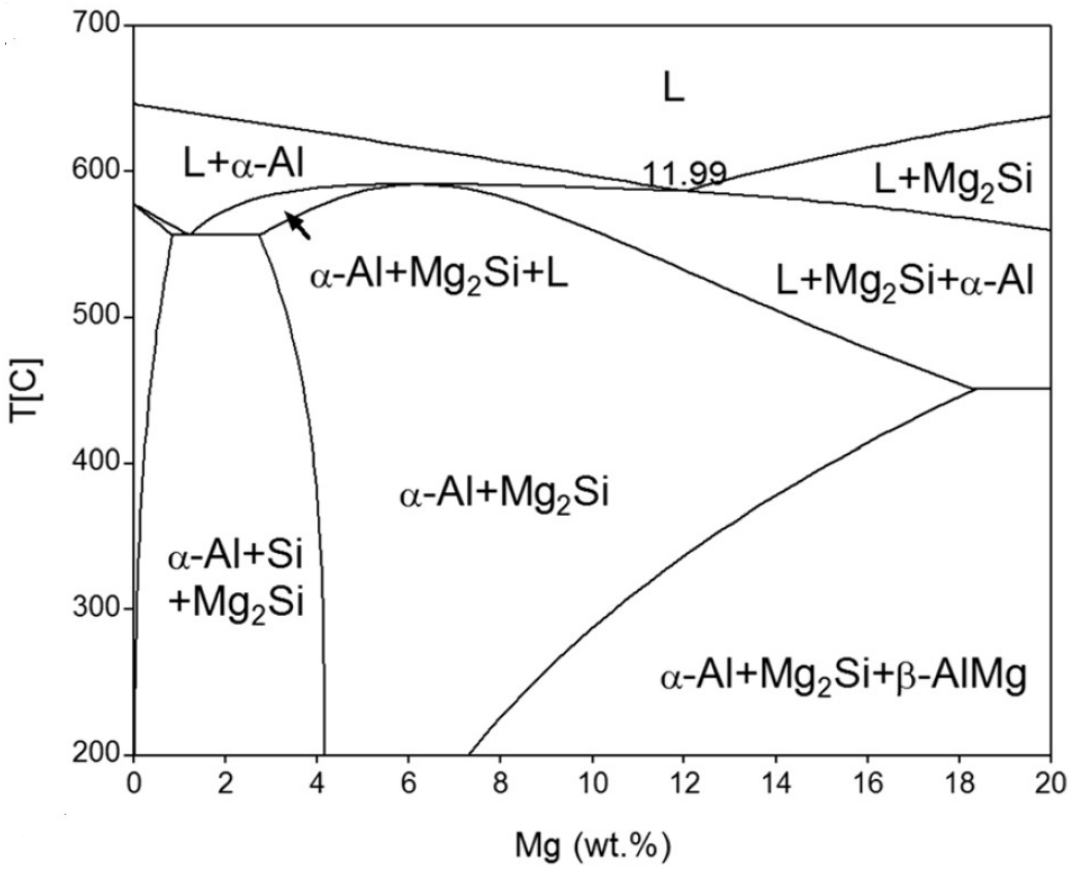

Figure 2.6 Calculated equilibrium phase diagrams of Al–Mg–Si alloys with varying Mg content.[101]

As Mg levels rise, the eutectic point shifts towards a lower Mg_2Si concentration, leading to a slower eutectic growth rate. Consequently, the volume fraction of Mg_2Si in the eutectic region decreases, transforming the eutectic Mg_2Si morphology from rod-like or lamellar structures into curved flake-like forms with increased eutectic spacing. This morphological change occurs due to the minimization of interfacial energy during solidification.

Moreover, at high Mg concentrations (above 9.6 wt.%), primary Mg_2Si particles begin to precipitate. These particles, which exhibit sharp-edged polyhedral shapes, tend to act as stress concentration sites, adversely affecting the alloy's mechanical performance. Additionally, increasing Mg levels enhances the strength of Al-Mg-Si alloys through solid solution strengthening and the formation of fine Mg_2Si precipitates that hinder dislocation movement. However, this improvement in strength comes at the expense of reduced ductility.

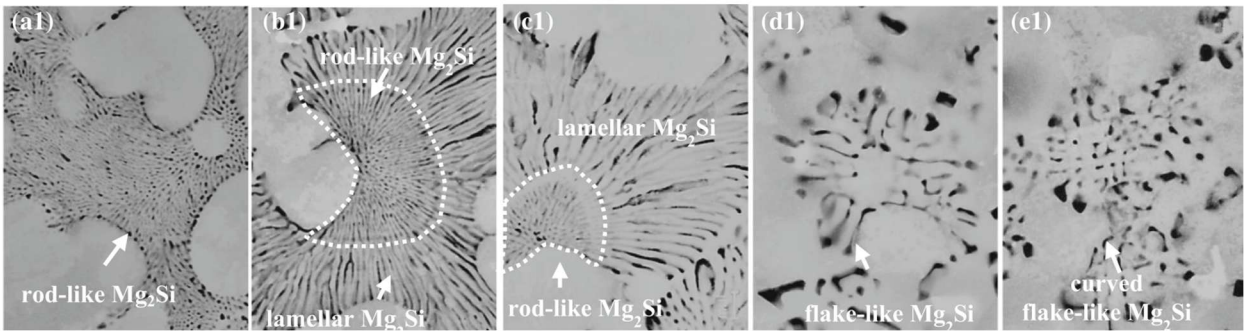

Figure 2.7 Effect of Mg on Morphology of Mg_2Si. [101]

The morphology of the eutectic Mg_2Si phase also changes with varying Mg levels. As Mg content increases, the eutectic Mg_2Si transforms from a rod-like or lamellar structure into a curved flake-like morphology with increased eutectic spacing as show in Figure 2.6. This transformation occurs due to the shift in the eutectic point towards a lower Mg_2Si concentration, which reduces the eutectic growth rate and results in a lower Mg_2Si volume fraction in the eutectic region. Despite these microstructural refinements, excessive Mg levels can lead to the precipitation of primary Mg_2Si particles, particularly at concentrations exceeding 9.6%. These primary Mg_2Si particles, which exhibit sharp-edged polyhedral shapes, can act as crack initiation sites, negatively impacting the alloy's mechanical properties. [101]

In terms of mechanical performance, increasing Mg content enhances the strength of Al-Mg-Si alloys but at the cost of reduced ductility as shown in Figure 2.7. The strengthening effect arises

from solid solution strengthening and the formation of fine Mg_2Si precipitates, which impede dislocation movement. However, the presence of coarse primary Mg_2Si particles in high-Mg alloys leads to premature fracture, lowering elongation and overall toughness. To balance strength and ductility, the Mg level should be carefully optimized to prevent excessive formation of primary Mg_2Si while still benefiting from the strengthening effects of eutectic Mg_2Si.[101]

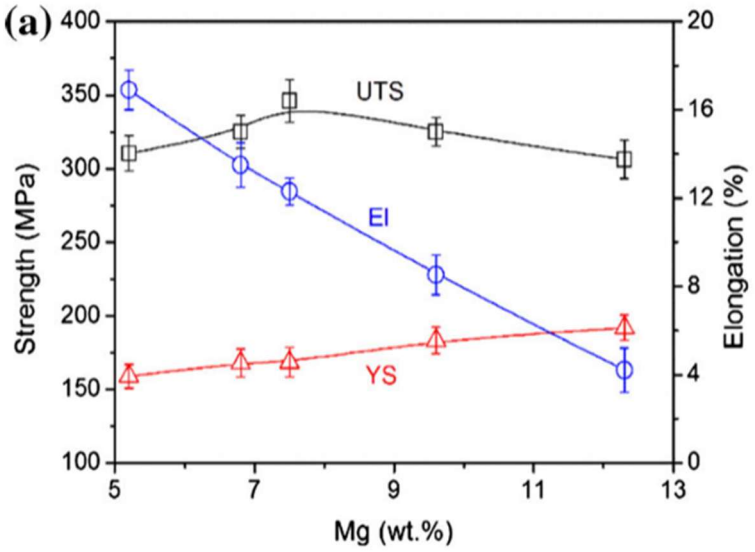

Figure 2.8 Effect of Mg on mechanical properties of Al-Mg-Si alloy. [101]

A study on Al-9Si-0.35Mn alloys revealed that adding up to 0.9 wt.% Mg increased strength but reduced ductility, primarily due to the formation of brittle intermetallic compounds and a slight increase in porosity.[106] A study demonstrated that increasing Mg levels improved the alloy's heat treatability and strength, although excessive Mg led to the formation of large, brittle intermetallics, reducing tensile strength and ductility.[107] Research indicates that an Mg/Si ratio of 2 offers high mechanical properties, with grain size analysis revealing that a ratio of 0.75 results in coarser grains and more spherical structures, which can affect the material's performance. [101]

2.8 Effect of Si in Al-Mg-Si alloy

Silicon (Si) has a significant impact on the phase diagram and microstructure of Al-Mg-Si alloys, affecting their solidification behavior and the morphology of the eutectic Mg_2Si phase. According to Zhu et al., increasing Si content reduces the liquidus temperature as shown in Figure 2.9, similar to magnesium (Mg), which helps in minimizing the formation of coarse primary α-Al grains. This leads to a more uniform microstructure and lowers inhomogeneity in die-cast alloys.[101]

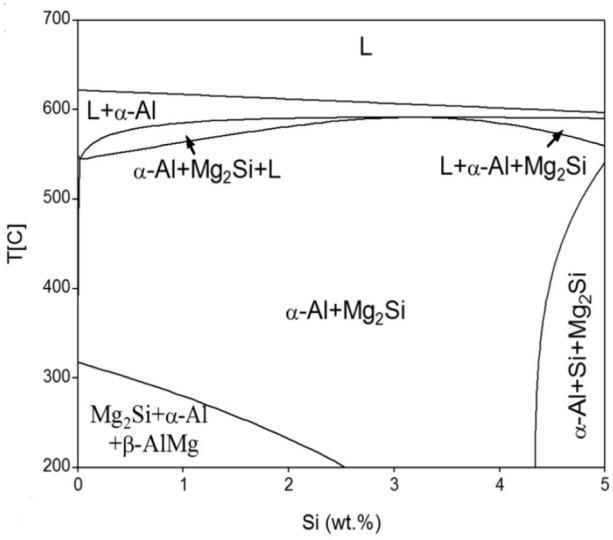

Figure 2.9 Calculated equilibrium phase diagrams of Al–Mg–Si alloys with varying Si content.[101]

Unlike Mg, which shifts the eutectic point to a lower Mg_2Si concentration and slows the eutectic growth rate, a higher Si content raises the Mg_2Si concentration in the eutectic region and accelerates its growth. Consequently, the fraction of Mg_2Si in the eutectic structure increases, refining the microstructure. The increasing Si content alters the shape and distribution of Mg_2Si, leading to a transition from a flake-like morphology to finer, more regular rod-like or lamellar structures as shown in Figure 2.10. This change encourages the development of rod-like or lamellar eutectic Mg_2Si with reduced eutectic spacing, in contrast to the flake-like morphology observed when Mg content is high.

Additionally, the presence of Si contributes to the strengthening of Al-Mg-Si alloys by increasing the volume fraction of Mg_2Si, which acts as a reinforcing phase. The finer and more uniform distribution of eutectic Mg_2Si helps achieve a better balance between strength and ductility.

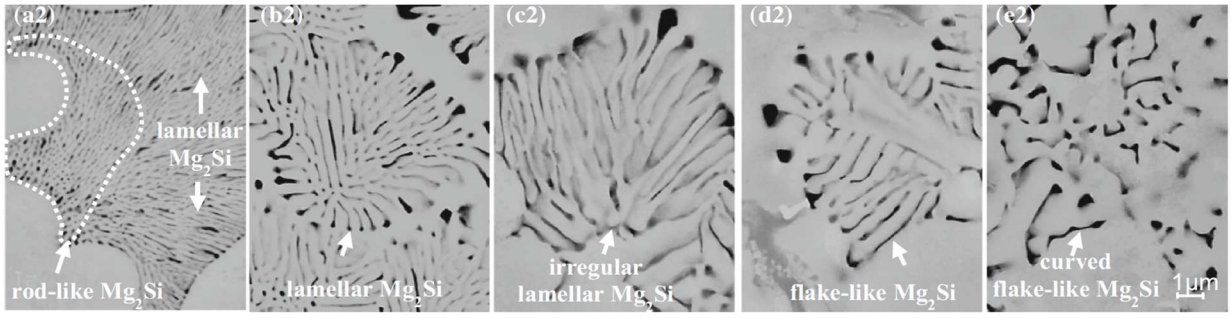

Figure 2.10 Effect of Mg on Morphology of Mg_2Si. [101]

Silicon (Si) content significantly influences the mechanical properties of Al-Mg-Si alloys. As Si levels increase, tensile strength improves notably; however, this enhancement is accompanied by a considerable reduction in elongation, indicating decreased ductility. Tensile tests revealed that Si increases both yield and ultimate tensile strength while causing a decrease in elongation. The study determined that for every 1 MPa increase in yield strength, Si addition results in a lower reduction in elongation (1.67%) compared to Mg addition (2.60%). [101]

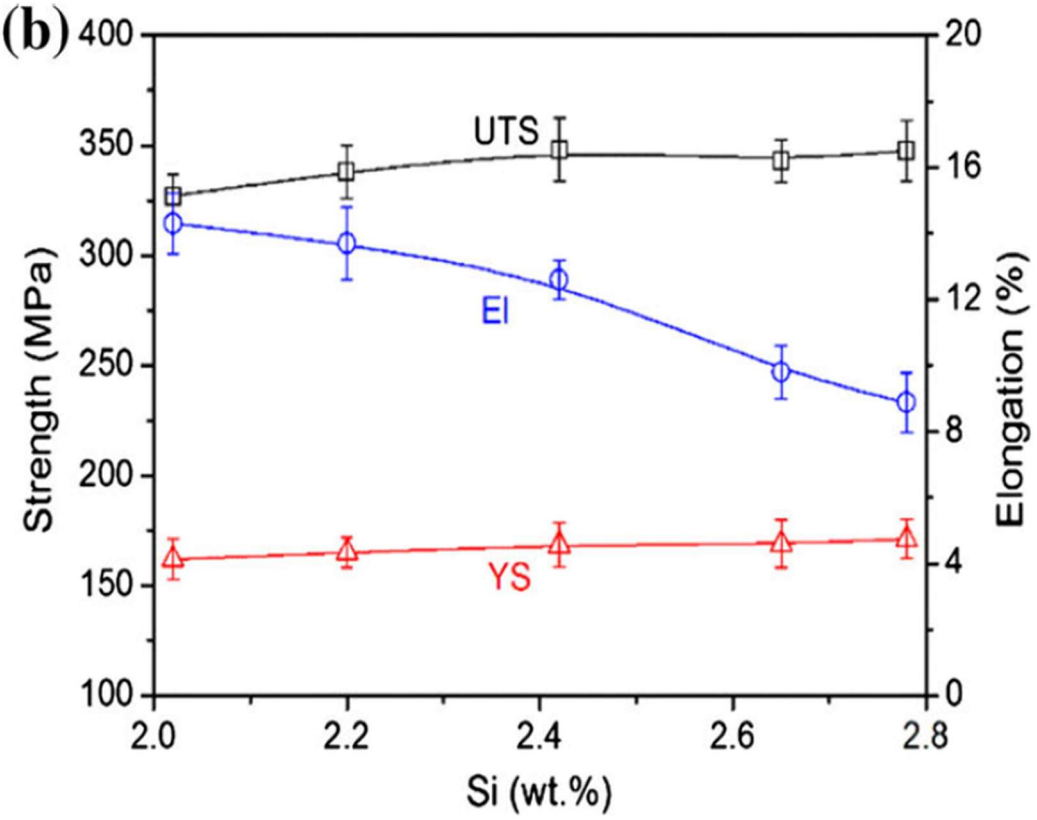

Figure 2.11 Effect of Mg on mechanical properties of Al-Mg-Si alloy. [101]

Hosch et. al found that refining eutectic Mg_2Si using Si enhances mechanical strength while reducing its adverse impact on elongation.[108] Similarly, Flemings et.al observed that higher Si levels result in a more compact eutectic structure, limiting defects that could otherwise weaken tensile properties.[109] Nordin et al. found that Si contributes to reducing microstructural inhomogeneity, further strengthening Al-Mg-Si alloys.[110]

2.9 Heat Treatment of Al-Mg-Si alloy

Al-Mg-Si alloys are heat-treatable and primarily undergo precipitation hardening, also known as age hardening, to modify their mechanical properties. This process relies on temperature-dependent changes in solubility, leading to the formation of fine secondary phase particles that hinder dislocation movement within the crystal structure. To facilitate precipitation, the alloy must be maintained at an elevated temperature for a specific period, a process referred to as aging. In age-hardenable aluminum alloys, aging at room or elevated temperatures results in the development of various precipitates within the matrix, contributing to enhanced strength.[111][112] However, the formation of these secondary phases, along with the presence of inclusions, introduces microstructural heterogeneity. This variation in microstructure leads to significant differences in corrosion potential between the matrix and intermetallic phases, allowing electron flow and accelerating anodic dissolution in the presence of an electrolyte.[101] The corrosion behavior of age-hardenable aluminum alloys evolves during the aging process, ranging from highly localized to more uniform corrosion, affecting different forms such as pitting, crevice, intergranular, and exfoliation corrosion.[101,113]

2.9.1 Precipitation Sequence During Aging of Al-Mg-Si Alloy

As Al-Mg-Si alloys undergo aging, they form metastable precursor phases before reaching the stable β (Mg_2Si) phase, following a complex precipitation sequence. The widely reported precipitation process for 6xxx series aluminum alloys typically progresses as follows:

SSSS (α) → GP zones → β″ (Mg_5Si_6) → β′ (Mg_9Si_5) → β (Mg_2Si, sTable)

Here, the supersaturated solid solution is represented by SSSS (α), while the metastable phases β″ (Mg_5Si_6), β′ (Mg_9Si_5), and equilibrium β (Mg_2Si) are associated with GP-zones. [[112][114][115][116]] Each phase differs in chemical composition, morphology, and crystal structure, as outlined in Table 2.8. These variations influence local chemistry and contribute to grain boundary degradation. In the peak-aged condition, the susceptibility of Al-Mg-Si alloys to intergranular corrosion (IGC) tends to increase with higher Si content due to enhanced precipitation along intergranular regions. Studies suggest that the primary cause of corrosion initiation is the significant potential difference between MgSi, Si particles, precipitate-free zones (PFZs), and solute-depleted regions, which promotes localized electrochemical activity.[113].

Table 2.8 Overview of precipitate phases in the Al-Mg-Si system

Precipitation Sequences	Composition	Morphology	Crystal structure	Reference
SSSS	Unknown	Point Defect	FCC	[117]
GP zone	Mg_xAl_5-xSi_6	Spherical Primarily	monoclinic	[118]
β″	Mg_5Si_6	Needles	Body cantered monoclinic	[119]
β′	$Mg_{1.8}Si$	Rods	Hexagonal	[120]
β	Mg_2Si	Plates or cubes	FCC	[118]

Research suggests that the susceptibility of Al-Mg-Si alloys to intergranular corrosion (IGC) increases with aging and reaches its peak at a specific hardness level. [85][89][93] This is primarily due to the formation of grain boundary precipitates during the aging process, which contribute to IGC vulnerability. The presence of microgalvanic cells at grain boundaries and the observed tendency for IGC suggest that these precipitates have a corrosion potential distinct from that of the matrix, leading to localized corrosion activity.[121] Additionally, slow quenching after solution heat treatment can enhance grain boundary precipitation, further increasing the risk of IGC.[117] However, overaging has been found to mitigate IGC susceptibility, though this comes at the expense of promoting pitting corrosion. Extended aging periods result in the growth and coarsening of precipitates. [122]

Heat treatment emerges as a pivotal metallurgical process that dramatically influences the alloys' microstructural evolution, mechanical performance, and electrochemical characteristics. Table 2.9 compiles data summarizing research findings from various research publication based on heat treatment of Al-Mg-Si alloy.

Table 2.9 Comparative Analysis of Heat Treatment Parameters and Their Effects on Al-Mg-Si Alloy properties.

Alloy Composition	Heat Treatment Type	Solution Treatment Temperature (°C)	Aging Temperature (°C)	Effect on Mechanical Properties	Electrochemical Properties	Reference
AA6061	T6	530-540	160-180	Increased yield strength (250-310 MPa). Improved hardness. Enhanced tensile strength	Reduced corrosion resistance. Increased pitting potential	Wang B et al. [123]
AA6082	T4	520-535	160-170	Improved formability. Moderate strength increase. Better ductility	Enhanced uniform corrosion resistance. Lower susceptibility to stress corrosion	El-Shennawy et.al [124]
Al-6Mg-1.2Si	Artificial Aging	540	180-200	Significant hardening. Peak strength at 180°C. Precipitation of β" phases	Improved localized corrosion resistance. Higher electrochemical stability	Pogatscher S et.al [125]

Al-5Mg-0.6Si	Interrupted Aging	525-535	150-170	Refined grain structure. Improved fatigue resistance. Balanced strength-ductility	Reduced galvanic corrosion potential. More stable passive film	Chen Y et.al.[126]
Commercial 6xxx Series	Optimized T6	535-545	175-185	Maximum hardness. Peak precipitation strengthening. Consistent mechanical properties	Moderate corrosion resistance. Controlled electrochemical behavior	Baruah M et al. [85]
Al-Mg-Si-Cu	Modified T6	510-525	170-190	Enhanced wear resistance Improved creep properties. Higher ultimate tensile strength	Complex electrochemical response. Improved pitting resistance	Shaha S et.al [127]
AA6063	Natural Aging	540-550	Room Temperature	Moderate initial strength. Gradual strength improvement. Good extrusion properties	Initial lower corrosion resistance. Self-healing passive film formation	Pratikno H et al.[128]
AA6082-T651	Overaging Treatment	540-550	200-220	Reduced peak strength. Improved ductility. Enhanced stress corrosion	More stable microstructure. Decreased susceptibility	Jangid Het. al. [129]

				cracking resistance	to localized corrosion	
Al-Mg-Si-Mn	Artificial aging	555	120	Fine precipitate distribution. Enhanced mechanical homogeneity. Improved yield strength	Uniform passive layer formation. Reduced electrochemical heterogeneity	Yin Z, et.al [130]
Al-6Mg-0.5Si-0.2Zr	Prolonged Aging	535-545	160-170 (Extended Time)	Sustained strength maintenance. Reduced precipitate coarsening. Improved long-term stability	Consistent corrosion behavior. Resistance to electrochemical degradation	Yin Z et.al [131]
AA6082 with Ce Addition	Modified Solution Treatment	530	180	Refined grain structure. Improved precipitation kinetics. Enhanced mechanical properties	Improved passive film characteristics. Reduced critical pitting potential	Vlach M et.al.[132]

The findings suggest that optimized solution treatment and aging processes significantly enhance hardness, tensile strength and corrosion properties. However, variations in alloy composition and heat treatment conditions lead to differing outcomes, emphasizing the need for further investigation.

2.10 Literature Related to Past Work

Liu S et.al investigates how varying silicon content influences the microstructure and mechanical properties of Al-Mg-Si-Zn alloys. The findings indicate that increasing silicon content enhances

tensile strength but reduces elongation due to changes in the crystalline structure.[133] Dwivedi D. et.al examines the combined effects of silicon content and heat treatment parameters on the mechanical properties of cast Al-Si-Mg alloys. Results show that higher silicon content, along with increased solution and aging temperatures, improves tensile strength.[134] Zhu X. et al. investigated the impact of varying magnesium and silicon levels on the microstructure and mechanical properties of Al-Mg-Si alloys. Their findings revealed that increasing the concentrations of these elements led to a more uniform distribution of primary α-Al and Al–Mg_2Si eutectics, thereby reducing microstructural inhomogeneity.[101] Maruyama N et.al analyzes effect of excess silicon in the pseudo-binary Al-Mg_2Si system which enhance the density of precipitates, thereby influencing the alloy's mechanical properties.[135]

The research by Kaygısız Y et.al demonstrates that T6 heat treatment (solution treatment at 530–550°C, followed by artificial aging at 160–180°C) reduces corrosion current density, indicating a lower corrosion rate and improved corrosion resistance. The study highlights that the aging process stabilizes precipitate phases, enhancing the electrochemical properties of the alloy.[136] El Garchani et.al explores the impact of artificial aging (T6 and T7 treatments) on the corrosion resistance of aluminum alloys. It suggests that aging at 150–200°C minimizes the size of corrosion products and refines the microstructure, leading to improved corrosion resistance. [63] Jang K et.al found that T6 heat treatment (solution treatment at 540–560°C, followed by aging at 155–180°C) optimizes mechanical properties and enhances corrosion resistance in Al-Si alloys. The findings indicate that prolonged aging may reduce susceptibility to pitting corrosion.[137] Jurczak Whighlights how different heat treatment parameters impact the mechanical and corrosion resistance of Al-Zn-Mg alloys. Solution heat treatment at 470–500°C and subsequent aging at 120–160°C are shown to refine the precipitate structure and improve corrosion performance.[138]

2.11 Research Gap

Based on the reviewed studies, there are still several unresolved aspects regarding the combined impact of alloy addition and heat treatment on the electrochemical properties of Al-Mg-Si alloys. The following key gaps are identifieds;

Research Gap 1: **Limited Understanding of Electrochemical Behavior**

While previous studies have explored the microstructural and mechanical effects of silicon addition, there is insufficient data on its influence on the electrochemical properties of Al-Mg-Si

alloys. The impact of silicon-induced phase formations on corrosion resistance requires further investigation.

Research Gap 2: Influence of Heat Treatment on Corrosion Mechanisms

Existing research primarily focuses on optimizing heat treatment parameters for mechanical strength enhancement. However, the correlation between different heat treatment conditions and the electrochemical stability of Al-Mg-Si alloys remains underexplored.

Research Gap 3: Optimizing Si Content for Electrochemical Performance

The influence of varying silicon levels on the corrosion behavior of Al-Mg-Si alloys has not been extensively analyzed. Identifying an ideal silicon composition that simultaneously enhances mechanical properties and corrosion properties is essential for improving the alloy's overall performance as sacrificial anode.

Research Gap 4: Synergistic Effects of Alloying and Heat Treatment

A combined effect silicon addition and heat treatment process to influence electrochemical properties is still lacking. Investigating how these factors interact can help establish optimized processing parameters to achieve superior electrochemical behavior of Al-Mg-Si alloy.

CHAPTER 3
EXPERIMENTAL WORK

3.1 Overview

This chapter outlines the materials and methods employed in the study. It details the raw materials used, casting procedures and furnace charge materials, along with the experimental setup. Additionally, it describes the experimental process, including the preparation of Al-Mg-Si alloys and the associated heat treatment procedures. The section further covers chemical analysis, mechanical property evaluations, microstructural examination, phase identification, corrosion rate assessment, anode efficiency measurement, and the analysis of corroded samples.

3.2 Materials and Methods

1.2.1 Raw Materials

This section provides an overview of the raw materials used in the study. The research utilizes commercially pure aluminum (99.7% wt%), silicon (99.9%), and magnesium (98.7%). Table 3-1 presents the chemical composition of these materials in terms of the weight percentages of Al, Mg, and Si. The commercially pure magnesium was sourced from C.K. Enterprise, Vadodara, while the aluminum wire, obtained from a GETCO High Tension Power contractor, has a high purity level of 99.7% with minimal impurities. Additionally, silicon was procured from Riddant Aluminium Pvt. Ltd., Sachin, Surat, ensuring the required composition for the study.

Table 3.1 Chemical composition of raw materials

	Al %	**Si %**	**Mg %**	**Fe %**	**Cu %**	**Mn %**	**Zn %**	**Ti %**	**Pb %**	**O %**
Aluminium wire	99.7	0.25	-	0.4	0.10	0.07	0.04	0.01	0.05	-
Silicon	0.005	99.9	-	0.01	-	-	-	0.001	-	0.02
Magnesium	-	-	98.8	-	-	-	-	-	-	1.24

Figure 3.1 shows an (a) aluminium wire (b) magnesium ingot, and c) silicon lumps. The aluminum wire used in this study contained trace impurities, including Cu, Si, Fe, Zn, Ti, Pb and Mn. These impurities may have influenced the material's properties and behavior during the research, making it important to acknowledge their presence. In contrast, the magnesium had a higher purity of

99.9% compared to the aluminum wire. Using high-purity materials is essential for ensuring accurate and reliable results, as impurities can alter material properties and impact the study's findings

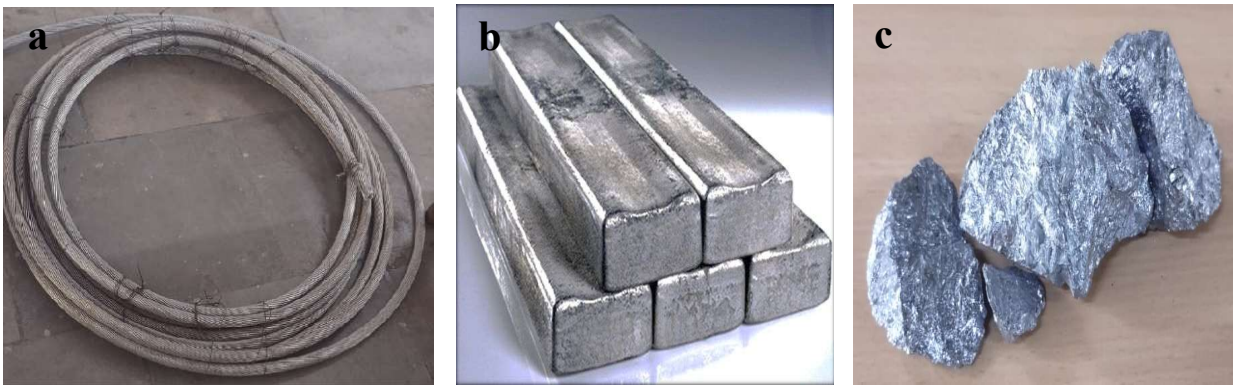

Aluminium wire **Magnesium ingot** **Silicon lumps**

Figure 3.1 (a) Aluminium wire, (b) Magnesium ingot, and (c) Silicon lump.

1.2.2 Casting of Al-Mg-Si Alloys

This section outlines the casting procedure used to produce the Al-Mg-Si alloy. The process begins with melting aluminum in an electric resistance furnace, followed by the addition of magnesium and silicon to the molten metal. The furnace temperature is maintained at approximately 820˚C to ensure complete melting. The casting process was conducted at the departmental facilities of Dr. S & S. S. Ghandhy College of Engineering & Technology, Surat, as shown in Figure 3.2.

Graphite crucibles and metallic dies are used for the melting process, both of which are thoroughly cleaned and dried beforehand to prevent contamination. The die used for casting is made of grey cast iron and consists of two halves. Molten metal is poured into the die, allowing it to solidify and form a rod-shaped casting. The dimensions of the die are illustrated in Figure 3.3.]

Figure 3.2 Electric Resistance Furnace at Dr. S & S. S. Ghandhy College of Engineering & Technology, Surat.

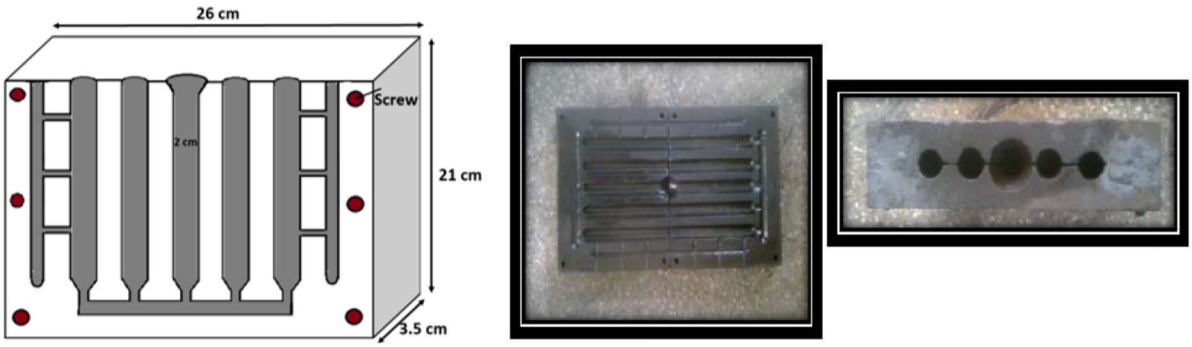

Figure 3.3 Metallic die.

During casting, magnesium and silicon are added to the molten aluminum in specific weight percentages. For the first composition, 6.5% magnesium by weight is introduced. In the other composition, 6.5% magnesium is combined with varying silicon concentrations of 1.5%, 3%, 4.5%, and 6% by weight. The molten mixture is continuously stirred to ensure uniform distribution of magnesium and silicon. Once thoroughly mixed, the alloy is poured into pre-designed metallic dies for solidification.

After pouring, the dies are left to cool at room temperature to allow the molten metal to solidify into rod-shaped castings. Once fully cooled, the rods are carefully removed using appropriate tools and inspected for any defects or irregularities. To achieve high-quality castings, it is essential to thoroughly clean and dry the crucibles and dies, as well as precisely measure and add the required amount of magnesium and silicon.

1.2.3 Alloying Materials and Charge Determination

The furnace charge calculation begins with determining the required quantity of raw materials to achieve the target alloy composition. The process follows a systematic approach, starting with defining the desired alloy composition. This involves selecting the appropriate proportion of magnesium to be combined with pure aluminium this study, five different alloy compositions have been selected, consisting of aluminum with 6.5% magnesium, while the silicon content varies from 0% to 6% in increments of 1.5%, as shown in Table 3.2.

Table 3.2 Summery of Designed Alloy

Sr. No.	Alloy Designation		Purpose Composition
	As cast	Heat Treated	
1	Base alloy (BA)	-	Al + 6.5% Mg
2	BA-1.5Si	BA-1.5Si – T6	Al + 6.5% Mg+ 1.5% Si
3	BA-3Si	BA-3Si – T6	Al + 6.5% Mg + 3%Si
4	BA-4.5Si	BA-4.5Si – T6	Al + 6.5% Mg+ 4.5%Si
5	BA-6Si	BA-6Si – T6	Al + 6.5% Mg + 6%Si

The next step is to determine the required amount of magnesium for each alloy composition. This is calculated using the following formula:

$$\text{Magnesium Quantity (g)} = (\text{Total Charge (g)} \times \%\ \text{Magnesium}) / 100$$

Similarly, for silicon addition, the amount needed for each composition is calculated using:

$$\text{Silicon Quantity (g)} = (\text{Total Charge (g)} \times \%\ \text{Silicon}) / 100$$

These calculation steps are repeated for silicon additions of 1.5%,3%, 4.5%, and 6%. Once the required amounts of aluminum, magnesium, and silicon for each alloy composition are determined, the next step is charge preparation. This involves accurately measuring the calculated quantities of each material and adding them to the furnace.

To proceed, the furnace is filled with weighted aluminum and heated to the target processing temperature of approximately 820˚C. Once this temperature is reached, magnesium is submerged into the molten aluminum and stirred with a stainless-steel rod to ensure uniform distribution. Afterward, silicon is added and the melt is allowed to homogenize for 30 minutes. After adding magnesium, drossing and degassing are essential to remove impurities from the molten mixture.

Once these processes are completed, the refined melt is ready to be poured into a metallic die. The molten metal is then allowed to cool and solidify within the die. After full solidification, the casting is removed as shown in Figure 3.4 and analyzed through various characterization techniques, including chemical composition assessment, mechanical property evaluation, and microstructural analysis etc.

Figure 3.4 Die Cast Al-Mg-Si Alloy.

3.3 Experimental Procedure

3.3.1 Die Casting of Designed Alloy

Commercially pure aluminum was placed in a graphite crucible and heated in an electric resistance furnace. The temperature was raised to 820°C to fully melt the aluminum. Once it molten, dross was removed and measured amounts of pure magnesium and silicon were added. The mixture was maintained at this temperature for 30 minutes to ensure thorough dissolution of the alloying elements. After the degassing carried out with chlorine Tablet, the molten alloy was poured into preheated metallic molds. All Al-6.5Mg-xSi alloys were produced using the same casting method as shown in Figure 3.5.

The chemical composition of the developed alloy is analyzed using Optical Emission Spectroscopy (OES). The mechanical properties, including hardness, are evaluated using appropriate testing techniques. To study the alloy's microstructure, metallographic preparation is carried out, followed

by analysis through optical microscopy. The identification of different phases and their elemental composition is performed using Energy-Dispersive Spectroscopy (EDS) and X-ray Diffraction (XRD). The detailed testing procedure for the developed alloys is illustrated in the Figure 3.6

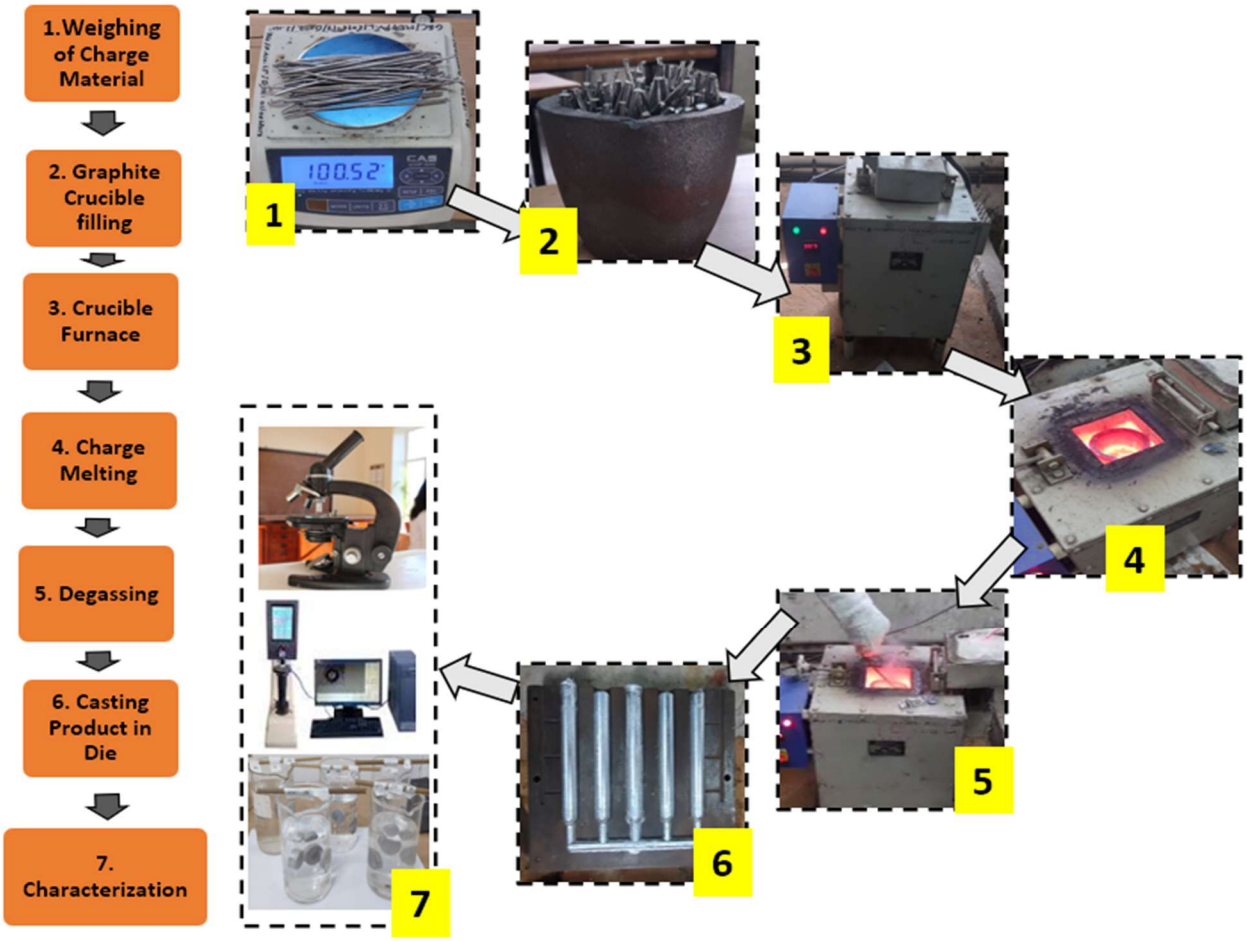

Figure 3.5 Procedure for development of Al-Mg-Si alloy casting.

The corrosion resistance of the alloy is assessed through standard weight loss methods and potentiodyamic studies in a 3.5% NaCl solution. Finally, the corroded samples are examined using Scanning Electron Microscopy (SEM) to evaluate the extent and characteristics of corrosion.

Anode performance measurement carried out as per DNV-RP-B401, involves evaluating the electrochemical efficiency (ε) of sacrificial anodes by calculating the ratio of the total electric charge transferred (Q) to the anode's mass loss (Δm), expressed in ampere-hours per kilogram (Ah/kg). Cylindrical test samples are extracted from manufactured anodes, thoroughly cleaned, weighed, and immersed in natural seawater for four days. After completion of the exposure period,

the anodes undergo cleaning and reweighing to determine mass loss, allowing for the calculation of electrochemical efficiency.

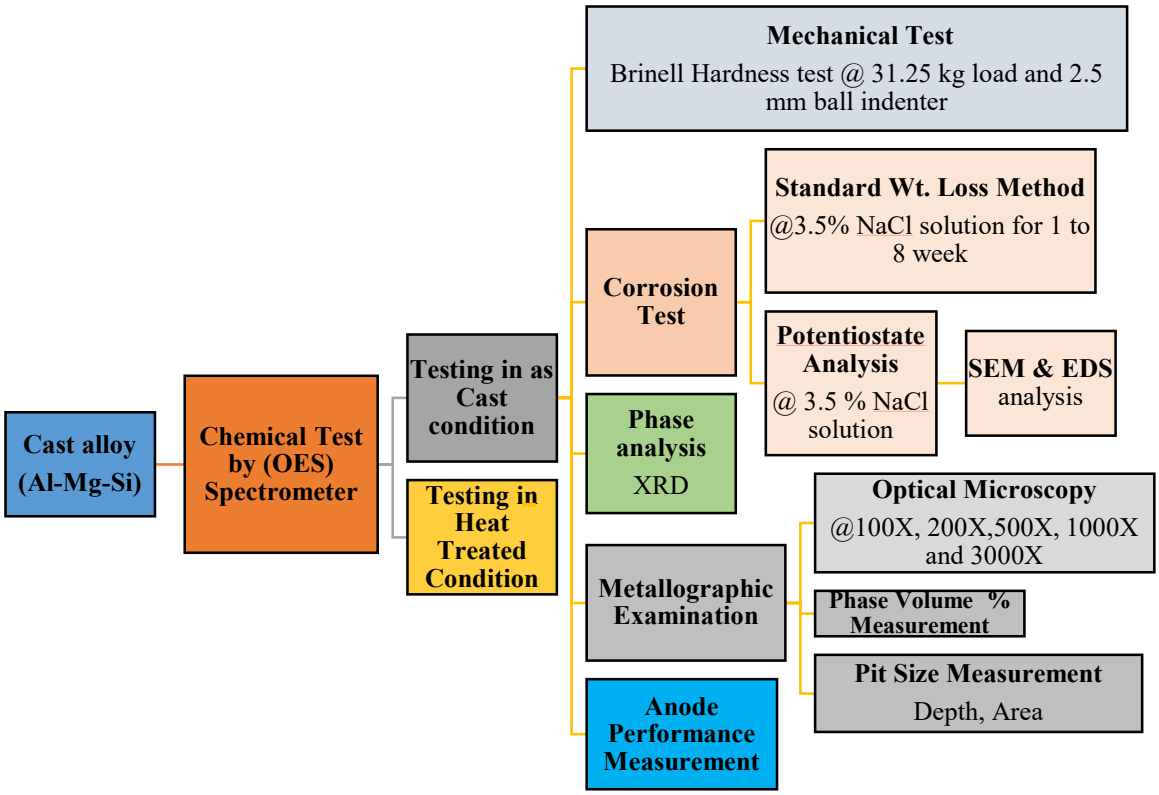

Figure 3.6 Detailed testing Plane for the experimental study.

3.3.2 Heat Treatment of Developed Alloys

The heat treatment process was conducted in the Muffle Furnace at the departmental facilities of Dr. S & S. S. Ghandhy College of Engineering & Technology, Surat as shown in Figure 3.7. The procedure involved solution treatment at 540°C for 1 hour, followed by water quenching to rapidly cool the material.

After quenching, the samples underwent aging treatment at 200°C for 4 hours, ensuring proper precipitation hardening. The final step involved air cooling, allowing controlled cooling to stabilize the material properties. The detailed heat treatment parameters are outlined in Table 3.3.

Figure 3.7 Muffle furnace at Dr. S & S. S. Ghandhy College of Engineering & Technology, Surat.

Table 3.3 Heat Treatment Parameters

Description	Parameters
SolutionTreatment Temperature	540 °C
Soaking Time	1 hr
Quenching Medium	Water Quench
Aging Temperature	200 °C
Soaking Time	4 hr
Quenching Medium	Air Cooling

The fabricated alloy is assessed for its mechanical properties, including hardness, using suitable testing techniques. Microstructural analysis is carried out through metallographic preparation and examination using optical microscopy.

The above heat-treatment schedule was successfully applied to all Al–6.5Mg–Si alloys. However, when the same solution-treatment condition (540°C for 1 h) was applied to the base Al–6.5Mg alloy (without silicon addition), severe surface oxidation was observed after solution treatment. Owing to this excessive oxidation, the specimen was considered unsuitable for subsequent ageing treatment and for reliable mechanical and corrosion characterization under identical heat-treatment conditions. Therefore, the heat-treated Al–6.5Mg control alloy was not included in the comparative investigation, whereas the as-cast Al–6.5Mg alloy was retained as the control sample throughout the study.

To evaluate the corrosion resistance, the alloy is immersed in a 3.5% NaCl solution and corrosion behavior is studied using the standard weight loss method and potentiodynamic analysis. Finally, the corroded samples undergo visual inspection and Scanning Electron Microscopy (SEM) analysis to examine surface modifications and microstructural changes resulting from the corrosion process.

3.4 Chemical Analysis

The chemical composition of the develop alloy was analyzed using the Bruker Q4 TASMANA, an advanced CCD-based optical emission spectrometer, at Aadhya Metal Testing, Baroda. This analysis followed the ASTM E1251:2017 standard, which outlines the procedure for examining aluminum and its alloys through spark-atomic emission spectrometry. [139] To begin the process, a cast rod sample was obtained and prepared by removing any surface impurities that could impact the accuracy of the results. Once cleaned, the sample was placed into the spectrometer's chamber, where a high-energy spark was generated on its surface to facilitate the chemical analysis.

The high-energy spark triggered the emission of light from the sample, which was then dispersed using a grating and captured by a CCD camera. This emitted light was analyzed to determine the chemical composition of the develop alloy, identifying the elements present and their respective concentrations. The acquired data was then compared against established reference standards to ensure the accuracy of the analysis. Overall, the ASTM E1251:2017 method is a reliable and widely used technique for the chemical analysis of aluminum and its alloys.

Figure 3.8 Optical Emission Spectroscopy.

3.5 Hardness Evaluation

Hardness, a key mechanical property associated with durability and strength, is measured by evaluating a material's resistance to indentation or penetration. The following steps outline the process for conducting hardness testing on an Al-Mg-Si alloy samples. First, a section of the developed alloy casting is cut using a suitable cutting tool. The sample is then thoroughly cleaned to remove any contaminants or surface irregularities. Next, a polishing machine equipped with 1200-grit paper is used to achieve a smooth and uniform surface. Once the polishing is complete, the sample is placed onto the Brinell hardness tester with 2.5 mm Ball indentor and a 31.25 kg load is applied in accordance with ASTM E10 Standard. [140] The load is maintained for 10 sec, to allow for proper indentation. After 10 sec, the load is removed and the indentation diameter is measured using a microscope or an optical measuring device. The measured indentation diameter is then used to calculate the hardness value of the aluminum alloy sample using the Brinell hardness formula and the obtained value is recorded. The Brinell hardness tester are shown in Figure 3.9.

Figure 3.9 Brinell Hardness tester at Dr.S &S.S.Ghandhy College of Engg. & Tech., Surat.

3.6 Microstructural Analysis and Phase Analysis

The preparation of metallographic samples for optical examination involves several sequential steps to ensure a representative and defect-free surface. First, sampling is carried out by carefully selecting a specimen from an appropriate region of the alloy so that its microstructure accurately reflects the bulk properties. The rod-shaped cast product is then cut into suitable dimensions, generally around 20 mm in diameter and 15 mm in height, using an automatic hacksaw cutting machine. Following this, grinding is performed to remove surface damage caused during sectioning. It begins with rough grinding using a an emery belt to produce a reasonably smooth surface and then progresses to fine grinding with silicon carbide abrasive papers of different grades (500–2000 grit) under wet conditions, where kerosene is used as a coolant and to wash away debris. The final step is polishing, which eliminates scratches from grinding and produces a flat, mirror-like surface suitable for microscopic analysis. Polishing is carried out on rotating wheels covered with quality polishing cloth, where a suspension of Al_2O_3 powder in distilled water is applied. For softer materials, polishing is performed at lower speeds to avoid surface distortion, ultimately yielding a smooth and reflective specimen surface. After polishing, the specimen is subjected to etching using Keller's solution (190 ml Distilled water, 5ml Nitric acid, 3 ml Hydrochloric acid, 2 ml hydrofluoric acid) for about 10 seconds to reveal its microstructural features. Once etched, the sample is carefully rinsed with water, air-dried for approximately 30 seconds, and then examined under Olympus DSX1000 Digital Microscope as well as a JEOL JSM 7900F scanning electron microscope (SEM) equipped with energy dispersive spectroscopy (EDS) for microstructural and compositional analysis at different magnifications as shown in Figure 3.10. Quantitative evaluation of phase volume fraction was performed using the Metal 11.1 image analysis system connected to a Radical optical microscope.

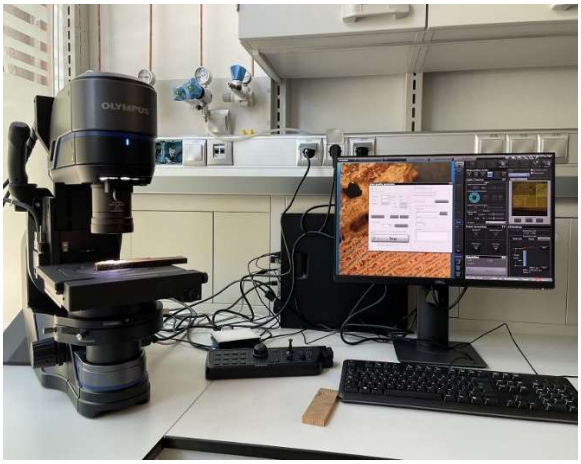

a) Olympus DSX1000 Digital Microscope

b) JEOL JSM 7900F scanning electron microscope (SEM) at IIT Gandhinagar

C) X-ray diffraction (XRD) on a Pan Analytical X'pert Pro system at MSU, Baroda.

Figure 3.10 Experimental set up for Microscopy, SEM and XRD analysis.

To identify the crystalline phases present in the alloy, X-ray diffraction (XRD) analysis was conducted using a *Panalytical X'Pert Pro* diffractometer at Maharaja Sayajirao University, Baroda (Figure 3.10). Prior to X-ray diffraction (XRD) analysis, the PANalytical X'Pert PRO diffractometer was calibrated using a standard silicon carbide (SiC) reference sample supplied by PANalytical in accordance with the manufacturer's recommended calibration procedure. The calibration was performed to verify the instrument alignment and ensure the accuracy of diffraction peak positions before data acquisition. All diffraction patterns were subsequently recorded under the calibrated instrument conditions. The equipment used a copper anode as the radiation source, producing Cu Kα radiation with a wavelength of 1.54060 Å, which is standard for phase

identification. The test specimen was prepared in cylindrical form (20 mm diameter, 2 mm thickness). Prior to testing, its surface was sequentially ground with silicon carbide papers of 500–2000 grit and subsequently polished on a cloth using an alumina suspension in distilled water. The polished sample was then placed in the sample holder for analysis.

The instrument was powered on and allowed to stabilize for nearly 30 minutes before measurement. After proper alignment of the specimen with the X-ray beam, the diffraction scan was carried out for 2–10 minutes, depending on the chosen parameters. Interaction of the X-rays with the atomic planes of the alloy produced characteristic diffraction peaks, which were recorded by the system's detector.

The collected data were analyzed with specialized software, where diffraction peaks were matched with standard reference patterns for phase identification. This confirmed the presence of the expected phases and provided valuable information regarding the alloy's crystallographic structure and microstructural features.

3.7 Corrosion Behavior Study

To investigate the corrosion resistance of the developed Al–Mg-Si alloy, two established techniques were employed: weight loss analysis and potentiodyanamic polarization.

The weight loss method provides a straightforward and cost-effective approach to quantify corrosion rate. Here, alloy samples are exposed to a corrosive medium for a specific duration. After exposure, the specimens are cleaned, dried, and weighed to determine the mass loss. The corrosion rate is then calculated based on the reduction in weight relative to the exposed surface area and exposure time. This method, though simple, delivers reliable long-term corrosion data and serves as a validation tool for electrochemical results.

Potentiodyanamic polarization is a widely used electrochemical method for understanding corrosion behavior. In this technique, the alloy specimen is immersed in an electrolyte and the variation of current response with applied potential is continuously monitored. The resulting polarization curves reveal important parameters such as corrosion potential (Ecorr) and corrosion current density (Icorr), which serve as indicators of corrosion tendency and rate.

3.7.1 Standard weight loss method

The corrosion behavior of the developed Al–Mg-Si based alloys was evaluated using the standard weight-loss technique, following the procedure outlined in ASTM G1-03 (2017). The experimental work was carried out in the Metallurgy department, Dr. S & S.S.Ghandhy College of Engineering & Technology, Surat, Gujarat as shown in Figure 3.11.

Figure 3.11 Experimental set up for standard weight loss method.

For the test, cylindrical specimens of 20 mm diameter and 10 mm height were prepared. To ensure uniformity and minimize surface irregularities, each sample was ground with 500 and 1000-grit emery paper to obtain a smooth finish. The initial weights of the specimens were measured with a four-digit precision analytical balance before immersion. The corrosion medium consisted of a 3.5 wt% NaCl solution, prepared by dissolving 3.5 g of sodium chloride powder in 100 ml of water. This solution was selected to simulate a chloride-rich environment similar to seawater. Three specimens from each alloy composition were used, and the average value was considered for corrosion rate determination to improve accuracy and minimize random error.

All the samples were completely immersed in the NaCl solution for a total duration of eight weeks. At the end of each weekly interval, a specimen from each set was removed from the corrosive medium. The retrieved specimens were thoroughly rinsed with distilled water, cleaned with acetone to remove residual contaminants, air-dried and finally reweighed using the analytical balance. The loss in weight of the specimens was recorded at each stage. The corrosion rate was calculated using the standard formula given in ASTM G1-03 (2017):

$$\text{Corrosion Rate (MPY)} = \frac{534W}{D\,A\,T}$$

Where:

W = Weight loss of the sample (g)
D = Density of the alloy (g/cm³)
A = Exposed surface area (in²)
T = Exposure time (h)

3.7.2 Potentiodynamic Polarization Study

The objective of this experiment was to determine the corrosion potential (*E*corr) and corrosion current density (*I*corr) of the developed alloy using a Gamry Reference 600 potentiostate, following the guidelines of ASTM G5 as shown in Figure 3.12.

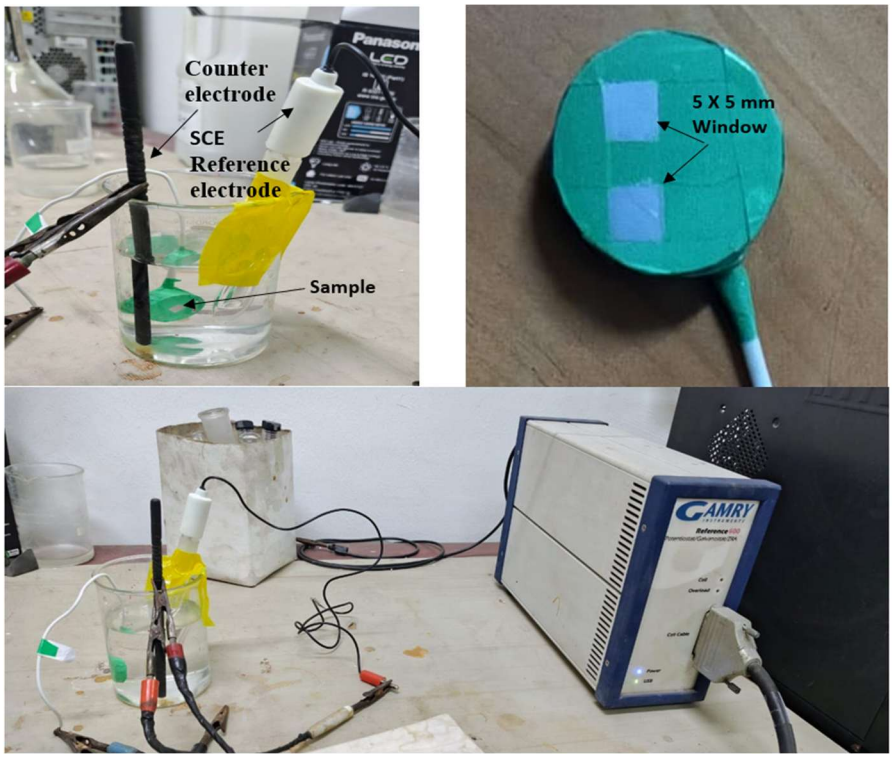

Figure 3.12 Experimental setup for potentiodynamic polarization.

For this purpose, cylindrical specimens measuring 10 mm in height and 20 mm in diameter were prepared (Figure 3.12). The potentiodynamic study was carried out in a three-electrode electrochemical cell configuration, where the alloy specimen acted as the working electrode, graphite served as the counter electrode, and a saturated calomel electrode (SCE) was used as the reference electrode. The corrosive medium consisted of a 3.5 wt% NaCl solution, and the exposed surface area of the specimen was restricted to a 5 × 5 mm window to maintain uniform testing conditions.

Prior to testing, the working electrode surface was carefully cleaned to eliminate any contaminants or oxide films that could interfere with the measurements. The specimen was then mounted in the working electrode holder and connected to the potentiostat along with the counter and reference electrodes.

The polarization study was performed by gradually varying the potential of the working electrode at a constant scan rate, sweeping from a negative value toward a positive value. During this process, the corresponding current response of the alloy was recorded, generating a polarization curve. From this curve, the corrosion potential (Ecorr) and corrosion current density (Icorr) were obtained, which are critical parameters for evaluating corrosion resistance.

3.8 Examination of Corrosion-Induced Surface Degradation

The evaluation of corroded specimens can initially be carried out through visual inspection, which offers a simple yet effective method to assess surface degradation. In this approach, the alloy surface is carefully examined for any visible signs of corrosion damage, either directly by the naked eye or with the aid of magnifying tools. Before inspection, the samples are cleaned to remove loose corrosion products and contaminants. The corroded surfaces are then scrutinized for features such as pitting and oxide film breakdown etc. These observations provide valuable information regarding the severity and nature of corrosion. Moreover, the type of corrosion detected often reflects the environmental exposure conditions, the alloy's chemical composition and potential factors contributing to corrosion initiation and progression.

To gain a more detailed understanding of the corrosion mechanism, scanning electron microscopy (SEM) was employed. SEM is a powerful characterization tool that generates high-resolution images of the material's surface, enabling the identification of microstructural features and localized corrosion damage. The corroded alloy samples were analyzed using SEM to observe the formation of pits, cracks, and surface deposits such as oxides and salts. In addition to morphology, SEM also provides elemental composition data of the corroded regions, revealing the presence of alloying elements, impurities, and corrosion products. Such detailed information assists in identifying the type of corrosion (e.g., pitting, uniform, or localized attack) and in understanding the underlying corrosion mechanisms.

3.9 Assessment of Anode Performance

The performance of sacrificial anodes was evaluated in accordance with DNV RP B401 guidelines to determine anode efficiency and consumption characteristics.[141] The experimental methodology involved preparation of test solutions, sample conditioning, current application, monitoring, and post-test analysis.

3.9.1 Preparation of Electrolyte and Equipment

A mild steel vessel containing 11 liters of natural seawater was used as the electrolyte medium. The coulometer solution was prepared following ASTM G97 standards, consisting of $CuSO_4$, $5H_2O$ (25 g), H_2SO_4 (27 ml), and ethyl/methyl alcohol (50 ml) in 900 ml distilled water. [142]

Figure 3.13 Experimental set up: MS vessel fills with electrolyte and specimen.

- **Anode Cleaning Solution**:

  Before test: methanol was used for surface cleaning.

  After test: a mixture of chromium trioxide (20 g) and phosphoric acid (30 ml per liter of water) was applied to remove corrosion products and deposits.

- **Test Setup**

  The prepared anode sample was placed in the coulometer setup as specified in DNV RP B401. An ammeter and variable resistance were connected in series with the specimen to regulate and measure current. The surface area of the cylindrical anode was calculated to normalize current density.

- **Current Application:**

  The test procedure involved applying current densities in four sequential stages:

- 1.5 mA/cm² × surface area
- 0.4 mA/cm² × surface area
- 4 mA/cm² × surface area
- 15 mA/cm² × surface area

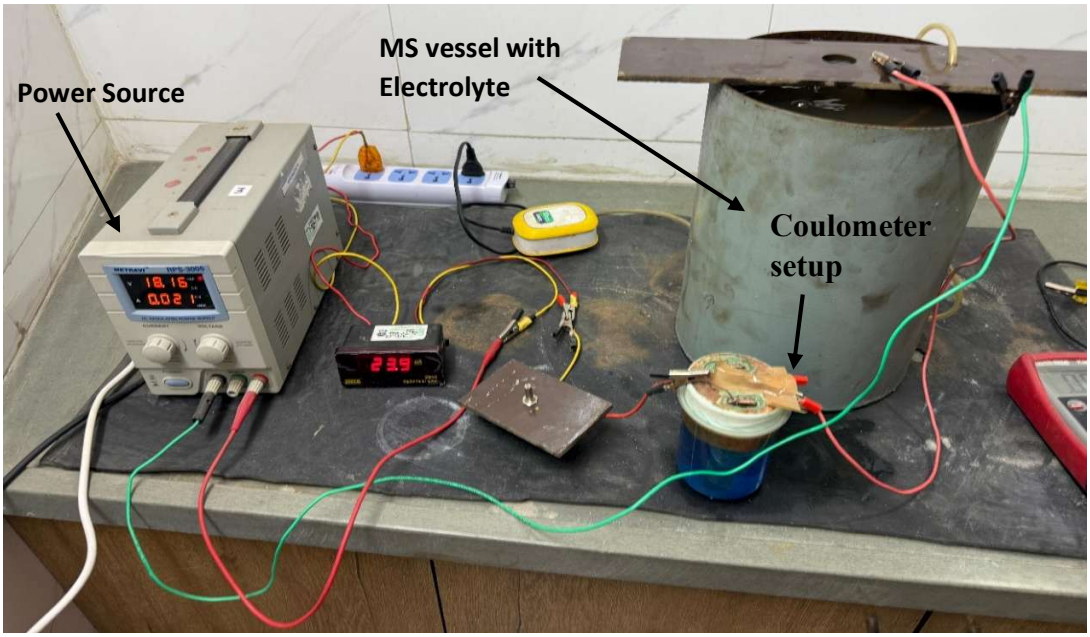

Figure 3.14 Experimental Set up for anode performance measurement as per DNV RP B401.

Each current density was maintained for 24 ± 1 hours daily, while continuously purging the electrolyte with air to prevent stagnation. The cycle was repeated for four consecutive days.

- **Monitoring and Measurement:**

  Open circuit and closed circuit potentials were measured immediately after applying current, and the current output was logged at four intervals daily (10:00 am, 1:00 pm, 4:00 pm, and 7:00 pm).

- **Post-Test Analysis**

  On the fourth day, the copper wire was removed and the sample was cleaned with the specified post-test solution to eliminate corrosion residues. The specimens were then dried and the final weight was recorded to calculate the consumption rate.

- **Performance Evaluation Parameters**

  The efficiency and reliability of sacrificial anodes were assessed by deriving key performance parameters from the experimental data. These parameters provided quantitative

insight into material consumption, electrochemical activity, and anodic behavior under simulated service conditions.

- **Consumption Rate (kg/A·yr)** This parameter represents the rate at which the anode material is consumed when delivering protective current. It is expressed in kilograms of anode material lost per ampere-year of service. A lower consumption rate indicates higher durability and longer service life of the anode under given operating conditions.
- **Current Capacity (Ah/kg)** Current capacity defines the total charge delivered per unit mass of anode consumed, measured in ampere-hours per kilogram. This value reflects the efficiency with which the anode material is converted into useful protective current. A higher current capacity corresponds to better utilization of the anode material, thereby improving cost-effectiveness and sustainability of the protection system.
- **Potential Measurements (V)** Both closed-circuit potential (CCP) and open-circuit potential (OCP) were recorded during the tests. OCP provides information about the natural electrochemical tendency of the anode in seawater, while CCP reflects the potential of the anode when delivering current to the system. These measurements are essential in determining the driving voltage available for cathodic protection and in assessing the stability of the anode under operating conditions.

Collectively, these parameters enable a comprehensive evaluation of sacrificial anode performance. They serve as critical indicators for predicting service life, ensuring adequate current delivery, and verifying compliance with international cathodic protection standards such as DNV RP B401.

3.10 Summary

This chapter presented the experimental procedures carried out to prepare and evaluate the Al–Mg alloy modified with silicon. The study comprised a series of characterizations, including chemical composition analysis, mechanical testing, microstructural examination, phase identification, corrosion evaluation, and anode performance assessment.

The experimental sequence began with a detailed description of the raw materials, charge calculations, alloy casting, and experimental setup, followed by the heat treatment procedure applied to the Al–Mg–Si alloys. Mechanical behavior was determined through hardness testing,

while the alloy's microstructure was investigated using optical microscopy (OM) and scanning electron microscopy (SEM). For phase identification, both energy-dispersive X-ray spectroscopy (EDS) and X-ray diffraction (XRD) were employed.

The corrosion performance of the alloys was evaluated using two approaches: potentiodynamic polarization studies and the standard weight-loss method, with post-corrosion analysis conducted through visual inspection and SEM observation. Furthermore, the anode performance of the developed alloys was examined in accordance with DNV RP B401 guidelines, where both the consumption rate and anode capacity were measured.

CHAPTER 4
RESULTS & DISCUSSION

4.1 Introduction

This chapter investigates the compositional changes in Al-Mg alloys arising from the addition of silicon to the alloy matrix. The chemical composition was determined using optical emission spectroscopy (OES), and the corresponding results are presented and discussed. To assess the effect of silicon content in combination with heat treatment, hardness measurements were performed. The findings from these analyses are presented in detail and critically interpreted in the following sections.

4.2 Effect of Silicon Addition on the Composition of Aluminum Alloys

The changes in alloy composition with varying silicon content were determined through optical emission spectroscopy (OES), and the results are summarized in Table 4.1. The analysis clearly demonstrates that the addition of silicon significantly alters the overall chemical balance of the Al–Mg system.

Table 4.1 Chemical composition of Al–6.5%Mg alloys with varying Si additions (wt.%) determined by OES.

Alloy / Elements	Alloy Identification	Mg %	Si %	Fe %	Cu %	Mn %	Zn %	Ti %	Pb %	Al %
Base Alloy-(Al6.5%Mg)	**BA**	6.47	0.25	0.47	0.11	0.06	0.04	0.01	0.06	92.48
(Al6.5Mg–1.5%Si)	**BA-1.5Si**	6.71	1.61	0.47	0.10	0.06	0.03	0.012	0.05	90.89
(Al6.5Mg–3%Si)	**BA-3Si**	6.76	3.03	0.47	0.09	0.05	0.04	0.011	0.04	89.43
(Al6.5Mg–4.5%Si)	**BA-4.5Si**	6.63	4.41	0.50	0.11	0.06	0.09	0.016	0.06	88.02
(Al6.5Mg–6%Si)	**BA-6Si**	6.76	5.61	0.54	0.11	0.06	0.03	0.014	0.06	86.70

Optical emission spectroscopy (OES) confirmed that the target silicon additions were successfully incorporated into the Al–6.5%Mg alloy system. The measured Si concentrations-1.61%, 3.03%, 4.41%, and 5.61% for alloys A through D, respectively show excellent agreement with the intended

levels of 1.5, 3.0, 4.5, and 6.0 wt.%. This close correlation validates the accuracy of the alloying procedure and demonstrates effective silicon integration into the matrix.

The magnesium content remained highly consistent across all alloy variants, with values ranging narrowly between 6.63% and 6.76%. Such stability suggests that the introduction of silicon does not significantly alter the bulk magnesium concentration, although a fraction of Mg is likely consumed in the formation of Mg_2Si intermetallic compounds.

As expected, the aluminum fraction progressively decreased with increasing silicon addition, declining from 92.48% in the base composition to 86.70% in the alloy containing 6% Si. This trend reflects the substitutional nature of alloying, wherein added silicon partially replaces aluminum within the matrix.

Trace elements, including Fe, Cu, Mn, Zn, Ti, and Pb, were also detected in minor concentrations across all compositions. Their levels exhibited slight variations with silicon addition. The measured silicon concentrations are sufficient to promote the formation of Mg_2Si intermetallic phases, which are known to exert a strong influence on microstructural evolution and mechanical response.

4.3 Effect of Silicon Addition on the Microstructure of Aluminum Alloys

4.3.1 Microstructural Evolution of As-Cast Al-Mg-Si Alloys

The microstructural evolution of the investigated aluminum-magnesium-silicon alloys is primarily governed by the phase equilibria of the Al-Mg binary and Al-Mg-Si ternary systems. Based on the Al-Mg binary phase diagram, the microstructure of the Al-Mg alloy without silicon is composed mainly of the α-Al solid solution and the intermetallic β-phase (Al_3Mg_2). [143,144] This phase constitution is consistent with thermodynamic predictions and confirms that magnesium remains partially dissolved in the aluminum matrix while also forming a distinct intermetallic compound at higher Mg concentrations.

With the incorporation of silicon, a notable modification in phase constitution is observed. According to the Al–Mg–Si ternary phase diagram, the addition of silicon promotes the formation of Mg_2Si as the dominant secondary phase, resulting in a dual-phase microstructure consisting of

α-Al matrix and Mg_2Si intermetallic particles. [97,145] The α-Al phase is observed as bright and continuous regions in the optical and scanning electron micrographs, indicating a homogeneous aluminum-rich matrix.

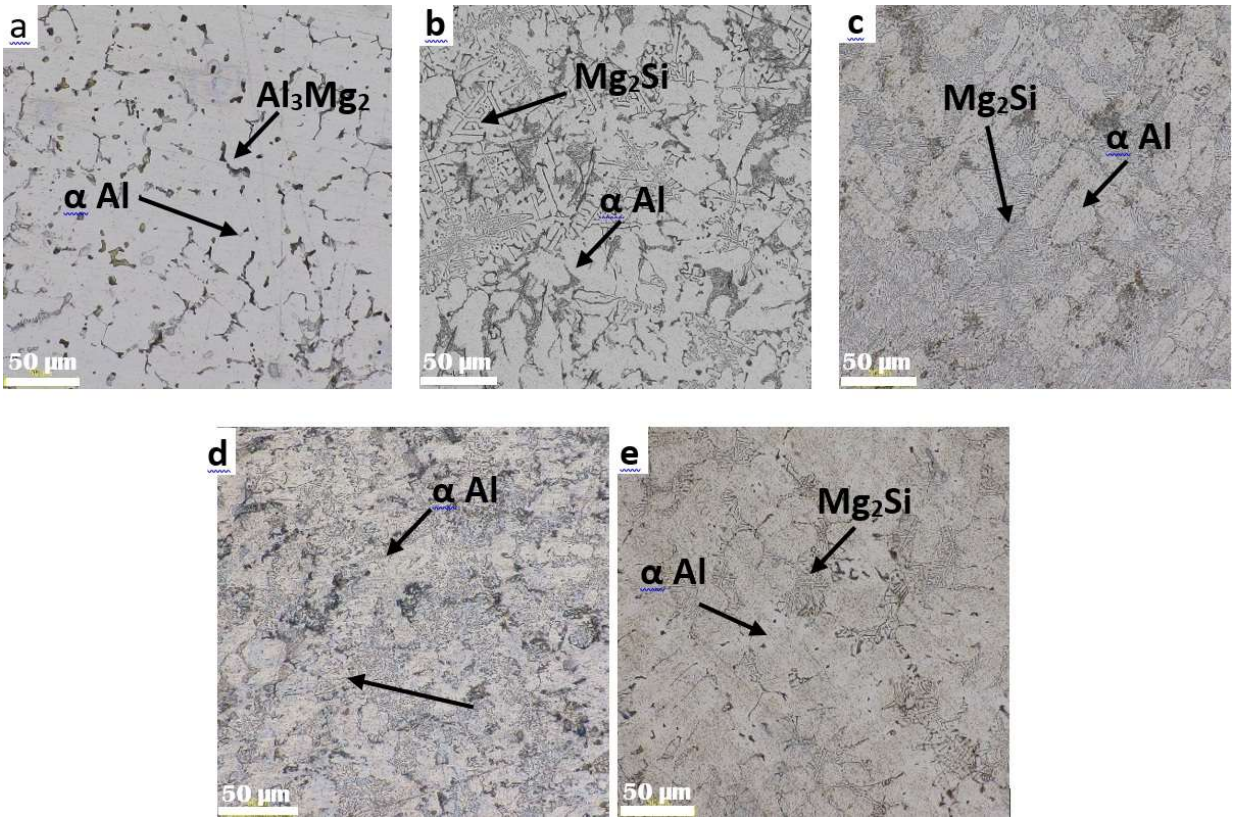

Figure 4.1 Microstructure of Al-6.5 %Mg alloys with varying Si content: (a) Al-6.5 %Mg, (b) Al-6.5 %Mg-1.5 %Si, (c) Al-6.5 %Mg-3 %Si, (d) Al-6.5 %Mg-4.5 %Si, and (e) Al-6.5 %Mg-6 %Si at 1000 X magnification, showing the evolution of Mg_2Si phases with increasing Si.

In the Al-6.5 wt.% Mg alloy without silicon (Figures 4.1a and 4.2a), the β-phase (Al_3Mg_2) appears as dark, irregular regions distributed along the interdendritic boundaries. This phase forms due to the limited solubility of magnesium in aluminum during solidification and is characteristic of high-magnesium aluminum alloys. The presence of Al_3Mg_2 is known to influence mechanical and corrosion behavior, particularly under aggressive environments.

Upon silicon addition (Figures 4.1(b-e) and 4.2(b-e)), the microstructure undergoes a distinct transformation, wherein Mg_2Si replaces Al_3Mg_2 as the primary secondary phase. This phase forms

through a preferential metallurgical reaction between magnesium and silicon during solidification. As silicon content increases, a progressive refinement of the Mg_2Si phase is observed, accompanied by an increase in particle number density and a more uniform spatial distribution. Such refinement suggests that silicon plays a crucial role in altering solidification kinetics and eutectic reactions within the alloy system.

The observed refinement and morphological modification of Mg_2Si particles with increasing silicon content are in good agreement with previous studies, which report that higher silicon levels promote the formation of finer and more evenly distributed eutectic Mg_2Si structures. [146] This behavior is often attributed to enhanced nucleation rates and restricted growth of Mg_2Si particles under silicon-rich conditions. The dark contrast of Mg_2Si particles within the microstructure, as confirmed by SEM and EDS analysis (Figure 4.2) and further validation their chemical identity is done by XRD analysis as shown in Figure 4.3.

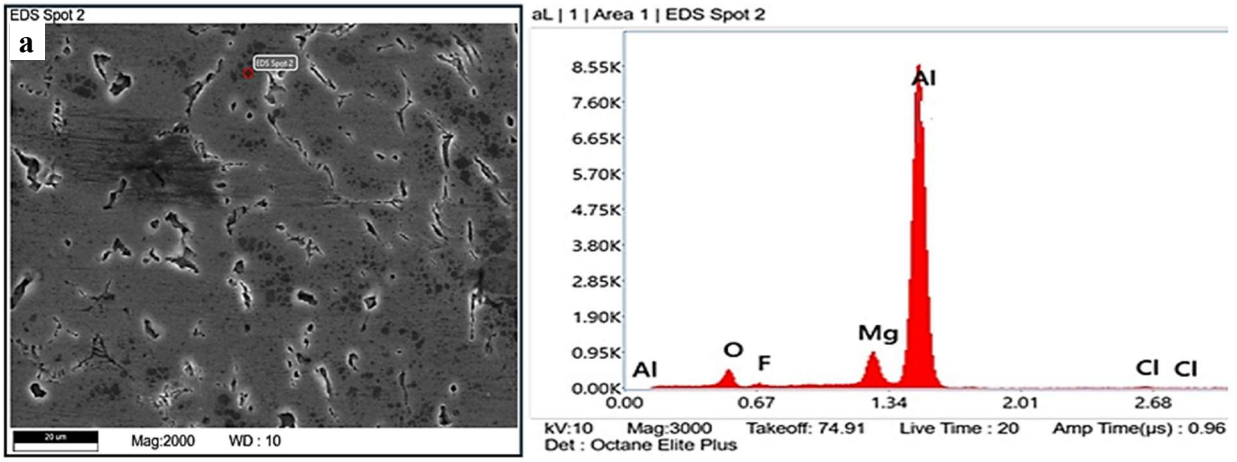

(BA) Al-6.5Mg

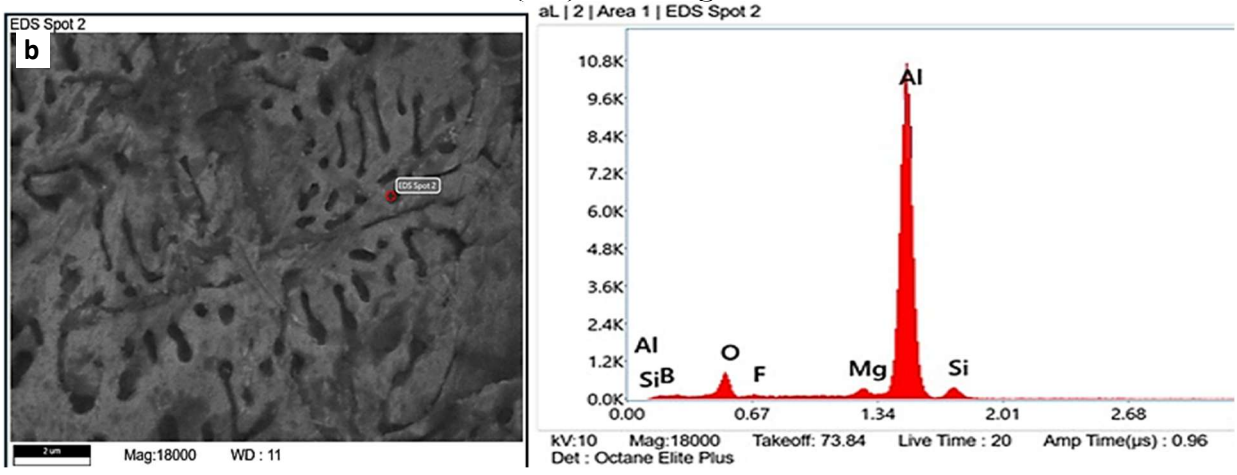

(BA-1.5Si) Al-6.5Mg-1.5Si

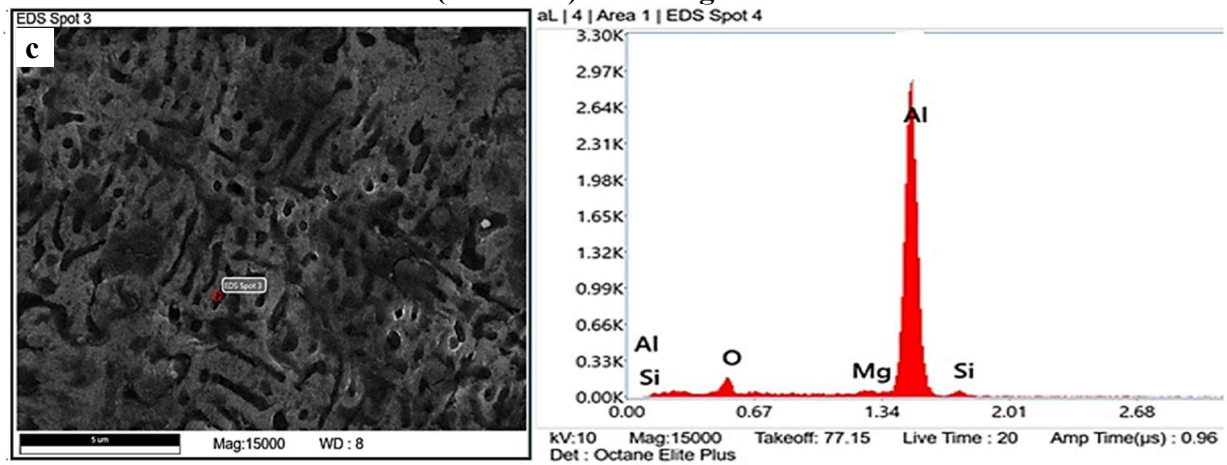

(BA-3Si) Al-6.5Mg-3Si

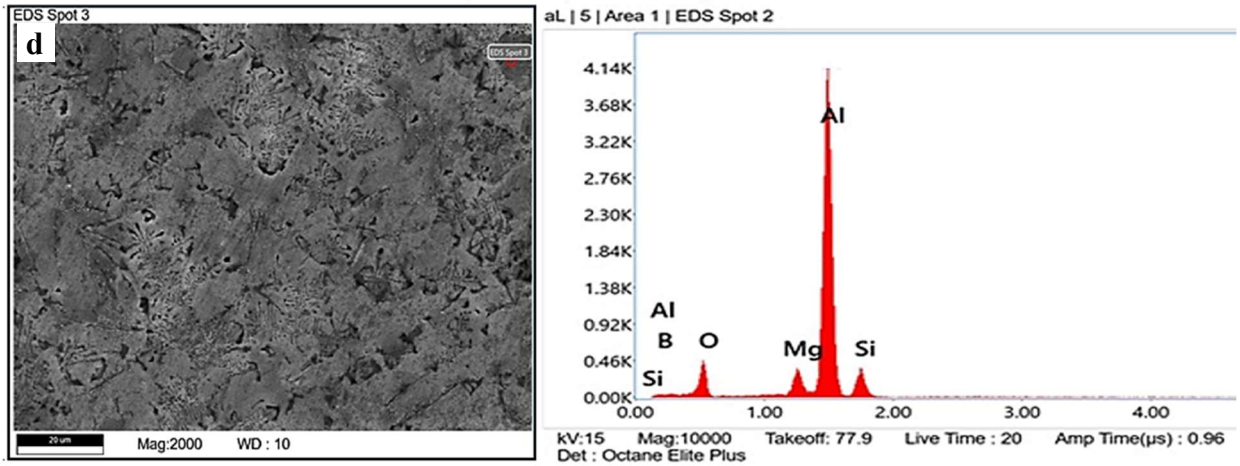

(BA-4.5Si) Al-6.5Mg-4.5Si

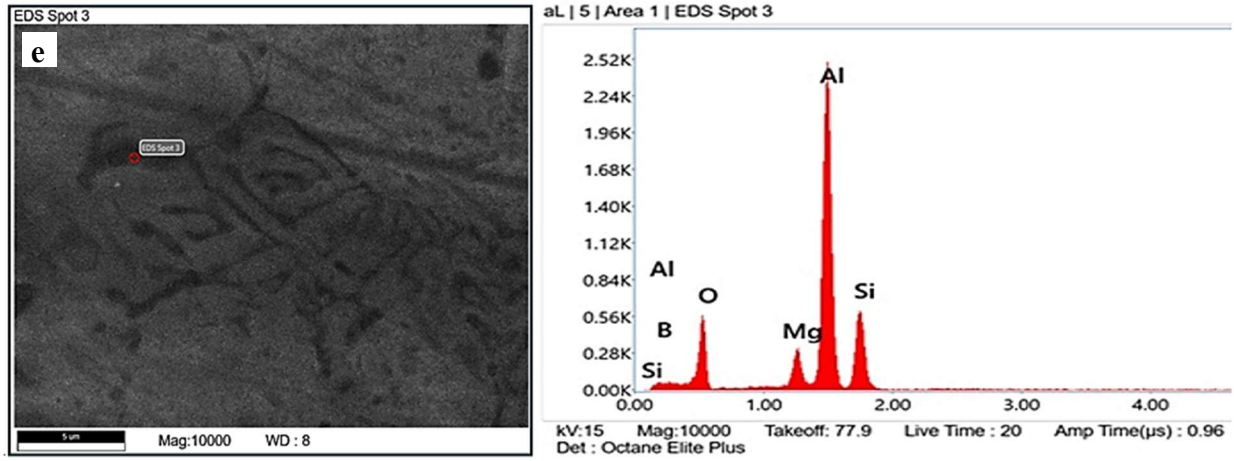

(BA-6Si) Al-6.5Mg-6Si

Figure 4.2 SEM images with marked analysis location (Spots) and corresponding EDS spectrum, confirming the presence of the phase Al_3Mg_2 and Mg_2Si. (a) BA (b) BA-1.5Si (c) BA-3Si (d) BA-4.5Si and (e) BA-6Si alloys.

Detailed microscopic examination (Figure 4.2) reveals that the α-Al matrix remains continuous and well connected, while Mg_2Si particles appear as discrete dark features embedded within the matrix. In the Al-Mg-Si alloy system, Mg_2Si is widely recognized as the principal strengthening and secondary phase, significantly influencing both mechanical and electrochemical properties. A clear relationship between silicon concentration and Mg_2Si morphology is evident; increasing silicon content results in a substantial refinement of the eutectic Mg_2Si phase, transforming it from coarse, irregular structures to finer and more uniformly dispersed particles. [101]

4.3.2 Phase Volume Fraction Analysis

To quantify the effect of silicon addition on phase evolution, phase volume fraction analysis was carried out using optical radical microscope with Metal 11.1 analytical software as represented in Table 4.2.

Table 4.2 Phase volume fraction and corresponding standard deviation of α-Al and Mg_2Si phases obtained from optical microscopy for Al–6.5Mg–xSi alloys.

Alloy Composition	α-Al (%)	Std.Dev.	Mg_2Si (%)	Std.Dev.
BA-1.5Si	81.19	±1.44	18.81	±0.42
BA-3Si	80.13	±1.23	19.87	±0.18
BA-4.5Si	78.70	±1.11	21.30	±0.26
BA-6Si	77.92	±1.05	22.08	±0.38

The phase volume fraction data obtained from optical microscopy demonstrate a clear and systematic influence of silicon content on the microstructural evolution of Al-6.5Mg-xSi alloys. As the silicon content increases from 1.5 wt.% to 6 wt.%, the volume fraction of the α-Al matrix decreases gradually from 81.19% to 77.92%. This reduction indicates progressive consumption of magnesium from the aluminum matrix due to the formation of Mg_2Si intermetallic compounds with increasing silicon availability.

In contrast, the Mg_2Si phase fraction increases steadily from 18.81% at 1.5 wt.% Si to 22.08% at 6 wt.% Si, confirming that silicon addition strongly promotes Mg_2Si formation in the Al-Mg-Si system. This inverse relationship between α-Al and Mg_2Si volume fractions is consistent with thermodynamic predictions and supports the phase evolution trends observed in SEM and XRD analyses.

The standard deviation values associated with α-Al phase fraction decrease slightly with increasing silicon content, from ±1.44 to ±1.05, suggesting improved uniformity of phase distribution at higher silicon levels. Similarly, the relatively low standard deviation values for Mg_2Si (ranging from ±0.18 to ±0.42) indicate good repeatability and reliability of the optical microscopy based image analysis. The reduced scatter in Mg_2Si measurements at intermediate silicon contents (3-4.5 wt.% Si) implies a more homogeneous dispersion of the intermetallic phase.

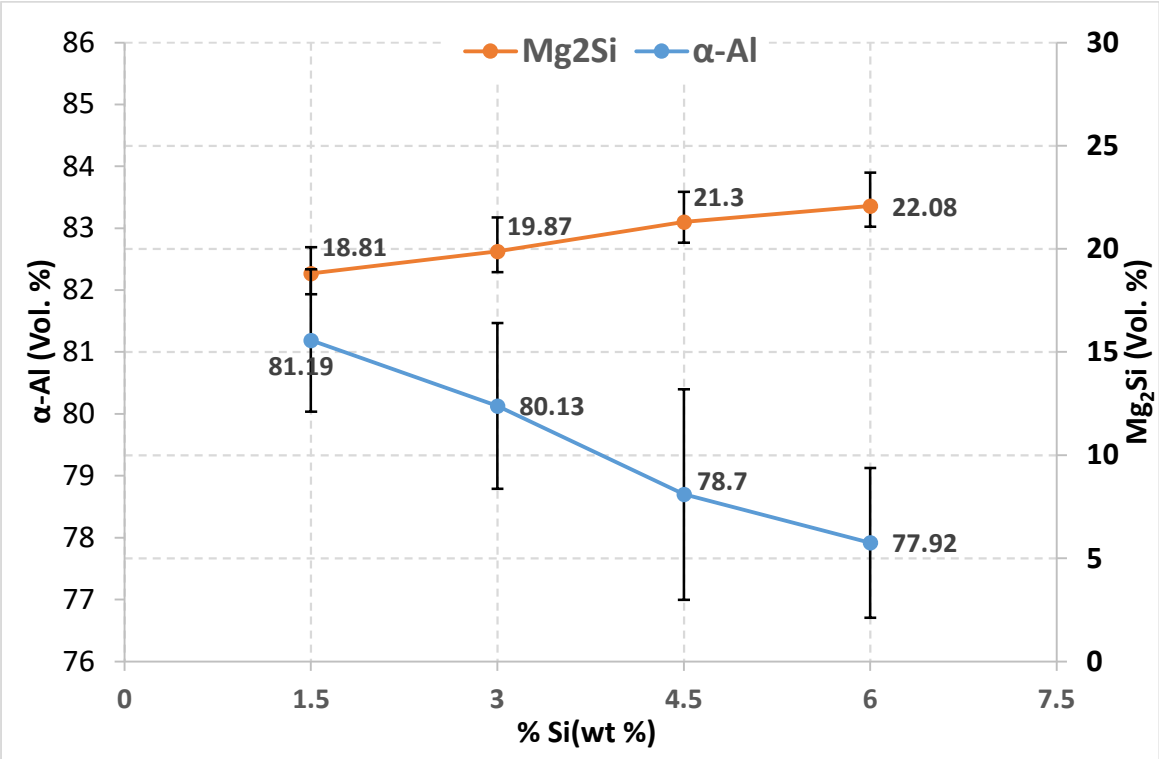

Figure 4.3 Volume fraction of α-Al and Mg_2Si phases in Al–6.5 %Mg alloys with varying Si content.

The measured volume fractions provide a quantitative basis for the observed changes in microstructure and enable direct correlation with hardness and electrochemical behaviors. As shown in Figure 4-3, phase analysis indicates that increasing the silicon content reduces the volume fraction of the α-Al phase while enhancing the formation of Mg_2Si higher Si additions are expected to influence α-Al grain, as suggested in previous studies. [101]

4.3.3 X-ray Diffraction (XRD) Analysis

The phase constitution of the Al–6.5Mg–xSi alloys was examined using X-ray diffraction (XRD) presented in Figure 4.4 and Table 4-3. The diffraction patterns are dominated by reflections corresponding to the face-centered cubic (FCC) α-Al matrix, with prominent peaks observed at 2θ values of approximately 38.2–38.5°, 44.8°, 64.6–65.1°, and 78.5°, which can be indexed to the (111), (200), (220), and (311) crystallographic planes, respectively. [147] These peaks confirm that α-Al remains the primary matrix phase across all investigated compositions, irrespective of silicon content or thermal condition.

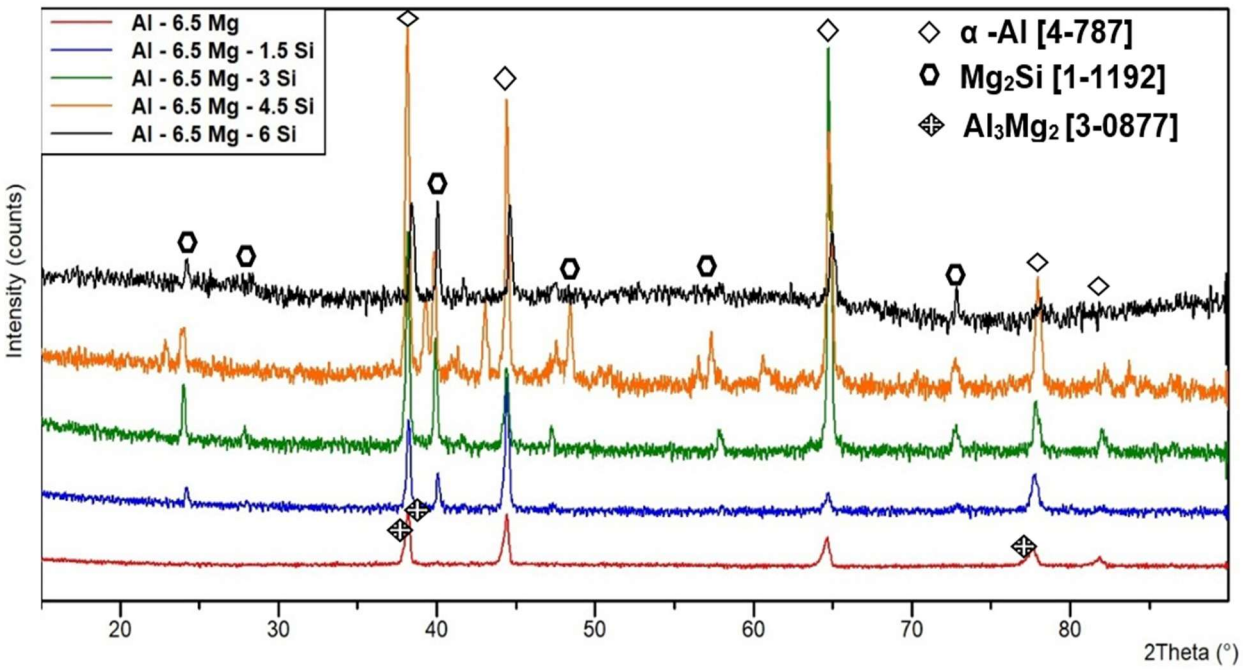

Figure 4.4 X-ray diffraction (XRD) patterns of the developed Al-6.5Mg-xSi alloys, showing the presence of α-Al, Mg_2Si, and Al_3Mg_2 phases.

In addition to the α-Al peaks, secondary diffraction maxima are detected at 2θ values around 24.1–24.3°, 40.0–40.1°, 47.7°, and 72.5°, corresponding to the characteristic reflections of the Mg_2Si intermetallic phase, indexed to the (111), (220), (311), and (511) planes. [148] The appearance of these peaks confirms the formation of Mg_2Si through the metallurgical reaction between magnesium and silicon in the Al–Mg–Si system. Minor peaks associated with the Al_3Mg_2 phase are also observed in alloys with lower silicon content, indicating partial retention of this phase when silicon availability is insufficient to fully consume magnesium.

Table 4.3 XRD peak positions (2θ), interplanar spacings (d), and Miller indices of α-Al matrix and secondary intermetallic phases (Mg_2Si and Al_3Mg_2) detected in Al–6.5Mg–xSi alloys.

α-Al			Mg_2Si			Al_3Mg_2		
2θ	**d spacing**	**Plane**	**2θ**	**d spacing**	**Plane**	**2θ**	**d spacing**	**Plane**
38.2152	2.35318	[111]	24.1372	3.68419	[111]	37.5997	2.39028	[140]
44.8182	2.02063	[200]	40.0439	2.24984	[220]	38.2398	2.35173	[147]
64.6487	1.44059	[220]	47.7056	1.90485	[311]	77.5468	1.23003	[531]
78.5847	1.21637	[311]	57.8007	1.59387	[440]			
81.769	1.17686	[222]	72.7318	1.29912	[511]			

The presence of the Al_3Mg_2 (β) phase is identified in Al-6.5Mg alloys through minor diffraction peaks appearing at 2θ values around 37.6°, 38.2°, and 77.5°, corresponding to the (140), (147), and (531) crystallographic planes, respectively. These reflections are consistent with reported XRD data for the Al_3Mg_2 intermetallic phase and confirm its formation in Al-Mg alloys containing high magnesium levels and limited silicon availability.

The Al_3Mg_2 phase is predominantly observed in the Al-6.5Mg alloy and in compositions with low silicon addition, where insufficient silicon is available to react with magnesium to form Mg_2Si. As the silicon content increases, the intensity of Al_3Mg_2 diffraction peaks progressively diminishes, indicating a reduction in its volume fraction. This behavior suggests that silicon preferentially combines with magnesium to form Mg_2Si, thereby suppressing the formation of the Al_3Mg_2 phase.

The gradual disappearance of Al_3Mg_2 peaks at higher silicon concentrations is metallurgically significant, as this phase is known to be electrochemically active and detrimental to corrosion resistance in Al-Mg alloys. Its replacement by Mg_2Si with increasing silicon content alters the phase balance and directly influences both mechanical and corrosion behavior. Furthermore, heat treatment promotes partial dissolution or redistribution of Al_3Mg_2, as evidenced by reduced peak intensity and slight peak broadening, indicating changes in phase stability and morphology.

A comparative evaluation of the diffraction patterns reveals a systematic increase in the intensity of Mg_2Si peaks with increasing silicon content from 1.5 wt.% to 6 wt.%. This trend indicates a progressive increase in the volume fraction of the Mg_2Si phase, consistent with the microstructural

observations from SEM and EDS analyses. At 1.5 wt.% Si, the Mg_2Si peaks are relatively weak and broadened, suggesting the presence of finely dispersed and small-sized precipitates. Such a refined distribution contributes to enhanced hardness and improved corrosion resistance by strengthening the matrix while minimizing localized electrochemical heterogeneity.

As the silicon content increases to 3 wt.% and 4.5 wt.%, the Mg_2Si diffraction peaks become sharper and more intense, reflecting coarsening and increased interconnectivity of the precipitates. While this evolution leads to further improvement in hardness due to a higher fraction of load-bearing intermetallics, it may also promote localized corrosion through micro-galvanic coupling between Mg_2Si particles and the α-Al matrix. At the highest silicon content of 6 wt.%, the pronounced Mg_2Si peaks indicate the formation of a nearly continuous intermetallic network, particularly along grain boundaries. This structural continuity is associated with embrittlement and an increased corrosion rate, despite yielding the maximum hardness among the studied alloys.

The lattice parameters of the major phases were calculated from the XRD data using multiple representative diffraction planes to improve accuracy. For cubic crystal structures, the lattice parameter was determined using the relation:

$$a = d * \sqrt{h^2 + k^2 + l^2}$$

where d is the interplanar spacing and (hkl) are the Miller indices of the corresponding diffraction planes. The calculated average lattice parameters for α-Al, Mg_2Si, and Al_3Mg_2 are summarized in Table 4-3. The α-Al phase exhibits an average lattice parameter of approximately 4.060 Å, while Mg_2Si and Al_3Mg_2 show lattice parameters of about 6.456 Å and 8.563 Å, respectively. These values are in close agreement with reported standard crystallographic data, confirming the reliability of phase identification and peak indexing.

The variation in lattice parameter of the α-Al matrix is strongly influenced by the nature and solubility of alloying elements. Magnesium, with an atomic radius of approximately 1.60 Å, is larger than aluminum (1.43 Å). When Mg atoms substitute into the α-Al lattice, they induce lattice expansion due to atomic size mismatch, resulting in an increase in the lattice parameter. In contrast, silicon has a significantly smaller atomic radius (~1.17 Å), and its substitutional dissolution within the α-Al lattice leads to lattice contraction.

In the Al-Mg-Si alloy system, the combined effect of magnesium and silicon governs the overall lattice distortion. At lower silicon contents, magnesium dominates the solid solution behavior, leading to an increase in the α-Al lattice parameter. With increasing silicon content, a greater fraction of silicon dissolves into the aluminum matrix, counteracting the expansion caused by magnesium and resulting in a gradual reduction in the lattice parameter. At higher silicon levels, excess silicon preferentially reacts with magnesium to form the Mg_2Si intermetallic phase, thereby reducing the amount of solute available for lattice distortion in the α-Al matrix. Consequently, further changes in the α-Al lattice parameter become less pronounced at high silicon concentrations.

4.3.4 Morphology of Mg_2Si

The morphology and phase constitution of Mg_2Si in cast Al-Mg-Si alloys were examined using Digital microscope and SEM coupled with EDS analysis, as presented in Figure 4.5 and 4.2(b-e). The SEM micrographs, along with marked analysis locations (spots) and corresponding EDS spectra, confirm the presence of Mg_2Si intermetallic phase across the investigated alloy compositions as shown in Figure 4.2. Same was also confirmed by XRD analysis as shown in Figure 4.4. Previous studies have reported that Mg_2Si can exist in multiple morphological forms, including lamellar, rod-like, fibrous, flake-like, and Chinese script-like structures, depending on alloy chemistry and solidification conditions. [96–98]

As shown in Figure 4.2(a), the Al-6.5Mg alloy primarily contains the Al_3Mg_2 phase, with no distinct Mg_2Si formation due to the absence of silicon. Upon the addition of 1.5% Si, as observed in Figure 4.2(b) and 4.5(a), fine and flake-like Mg_2Si particles begin to form within the α-Al matrix. The corresponding EDS spectrum confirms the presence of Mg and Si peaks, validating the formation of the Mg_2Si phase. [104] This fine morphology indicates limited growth and a relatively uniform distribution of the intermetallic phase.

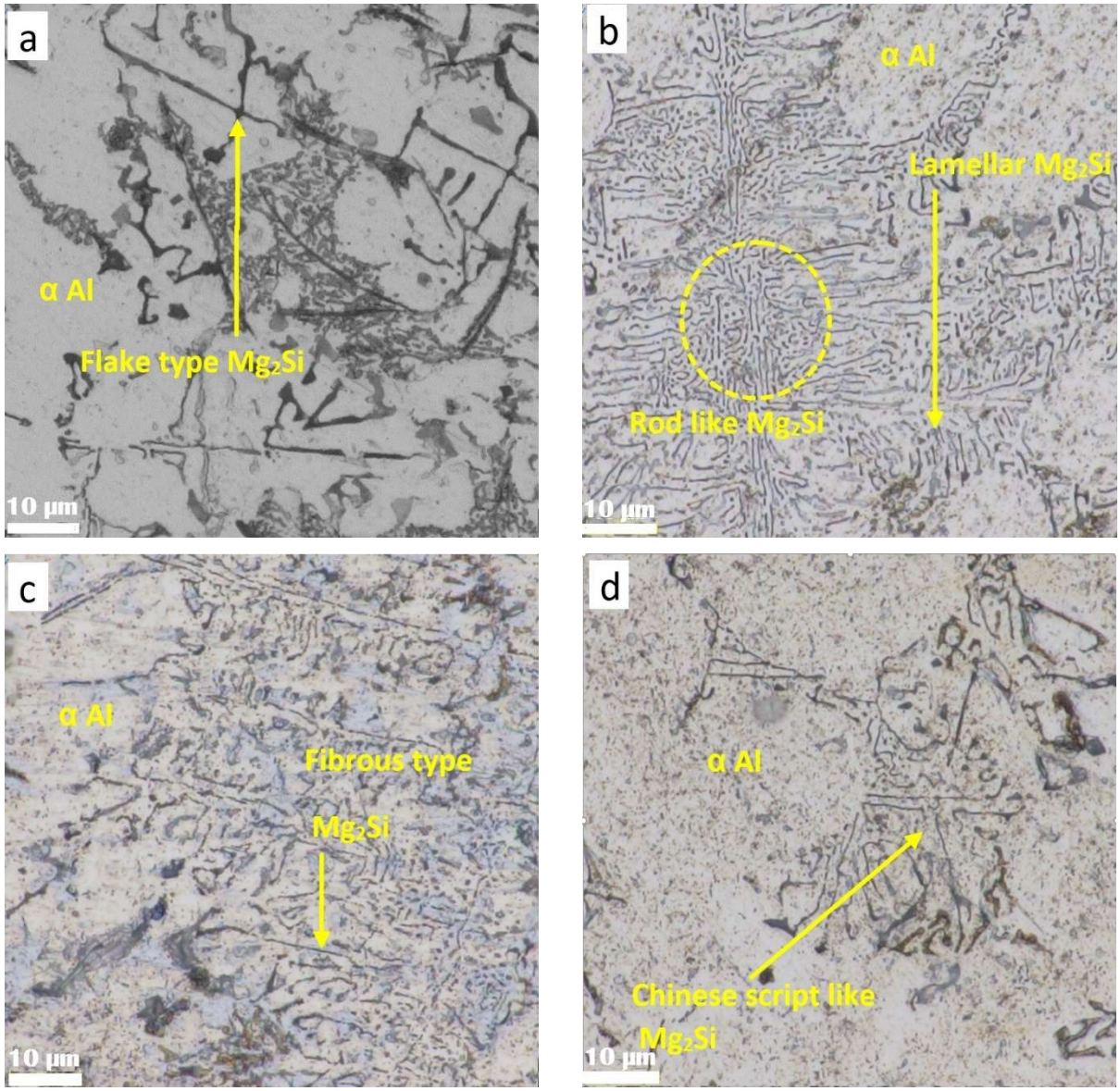

Figure 4.5 Morphology of Mg_2Si particles in Al–6.5 %Mg alloys with different Si contents: (a) 1.5 %Si, (b) 3 %Si, (c) 4.5 %Si, and (d) 6 %Si at 3620 X magnification.

With further increase in silicon content to 3%, the Al-6.5Mg-3%Si alloy (Figure 4.2(c) & 4.5(b)) exhibits coarser Mg_2Si particles with rod-like and lamellar morphologies. EDS analysis at selected spots confirms enrichment of Mg and Si, indicating well-developed Mg_2Si intermetallics.[92] In the Al-6.5Mg-4.5%Si alloy (Figure 4.2(d) & 4.5(c)), the Mg_2Si phase transforms into irregular and fibrous morphologies, suggesting increased interconnection and growth of the phase during solidification.

At the highest silicon content of 6%, as shown in Figure 4.2(e) & 4.5(d), the Mg_2Si phase predominantly appears as a fine Chinese script-like morphology distributed throughout the aluminum matrix. This interconnected Mg_2Si network significantly alters the microstructural characteristics of the alloy.

These observed morphological changes in Mg_2Si have a pronounced effect on the mechanical and corrosion behavior of the alloys. Fine and uniformly dispersed Mg_2Si particles, as seen in the Al-6.5Mg-1.5%Si alloy, contribute to improved hardness while maintaining better corrosion resistance. In contrast, the formation of coarser, fibrous, or networked Mg_2Si morphologies at higher silicon contents enhances hardness through structural continuity but adversely affects corrosion resistance and operational stability due to micro-galvanic effects and phase connectivity. [104,149]

4.3.5 Microstructural Evolution of Heat Treated Al-Mg-Si Alloys

The microstructural characteristics of the Al-6.5Mg-xSi alloys undergo substantial modification following the application of T6 heat treatment, consisting of solution treatment followed by artificial aging. In contrast to the as-cast condition, where Mg_2Si appears in morphologies such as flake-like, rod-shaped, fibrous, and Chinese script-like structures-the heat-treated condition exhibits a markedly refined and homogenized microstructure, as shown in Figures 4.6(a–d).

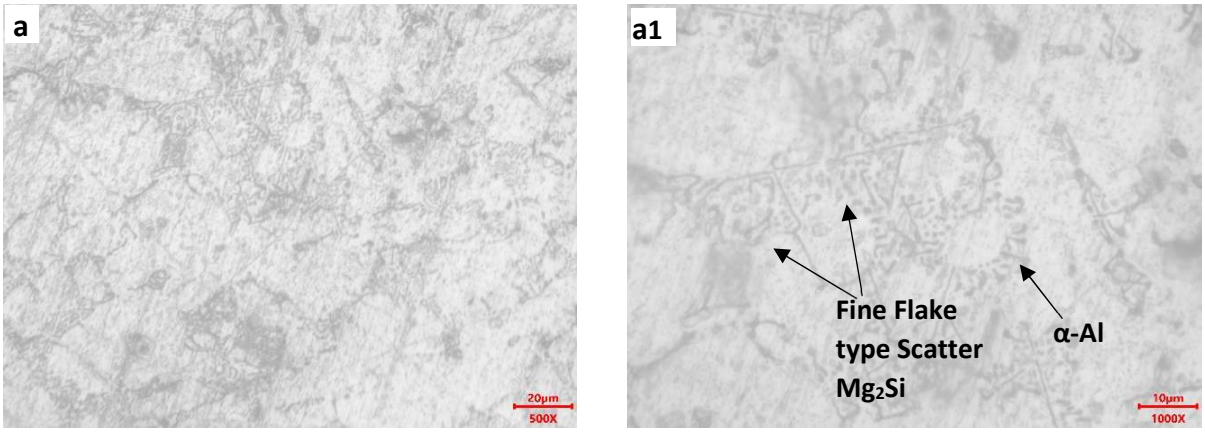

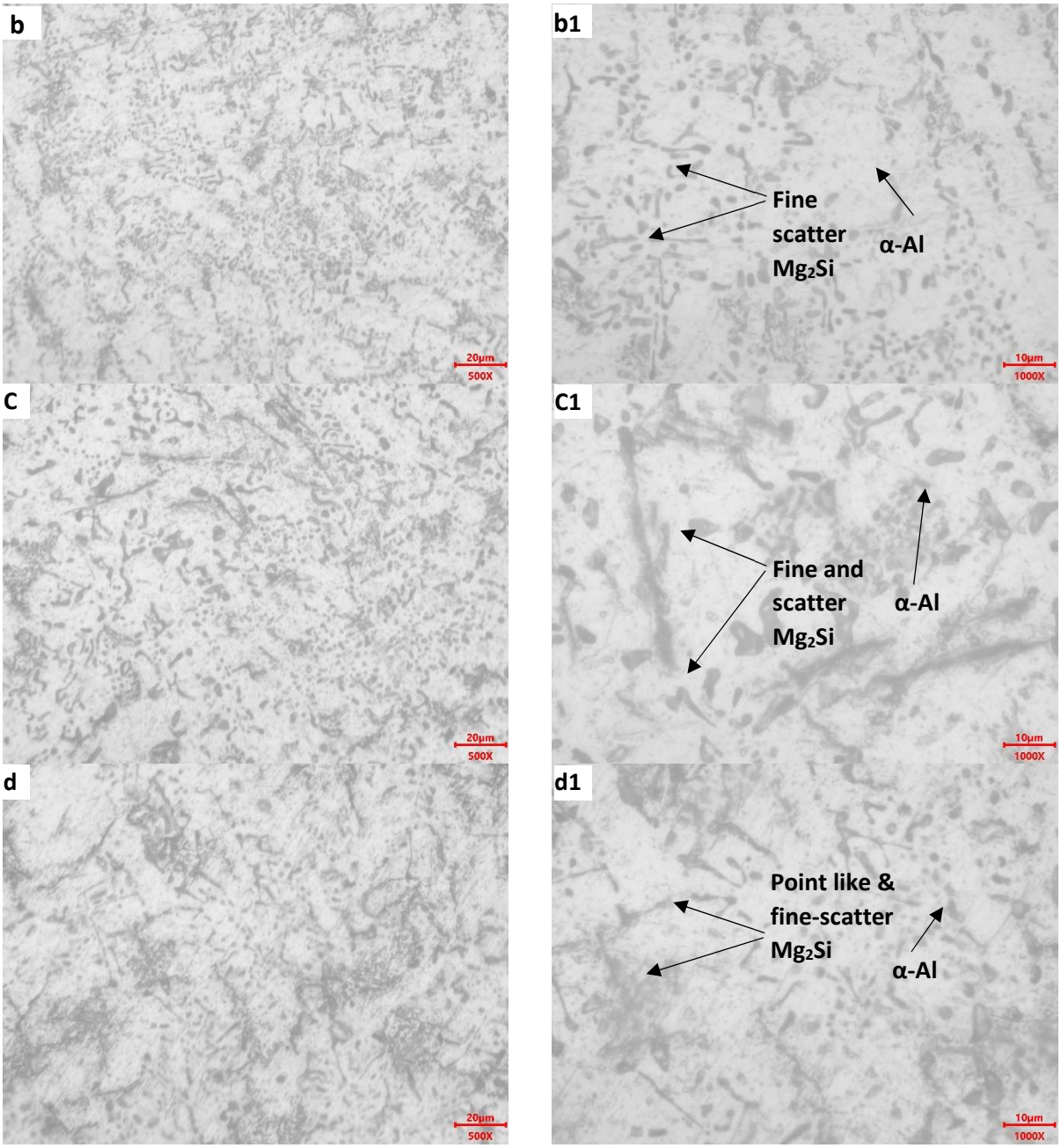

Figure 4.6 Microstructure of Al-6.5%Mg-xSi alloys in the T6 heat-treated condition showing the evolution of Mg_2Si precipitates: (a-d) at 500x and (a1-d1) at 1000x magnification. (a, a1) BA-1.5Si-T6, (b, b1) BA-3Si-T6, (c, c1) BA-4.5Si-T6, and (d, d1) BA-6Si-T6 alloys.

The overall transformation in microstructure from the as-cast to the T6 heat-treated condition is systematically illustrated in Figure 4.7, highlighting the dissolution of coarse Mg_2Si phases and their subsequent refinement into fine precipitates.

During the solution treatment stage, the coarse and morphologically heterogeneous Mg_2Si phases formed during solidification progressively dissolve into the α-Al matrix, leading to the formation of a supersaturated solid solution. This dissolution effectively eliminates the primary Mg_2Si networks and discontinuous morphologies observed in the as-cast alloys, irrespective of silicon content.[68,150–152] The removal of these coarse intermetallic phases improves microstructural uniformity and reduces micro-galvanic heterogeneities present in the as-cast state.

Subsequent artificial aging promotes controlled reprecipitation of the Mg_2Si phase from the supersaturated matrix. Unlike the coarse and interconnected Mg_2Si structures observed prior to heat treatment, the reprecipitated Mg_2Si appears in the form of fine, uniformly dispersed, and intermittent point-like precipitates. This transformation is consistently observed across all heat-treated alloy variants, indicating a convergence toward a similar refined precipitate distribution regardless of the initial as-cast Mg_2Si morphology. Such a refined precipitate structure is known to be highly effective in strengthening the aluminum matrix while simultaneously improving electrochemical stability.[153]

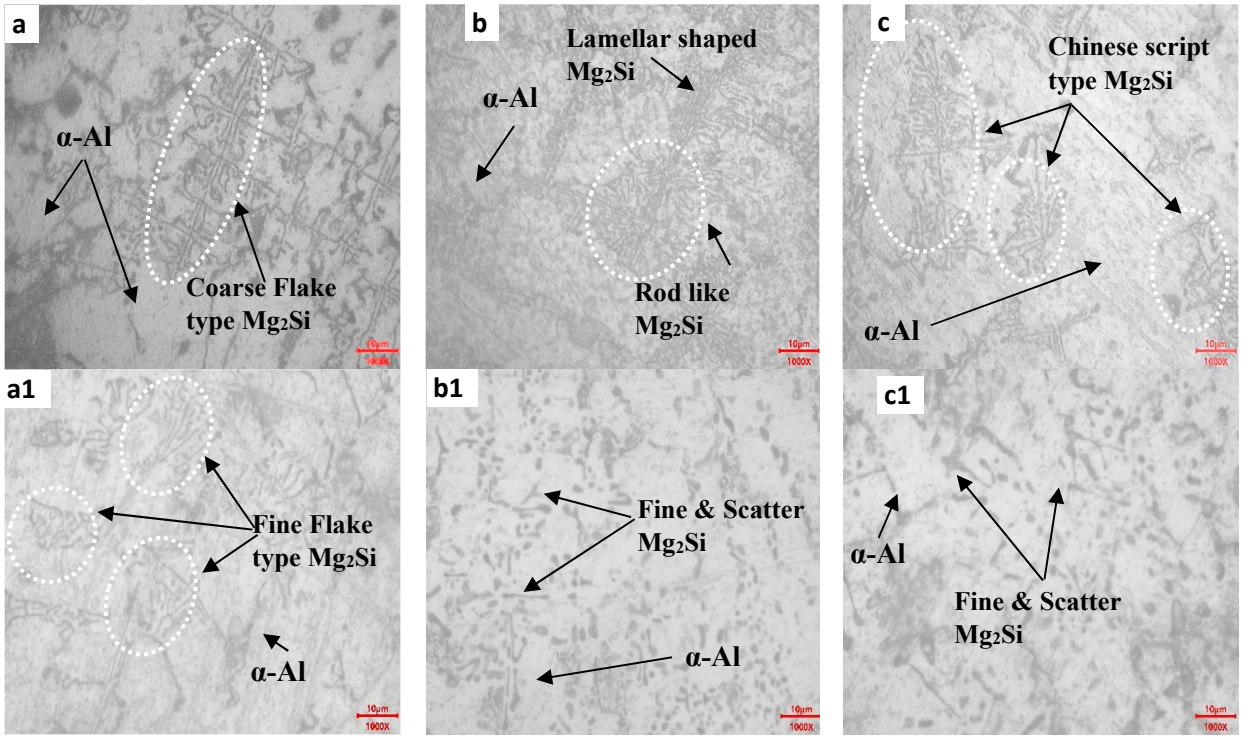

Figure 4.7 Microstructures of Al–6.5Mg–xSi alloys in as-cast (a–c) and heat treated (a1–c1) conditions for 1.5%, 3%, and 6% Si at 1000× magnification.

A detailed alloy wise microstructural evaluation reveals that in the BA-1.5Si-T6 alloy, the T6-treated microstructure is characterized by a fine, flake-like, and uniformly scattered Mg_2Si precipitate distribution, as observed in Figures 4.6(a-a1). The absence of coarse or interconnected Mg_2Si phases indicates effective dissolution during solution treatment followed by homogeneous reprecipitation during artificial aging, as illustrated in Figure 4.7(a–a1). Similarly, the BA-3Si-T6 alloy exhibits a refined microstructure dominated by fine, dispersed Mg_2Si precipitates distributed throughout the α-Al matrix, as shown in Figures 4.6(b–b1). Compared to the as-cast condition, the previously observed rod-like and lamellar Mg_2Si morphologies are completely replaced by a scattered, point-like precipitate structure as shown in Figure 4.7(b-b1).

In the BA-4.5Si-T6 alloy, the heat-treated microstructure closely resembles that of the 3% Si alloy, with Mg_2Si appearing as fine and uniformly scattered precipitates, as shown in Figures 4.6(c–c1). The fibrous and irregular Mg_2Si structures present in the as-cast condition are no longer observed, confirming the effectiveness of the T6 treatment in homogenizing the microstructure.

For the BA-6Si-T6 alloy, the T6 heat-treated microstructure also reveals a fine, point-like, and scattered Mg_2Si precipitate distribution, as illustrated in Figures 4.6(d–d1). Despite the high silicon content and the presence of Chinese script-like Mg_2Si in the as-cast state, the heat treatment leads to a uniform and refined precipitate morphology as shown in Figure 4.7(c-c1).

The presence and evolution of the Mg_2Si phase in the heat-treated condition are confirmed through complementary compositional and phase analyses. Initially, SEM-EDS analysis was carried out to verify the presence of the Mg_2Si phase after T6 heat treatment. The EDS spectra obtained from selected regions reveal localized enrichment of magnesium and silicon, confirming the reprecipitation of Mg_2Si within the α-Al matrix, as shown in Figure 4.8.

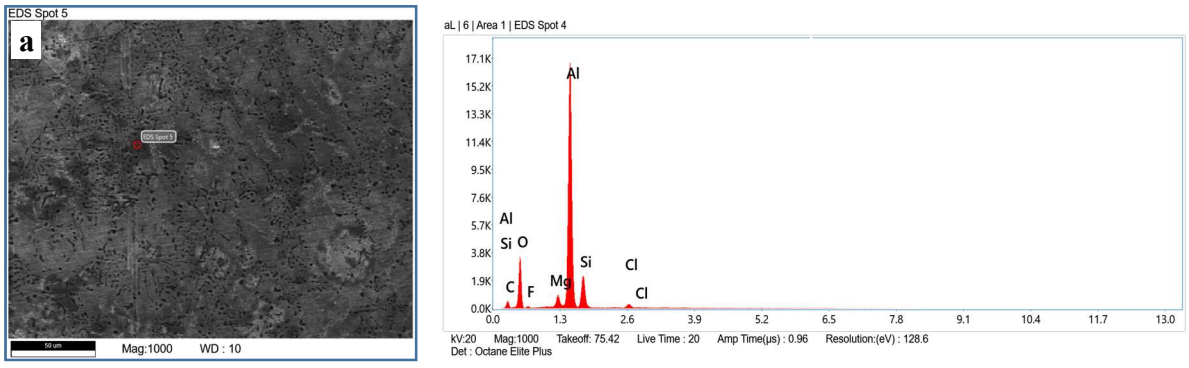

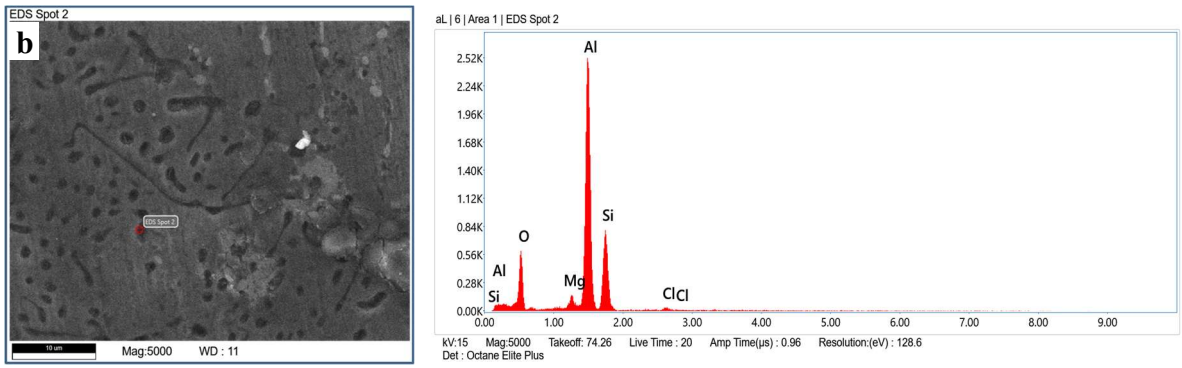

Figure 4.8 SEM micrographs and corresponding EDS spectra confirming the presence of the Mg_2Si phase in T6 heat-treated alloys: (a) BA–4.5Si-T6 and (b) BA–6Si-T6.

X-ray diffraction (XRD) analysis was performed to identify and validate the phase constitution of the T6 heat-treated alloys. The XRD patterns exhibit characteristic Mg_2Si peaks even after heat treatment, indicating that the Mg_2Si phase remains stable despite significant morphological refinement, as illustrated in Figure 4.9. Moreover, the XRD data of the heat-treated condition, presented in Table 4.4, closely resemble those of the as-cast alloys, confirming that the T6 heat treatment modifies the morphology and distribution of the Mg_2Si phase without introducing new phases or eliminating existing ones.

Table 4.4 XRD peak positions (2θ), interplanar spacings (d), and Miller indices of α-Al matrix and intermetallic phase Mg_2Si detected in Al–6.5Mg–xSi alloys in as heat treated condition.

α-Al			**Mg_2Si**		
2θ	**d spacing**	**Plane**	**2θ**	**d spacing**	**Plane**
38.2152	2.35318	[111]	24.1372	3.68419	[111]
44.8182	2.02063	[200]	40.0439	2.24984	[220]
64.6487	1.44059	[220]	47.7056	1.90485	[311]
78.5847	1.21637	[311]	57.8007	1.59387	[440]
81.769	1.17686	[222]	72.7318	1.29912	[511]

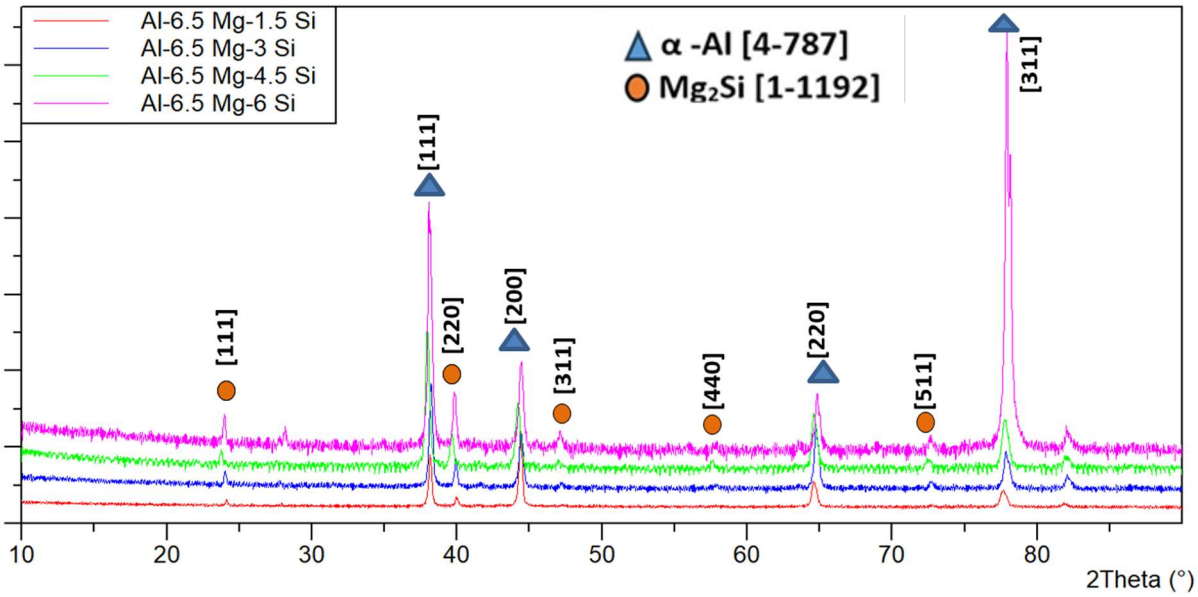

Figure 4.9 X-ray diffraction (XRD) patterns of the developed Al-6.5Mg-xSi alloys, showing the presence of α-Al, Mg_2Si phases.

4.4 Effect of Silicon Addition on the Hardness of Aluminum Alloys

Brinell hardness testing was carried out using a 2.5 mm diameter steel ball indenter under a load of 31.25 kg, following ASTM E10 standards. Measurements were taken at five different positions on each sample and the average values with standard deviations are presented in Table 4.5 and Figure 4.10.

Table 4.5 Brinell hardness values of pure Al, Al-6.5%Mg, and Al-6.5%Mg-Si alloys in as-cast and heat-treated conditions.

Alloy Composition	As-Cast Avg.	Std. Dev.	Heat-Treated Avg.	Std. Dev.
Pure Al	38	1.1	–	–
BA (Al–6.5Mg)	56	2.3	–	–
BA–1.5Si	82	1.9	75	1.2
BA–3Si	67	1.7	82	1.6
BA-4.5Si	70	2.2	103	2.0
BA–6Si	83	2.9	107	2.2

The as-cast hardness of pure aluminum was 38 HB, consistent with its soft, ductile nature. The incorporation of 6.5 wt.% Mg substantially increased hardness to 56 HB, demonstrating the solid-

solution strengthening effect of Mg in the Al matrix. [92] Hardness is greatly improved due to the formation of the Al_3Mg_2 (beta) phase as shown in Figure 4.1a. [154]

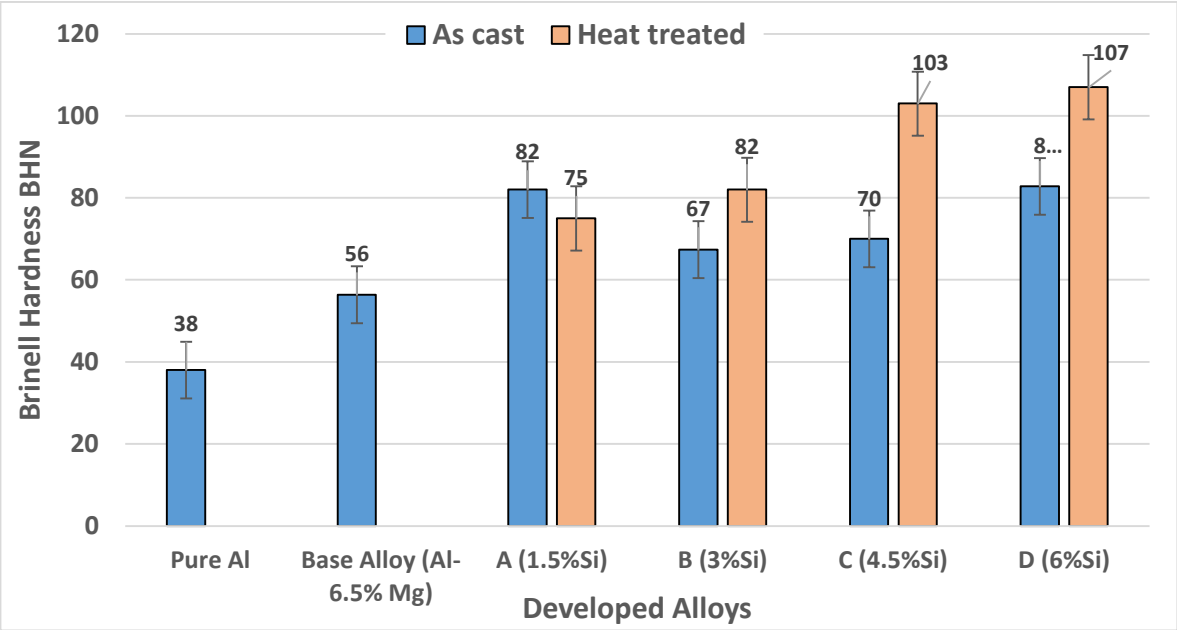

Figure 4.10 Effect of Si addition and heat treatment on hardness of Al-6.5% Mg alloys.

Silicon addition further modified the hardness response. The alloy containing 1.5 wt.% Si (Alloy A) showed a sharp increase to 82 HB, which can be attributed to the refinement of the dendritic α-Al structure as shown in Figure 4.11 and uniform dispersion of Mg_2Si precipitates plays a key role in strengthening. Along with Mg_2Si, the Al_3Mg_2 phase is also present and both are much harder and more rigid than the aluminum matrix. These intermetallic compounds act as obstacles to dislocation motion, effectively restricting plastic deformation and thereby enhancing hardness. [49,117,155] However, intermediate Si levels (3.0 and 4.5 wt.%) exhibited reduced hardness values of 67 and 70 HB, respectively. This decline is associated with the coarsening of Mg_2Si particles as shown in Figure 4.1(c, d), which decreases their ability to impede dislocation motion effectively. At the highest silicon level (6 wt.%), hardness rose again to 83 HB, indicating that a sufficient density of intermetallic phases compensated for particle coarsening and restored strengthening efficiency.

Heat treatment further enhanced hardness, as shown in Figure 4.12. The Alloy A (Al-6.5Mg-1.5% Si) alloy exhibited only slight decrease in hardness after heat treatment (from 82 to 75 HB), suggesting limited precipitation effects at lower Si levels. This reduction can be associated with

the partial coarsening and redistribution of Mg_2Si particles, which reduces their ability to act as effective dislocation barriers.

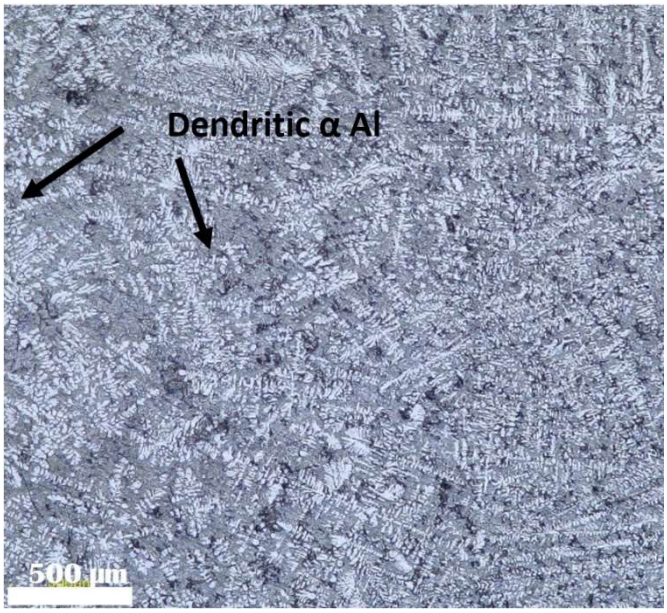

Figure 4.11 Microstructure of Al-6.5 %Mg-1.5 %Si alloy at 100 X magnification, highlighting the dendritic α-Al matrix.

In contrast, alloys with higher Si content responded strongly to heat treatment, with hardness values increasing to 82 (3% Si), 103 HB (4.5% Si) and 107 HB (6% Si). This substantial improvement-up to ~47% in compared to the as-cast condition-can be attributed to the precipitation and redistribution of fine Mg_2Si intermetallic during thermal processing, which refine the microstructure and strengthen the matrix.

The observed hardness trends are in good agreement with previously reported studies on Al–Mg–Si alloys, which have demonstrated that increasing Mg_2Si precipitation enhances hardness through precipitation strengthening, whereas coarsening of Mg_2Si particles reduces the strengthening efficiency. Similar behaviour has been reported by Polmear et al. [156], Totten and MacKenzie [157], Mondolfo [158], and Marioara et al. [159], confirming that the hardness variation observed in the present investigation is consistent with established precipitation-hardening mechanisms.

The combined effects of Mg and Si addition, supported by heat treatment, significantly improved hardness compared to pure aluminum. The strengthening mechanism arises from both solid-

solution effects and precipitation hardening due to Al_3Mg_2 and Mg_2Si phases. Importantly The results emphasize the non-linear influence of silicon content on hardness, which is governed by the competing effects of Mg_2Si formation, particle coarsening, and precipitation strengthening following heat treatment.

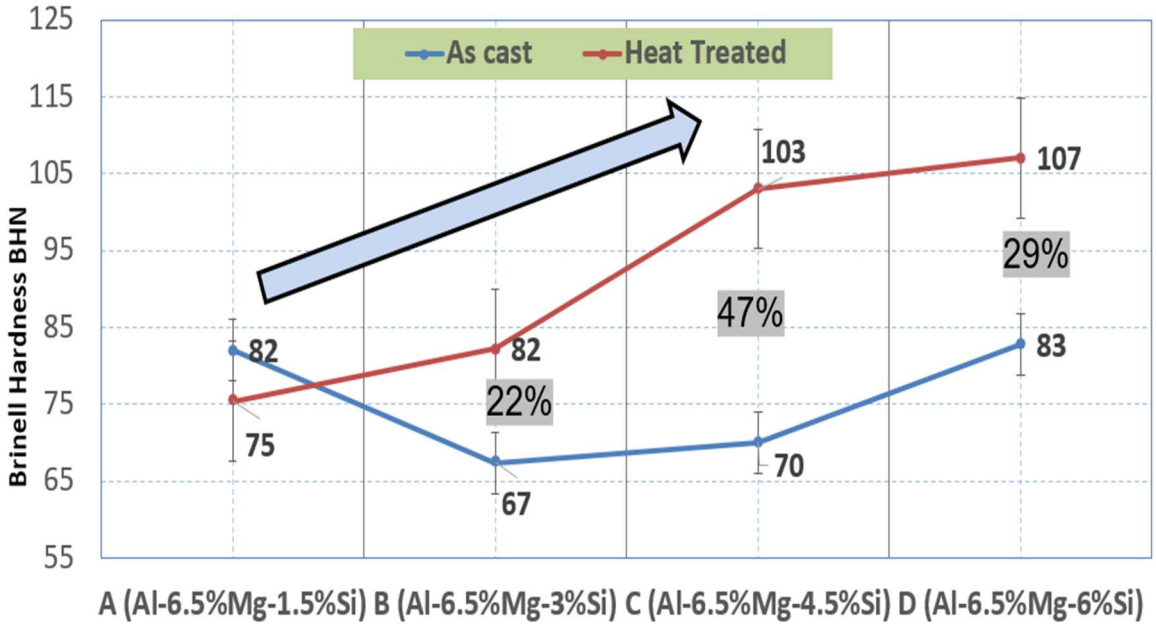

Figure 4.12 Comparison of hardness in as cast and heat-treated condition.

4.5 Corrosion

In this section, the corrosion behavior of Al-Mg sacrificial anodes with varying Si content is evaluated in both the as-cast and heat-treated conditions. The primary objective of this study is to assess the effectiveness of silicon (Si) as an alloying element in modifying and improving the corrosion performance of aluminum-based sacrificial anodes. Corrosion behavior was investigated using two complementary techniques: the standard weight loss method, which provides long-term corrosion rate data, and potentiodynamic polarization studies, which offer insight into electrochemical characteristics such as corrosion potential and kinetics.

4.5.1 Corrosion study by Weight Method-As Cast

The data presented in Table 4.6, summarize the progressive weight loss of Al–6.5Mg–xSi sacrificial anodes over an exposure period of 1 to 8 weeks, providing a quantitative basis for evaluating corrosion rate trends with respect to silicon content and exposure time.

Figure 4.13 reveals the variation in corrosion rates of Al-6.5Mg-xSi alloys over an eight-week exposure period, evaluated using the standard weight loss method. The corrosion rate trends clearly demonstrate the influence of silicon content on the corrosion performance of these alloys for sacrificial anode applications.

Table 4.6 Weekly weight loss measurements (1–8 weeks) obtained from the standard weight loss method for Al–6.5Mg–xSi sacrificial anodes.

	Corrosion Rate (MPY)							
Composition	**1 week**	**2 week**	**3 week**	**4 week**	**5 week**	**6 week**	**7 week**	**8 week**
BA	0 ± 0	0 ± 0	0.21 ± 0.008	0.24 ± 0.015	0.29 ± 0.012	0.31 ± 0.019	0.25 ± 0.010	0.24 ± 0.014
BA-1.5Si	0 ± 0	0 ± 0	0.20 ± 0.009	0.22 ± 0.011	0.22 ± 0.017	0.25 ± 0.013	0.28 ± 0.019	0.24 ± 0.012
BA-3Si	0 ± 0	0 ± 0	0.21 ± 0.010	0.23 ± 0.014	0.28 ± 0.018	0.30 ± 0.011	0.30 ± 0.020	0.28 ± 0.016
BA 4.5Si	0 ± 0	0 ± 0	0.21 ± 0.007	0.23 ± 0.012	0.26 ± 0.015	0.28 ± 0.018	0.22 ± 0.010	0.22 ± 0.013
BA-6Si	0 ± 0	0 ± 0	0.26 ± 0.013	0.28 ± 0.016	0.31 ± 0.020	0.37 ± 0.018	0.32 ± 0.015	0.31 ± 0.017

The Al-6.5Mg alloy exhibits stable and relatively low corrosion rates throughout the test duration, reaching a maximum of 0.31 mpy at six weeks before decreasing slightly to 0.24 mpy at eight weeks. This behavior indicates a relatively uniform and controlled corrosion process.

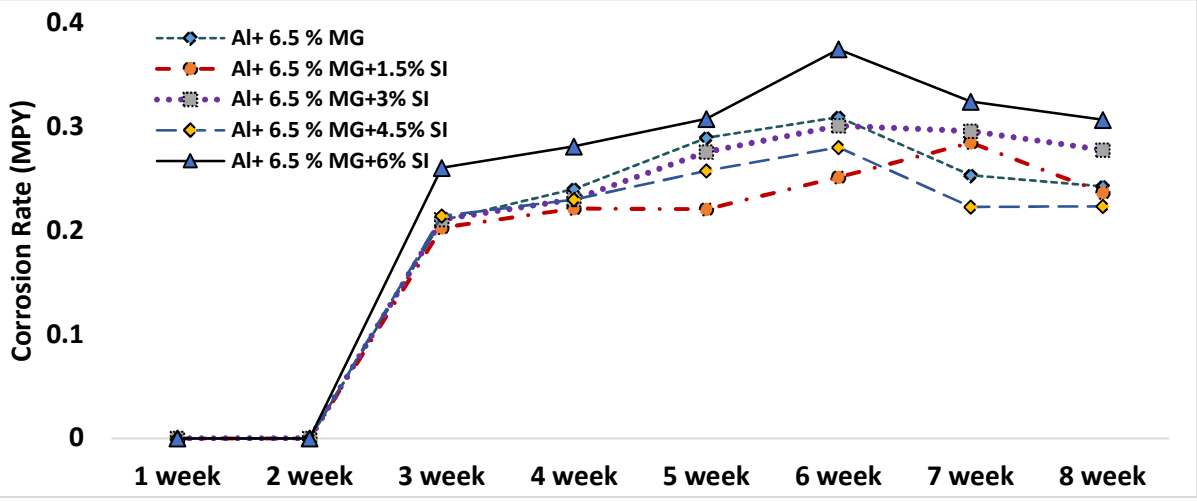

Figure 4.13 Variation of corrosion rates over time for Al-6.5 %Mg alloys with different Si contents measured using the standard weight loss method in 3.5 % NaCl solution.

The addition of 1.5 wt.% Si results in a similar corrosion trend, with a marginally reduced peak corrosion rate of 0.28 mpy observed at seven weeks. This suggests that low silicon addition does not adversely affect corrosion behavior and may even contribute to improved stability. In contrast, alloys containing higher silicon contents (3.0, 4.5, and 6.0 wt.%) exhibit progressively higher corrosion rates. The Al-6.5Mg-6%Si alloy shows the highest corrosion rate, reaching approximately 0.37 mpy at six weeks and maintaining an elevated rate thereafter. These results indicate that while the base Al-6.5Mg alloy and the 1.5% Si variant maintain consistent corrosion behavior, higher silicon additions accelerate corrosion.

The observed corrosion trends can be directly correlated with the morphology and distribution of the Mg_2Si phase in the as-cast microstructure. At lower silicon contents, Mg_2Si particles are fine and uniformly dispersed within the aluminum matrix, minimizing potential differences and reducing micro-galvanic coupling as shown in Figure 4.1. This microstructural condition promotes relatively uniform corrosion. With increasing silicon content, Mg_2Si particles become coarser and tend to form semi-continuous or network-like structures along grain boundaries. These continuous Mg_2Si morphologies act as preferential cathodic sites, enhancing micro-galvanic interactions between the Mg_2Si phase and the α-Al matrix, thereby accelerating localized corrosion. Similar observations have been reported in earlier studies, which indicate that fine Mg_2Si dispersions favor uniform corrosion, whereas interconnected networks promote localized attack. [156,157]

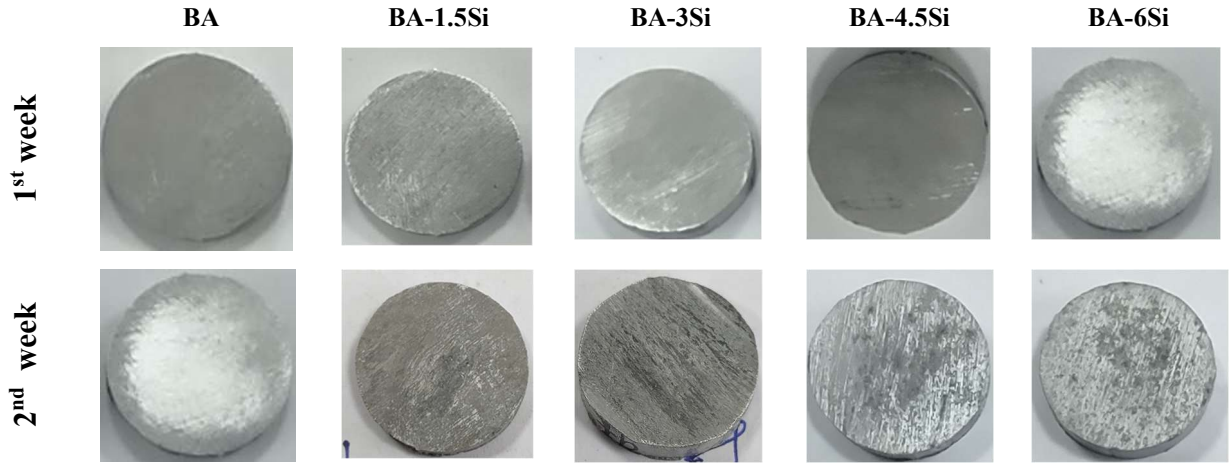

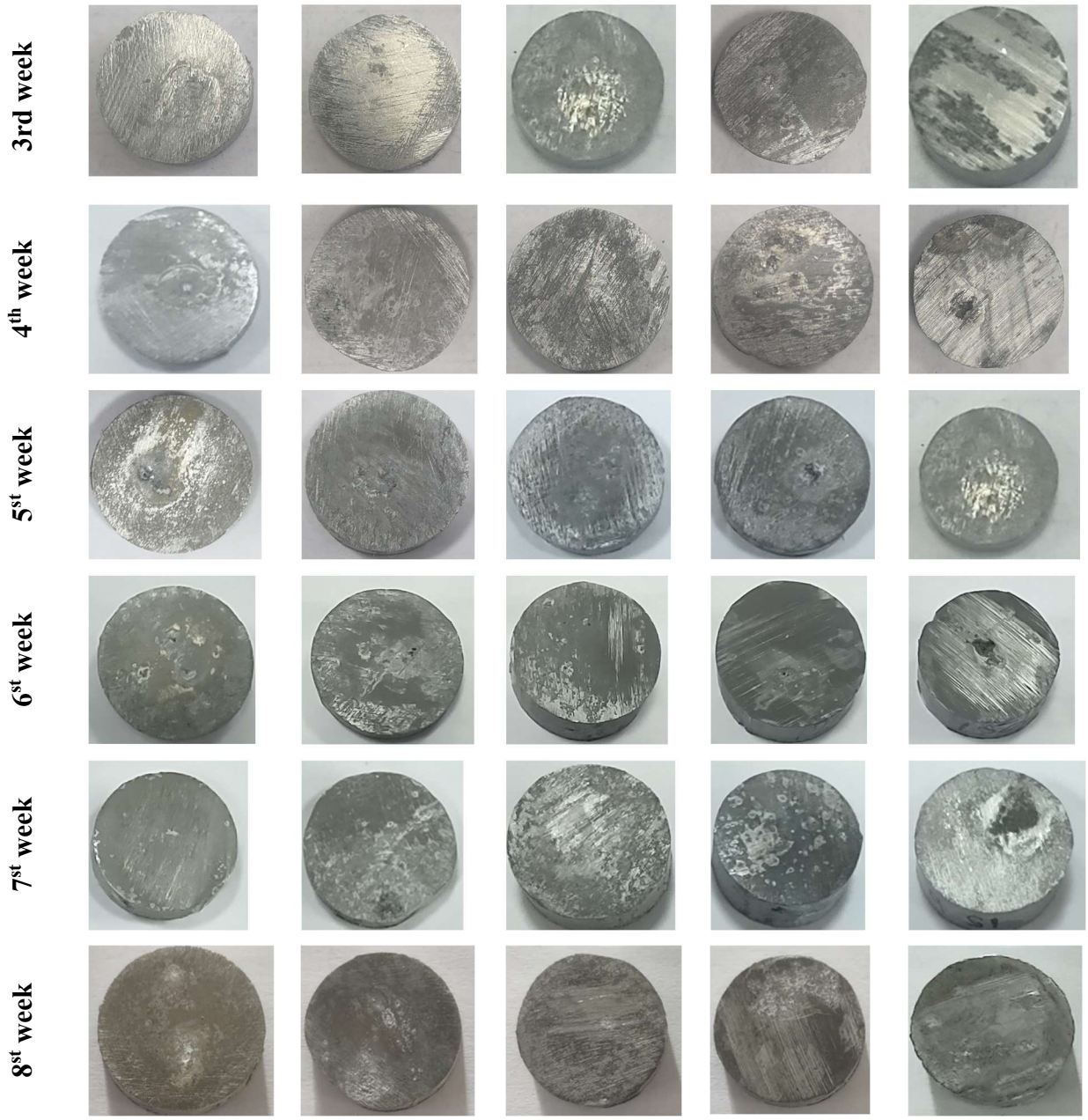

Figure 4.14 Surface morphologies of Al–6.5Mg–xSi alloys in the as-cast condition after weekly exposure to the corrosive medium.

Surface examinations were conducted after each week of exposure, and the resulting surface morphologies are presented in Figure 4.14. Surface examination after two weeks of exposure reveals the initiation of pitting, which becomes more pronounced with increasing exposure time and silicon content. The surface morphology images presented in Figure 4.14 are intended for qualitative assessment of the corrosion behavior. Quantitative image analysis of the corroded area

was not carried out in the present work. Further surface examination was carried out using a digital microscope at 72× magnification on samples exposed for six weeks, during which pit size measurements were also performed; the corresponding surface features and pit characteristics are shown in Figure 4.15.

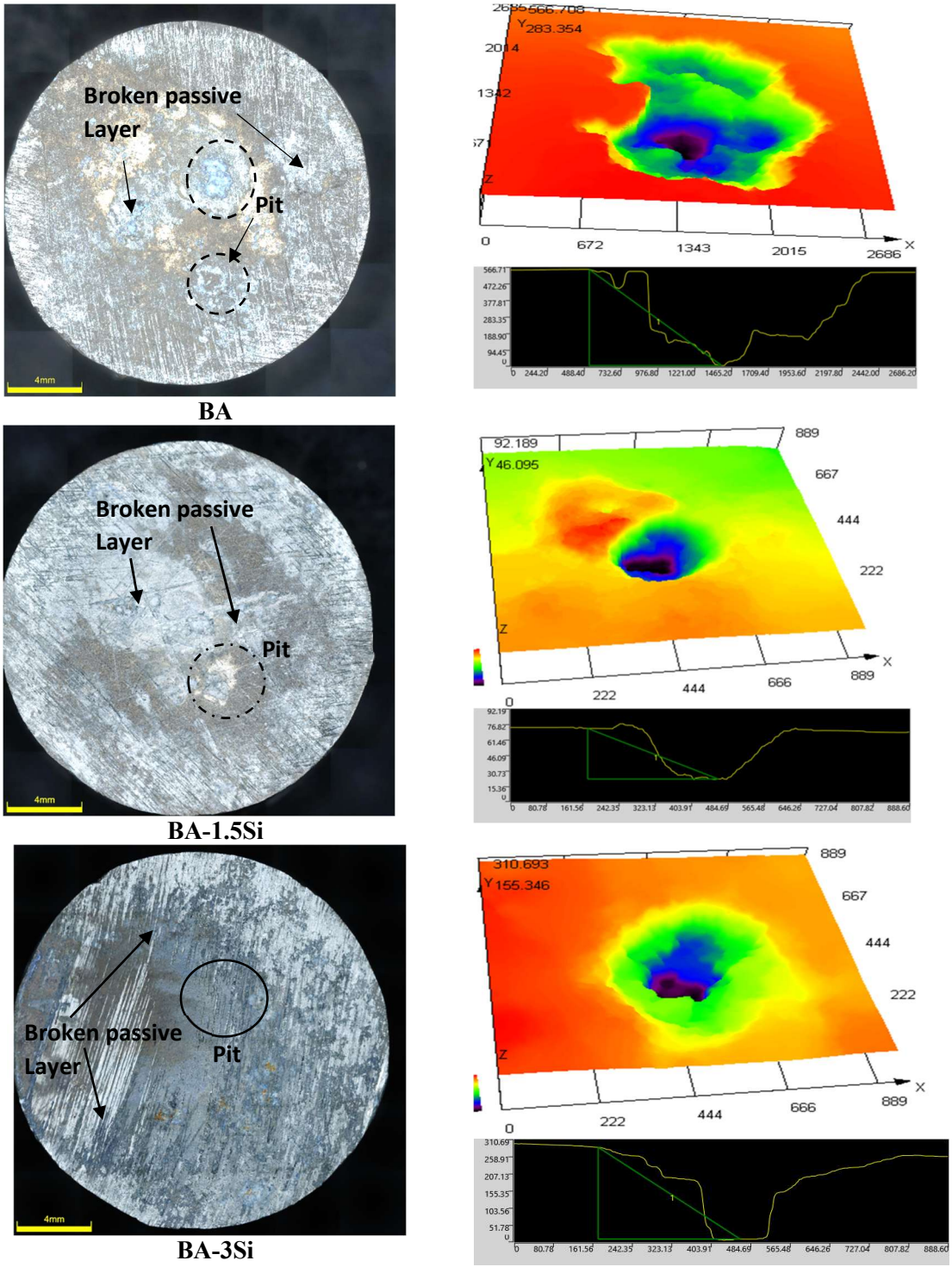

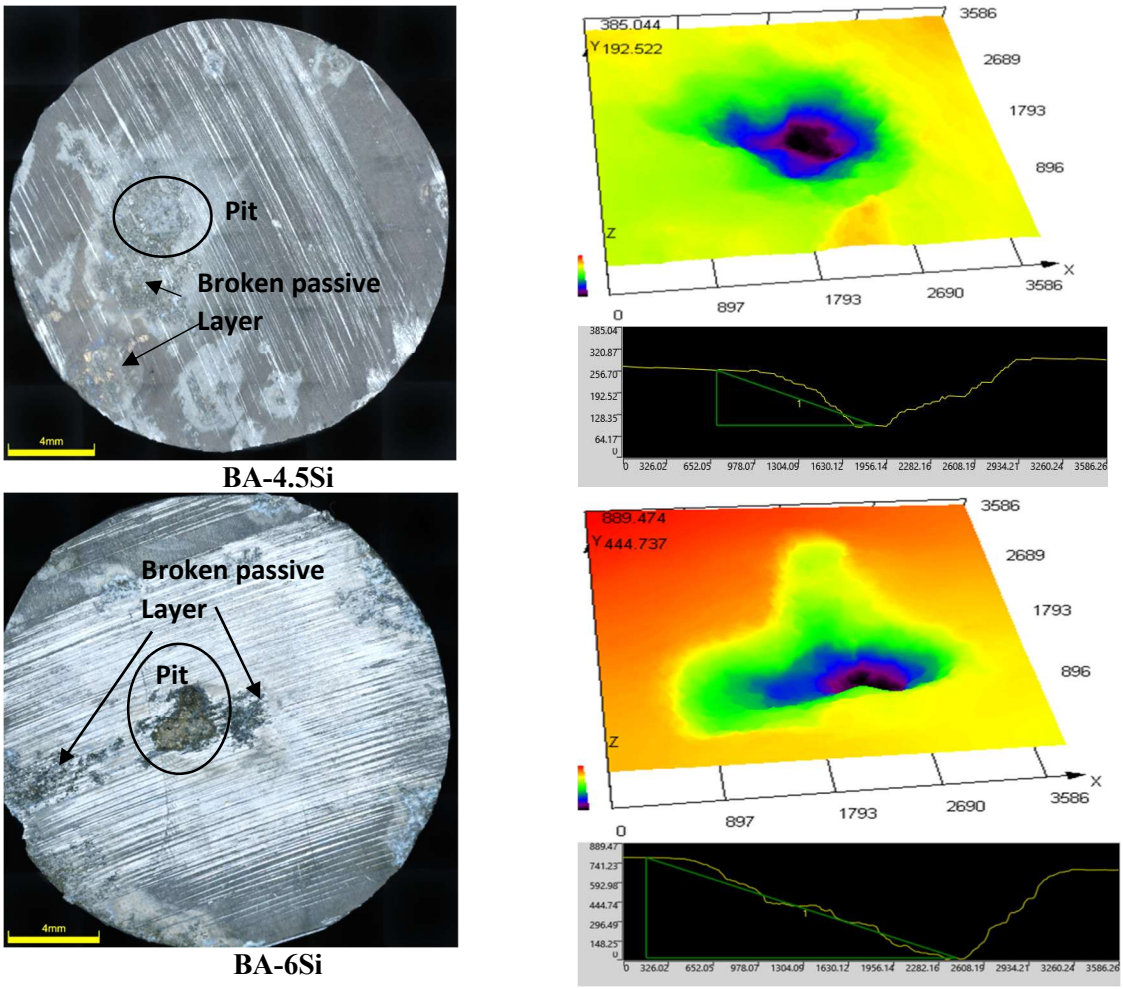

Figure 4.15 Surface morphology and pit dimension measurements of Al–6.5 %Mg–xSi alloys after 6 weeks of exposure to 3.5 % NaCl solution.

Pit size measurements show a wide variation in pit width and depth among different alloy compositions. This variation highlights the strong influence of silicon content on surface morphology and localized corrosion susceptibility in the as-cast Al–6.5Mg–xSi alloys.

Pitting corrosion in aluminum alloys is a complex phenomenon influenced by several factors, including pH, temperature, aggressive ions, and surface condition. [158] The breakdown of the naturally formed oxide film has been attributed to penetration, film-breaking, and adsorption mechanisms, as widely discussed in the literature. [159,160] Pitting typically proceeds through initiation and growth stages, during which chloride ions adsorb onto and penetrate the oxide layer, leading to localized film rupture and sustained metal dissolution. [161,162]

In aluminum alloys containing intermetallic phases, pit development is further influenced by the electrochemical behavior of these particles, which may act as anodic or cathodic sites relative to the surrounding matrix. [95] Two dominant pit morphologies are generally observed: circumferential pits, resulting from localized matrix dissolution around cathodic particles, and selective dissolution pits, where intermetallic particles dissolve or detach from the matrix. These pit morphologies reflect the combined effects of galvanic coupling, local pH variations, and intermetallic activity, all of which play a crucial role in determining corrosion performance. [95,163]

4.5.2 Corrosion Study by Weight Loss Method – Heat Treated Condition (T6)

To evaluate the corrosion behavior of heat-treated Al-6.5%Mg-xSi sacrificial anodes in heat treated condition, a standard weight loss method was employed over an exposure period of eight weeks. Corrosion rates were calculated in terms of mils per year (MPY) at weekly intervals, allowing assessment of the onset and progression of corrosion with exposure time. The measured corrosion rate data for all heat-treated alloy compositions are summarized in Table 4.7.

The corrosion behavior of the Al.6.5Mg-xSi alloys in the T6 heat-treated condition shows a noticeable increase in corrosion rate compared to the as-cast state, as illustrated in Figure 4.16. This increase is attributed to the significant microstructural reconfiguration induced by solution treatment and artificial aging. Although T6 heat treatment refines the Mg_2Si phase (Figure 4.1) and improves mechanical properties (Figure 4.12), it also modifies the electrochemical characteristics of the alloy.

During T6 treatment, coarse Mg_2Si phases dissolve during solution treatment and subsequently reprecipitate as fine, point-like, and uniformly dispersed particles during aging (Figure 4.7). While this refined precipitate distribution enhances hardness, it also increases the number density of Mg_2Si matrix interfaces. These interfaces act as numerous micro-cathodic sites, intensifying micro-galvanic coupling with the α-Al matrix and thereby accelerating corrosion.

Table 4.7 Weekly corrosion rate (MPY) of Al-6.5%Mg-xSi alloys in the heat-treated (T6) condition measured using the standard weight loss method over an 8-week exposure period.

Composition	1 week	2 week	3 week	4 week	5 week	6 week	7 week	8 week
BA-1.5Si-T6	0 ± 0	0.06 ± 0.005	0.22 ± 0.010	0.24 ± 0.013	0.25 ± 0.018	0.28 ± 0.015	0.30 ± 0.020	0.26 ± 0.014
BA-3Si-T6	0 ± 0	0.07 ± 0.006	0.24 ± 0.011	0.26 ± 0.015	0.30 ± 0.019	0.33 ± 0.013	0.32 ± 0.022	0.30 ± 0.018
BA-4.5Si-T6	0 ± 0	0.06 ± 0.005	0.23 ± 0.009	0.25 ± 0.013	0.28 ± 0.017	0.31 ± 0.020	0.25 ± 0.012	0.24 ± 0.014
BA-6Si-T6	0 ± 0	0.08 ± 0.007	0.28 ± 0.014	0.30 ± 0.018	0.34 ± 0.021	0.40 ± 0.020	0.35 ± 0.017	0.34 ± 0.019

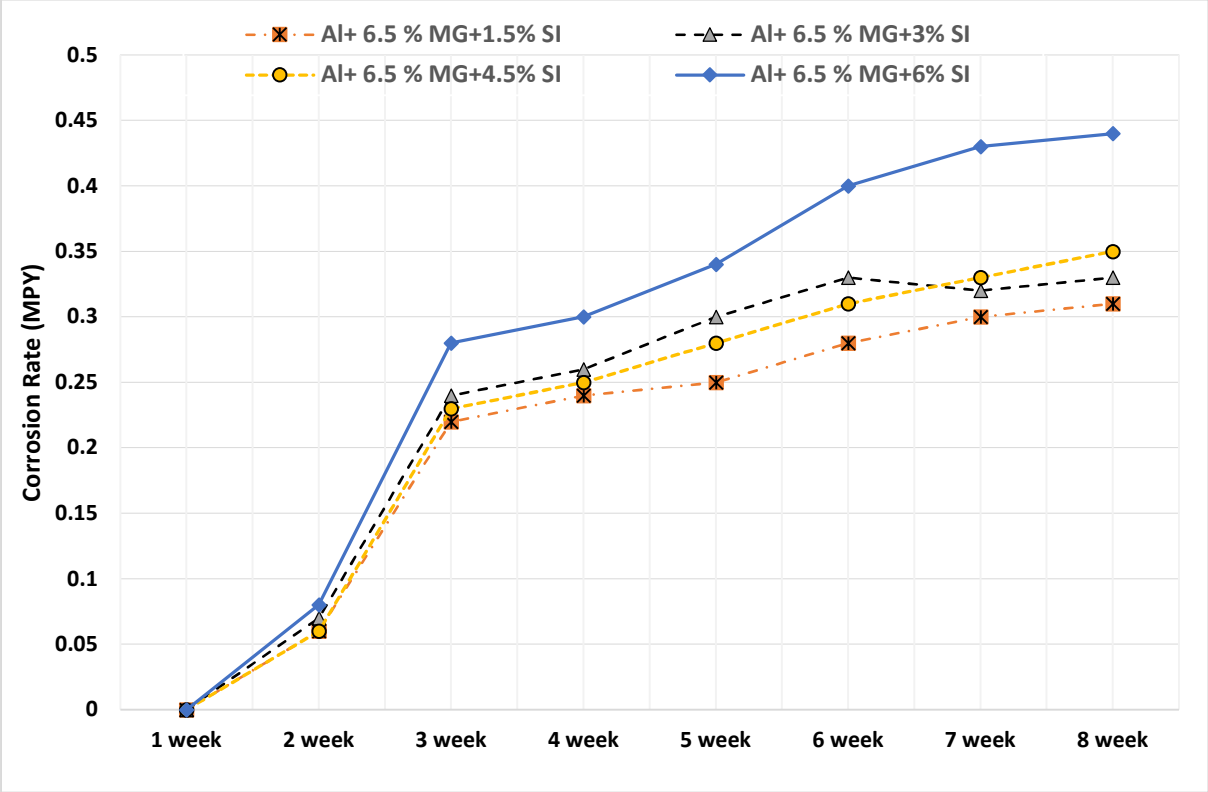

Figure 4.16 Corrosion rate variation of T6 heat-treated Al-6.5%Mg-xSi alloys with different Si contents in 3.5 %NaCl solution.

The increase in corrosion rate is more pronounced in alloys with higher silicon content, where the volume fraction of reprecipitated Mg_2Si is greater. Although the precipitates are finer than in the as-cast condition, their uniform dispersion throughout the matrix results in widespread

galvanic interactions, leading to increased general corrosion. This behavior explains the higher corrosion rates observed in heat-treated alloys compared to their as-cast counterparts.

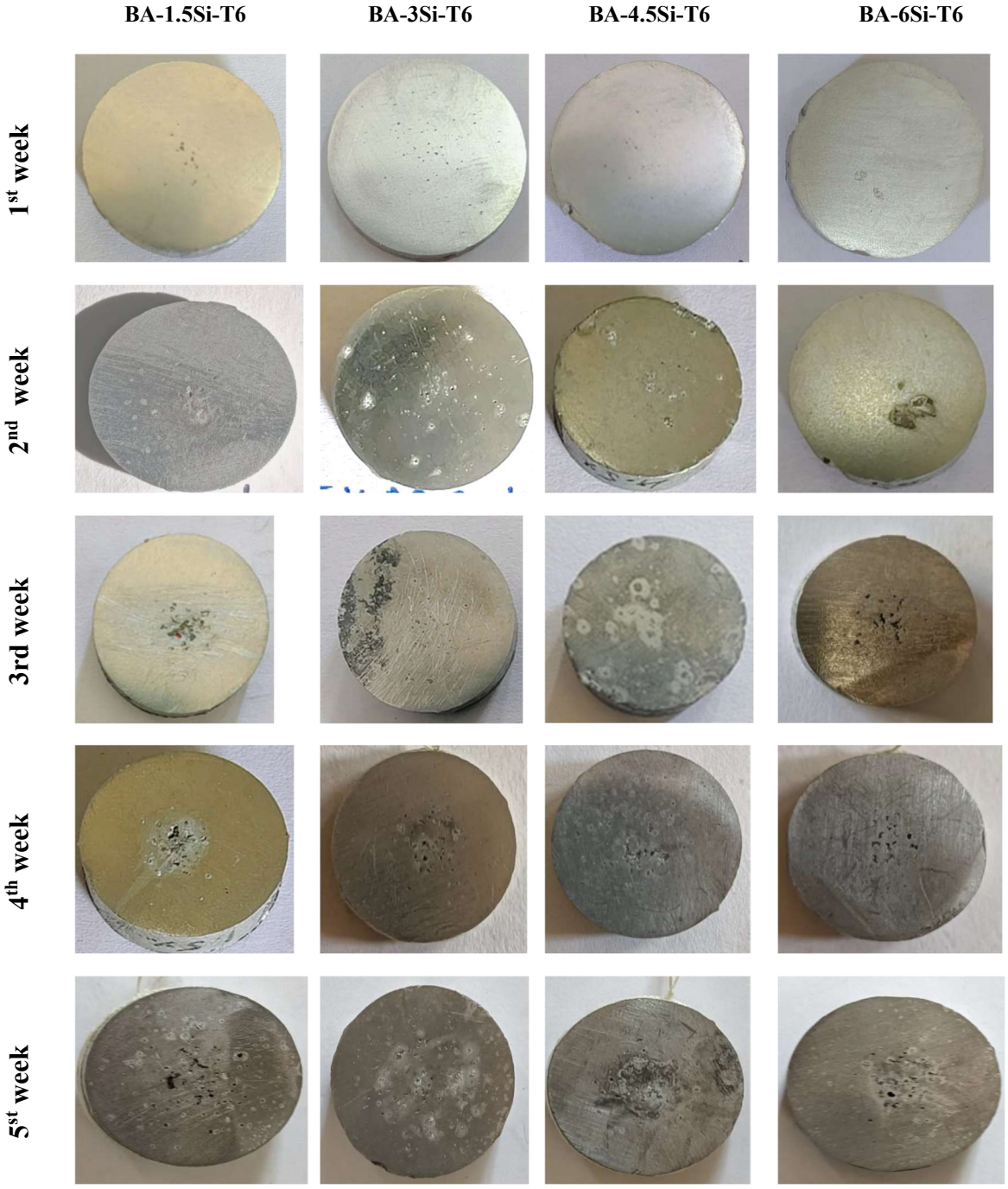

Figure 4.17 Surface morphologies of Al–6.5Mg–xSi alloys in the heat treated condition after weekly exposure to the corrosive medium.

Additionally, heat treatment alters surface properties and redistributes alloying elements within the matrix, which may further destabilize the passive oxide film and promote pit initiation. Surface observations confirm an increased density of pits in the heat-treated condition as shown in Figure 4.17, although the pits tend to be more uniformly distributed compared to the localized attack observed in as-cast high-Si alloys. This transition from localized to more uniform corrosion is characteristic of microstructures containing finely dispersed cathodic precipitates.

T6 heat treatment significantly enhances mechanical performance through precipitation strengthening, it adversely affects corrosion resistance by increasing micro-galvanic activity. These results highlight the inherent trade-off between mechanical strength and corrosion performance in Al-Mg-Si alloys and emphasize the importance of optimizing silicon content and heat treatment parameters for sacrificial anode applications.

4.5.3 Potentiodynamic Polarization Test

Potentiodynamic polarization experiments were conducted in 3.5 wt.% NaCl solution to evaluate the electrochemical corrosion behavior of Al-6.5Mg-xSi alloys in both as-cast and T6 heat-treated conditions. The polarization curves obtained from these tests in as-cast condition are presented in Figure 4.18, while the corresponding electrochemical parameters including corrosion potential (*E*corr) and corrosion current density (*I*corr) are summarized in Table 4.8 for both as-cast and T6 heat treated condition. These parameters provide direct insight into the anodic activity, driving potential, and current efficiency of the alloys when considered for sacrificial anode applications.

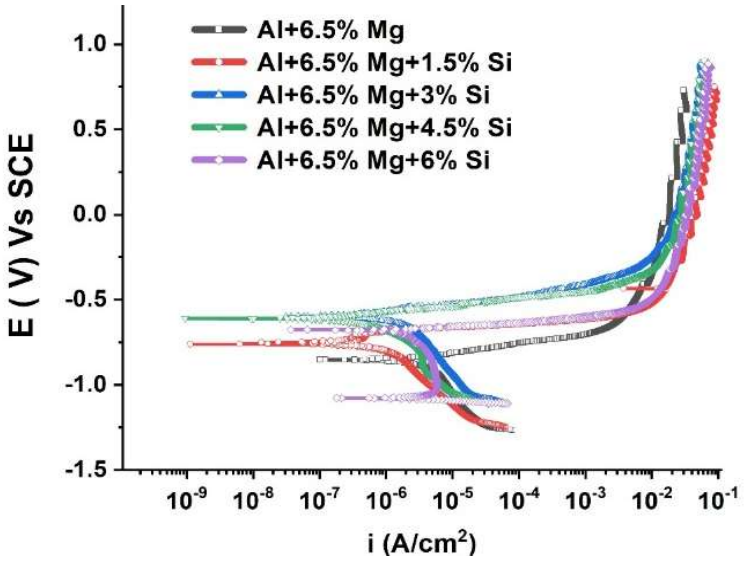

Figure 4.18 Potentiodynamic polarization curves of the developed Al-6.5Mg-xSi alloys in 3.5 % NaCl solution (As-Cast).

Table 4.8 Electrochemical corrosion parameters *E*corr and *I*corr of Al-6.5Mg-xSi alloys in as-cast and Heat-treated conditions

Name	Condition	*E*corr (mV)	*I*corr (μA/cm^2)
BA	As Cast	-852±18	1.520±0.028
Al+6.5%Mg+1.5%Si		-745.0±14	0.410±0.006
Al+6.5%Mg+3% Si		-599.0±12	1.690±0.032
Al+6.5%Mg+4.5% Si		-610±10.5	2.584±0.053
Al+6.5%Mg+6%Si		-677.0±13.5	3.620±0.072
Al+6.5%Mg+1.5%Si	Heat Treated	–955±18	7.51±0.15
Al+6.5%Mg+3% Si		–858±15	2.18±0.04
Al+6.5%Mg+4.5% Si		-1.03±18	1.30±0.021
Al+6.5%Mg+6%Si		–946±16.5	4.64±0.09

4.5.4 As-Cast Condition

In the as-cast condition, the base Al–6.5%Mg alloy exhibits a highly negative corrosion potential (-852.0 mV) with a moderate corrosion current density (1.520 μA/cm²), indicating strong anodic behavior suitable for sacrificial applications. The addition of silicon significantly influences the electrochemical response. A small Si addition (1.5%) shifts the *E*corr positively to -745.0 mV while markedly reducing *I*corr to 0.41 μA/cm², reflecting improved surface stability and reduced corrosion rate. This behavior suggests the formation of a relatively protective oxide layer supported by a fine and uniform Mg_2Si dispersion.

Further increasing the Si content to 3% results in a more noble *E*corr value (-599.0 mV), indicating enhanced corrosion resistance; however, the *I*corr increases to 1.690 μA/cm², suggesting the onset of localized electrochemical activity. At higher Si levels (4.5% and 6%), the corrosion current density increases substantially, reaching a maximum of 3.620 μA/cm² for the 6% Si alloy. Despite a moderately negative *E*corr (-677.0 mV), the high *I*corr indicates accelerated anodic dissolution. This behavior is attributed to the formation of coarse and interconnected Mg_2Si morphologies, which act as preferential electrochemical sites and promote micro-galvanic coupling with the α-Al matrix.

Pitting behavior plays a crucial role in this response. During anodic polarization, metastable pitting is observed as transient current spikes at lower potentials, while stable pits form beyond the breakdown potential, leading to sustained current increases and material loss.[164] In as-cast alloys, these pits preferentially initiate near Mg_2Si-matrix interfaces and grain boundaries where passive film continuity is disrupted.[165]

The increased current density observed for high-Si containing alloys confirms weaker passivation and a greater susceptibility to localized corrosion. The variation in electrochemical behavior of the Al-Mg-Si alloys in 3.5 wt.% NaCl solution highlights the critical role of silicon content in optimizing corrosion resistance for sacrificial anode applications. Figure 4.19 presents SEM micrographs of the Al-Mg-Si alloys after potentiodynamic polarization testing, illustrating the surface features and corrosion morphologies developed as a result of electrochemical evaluation.

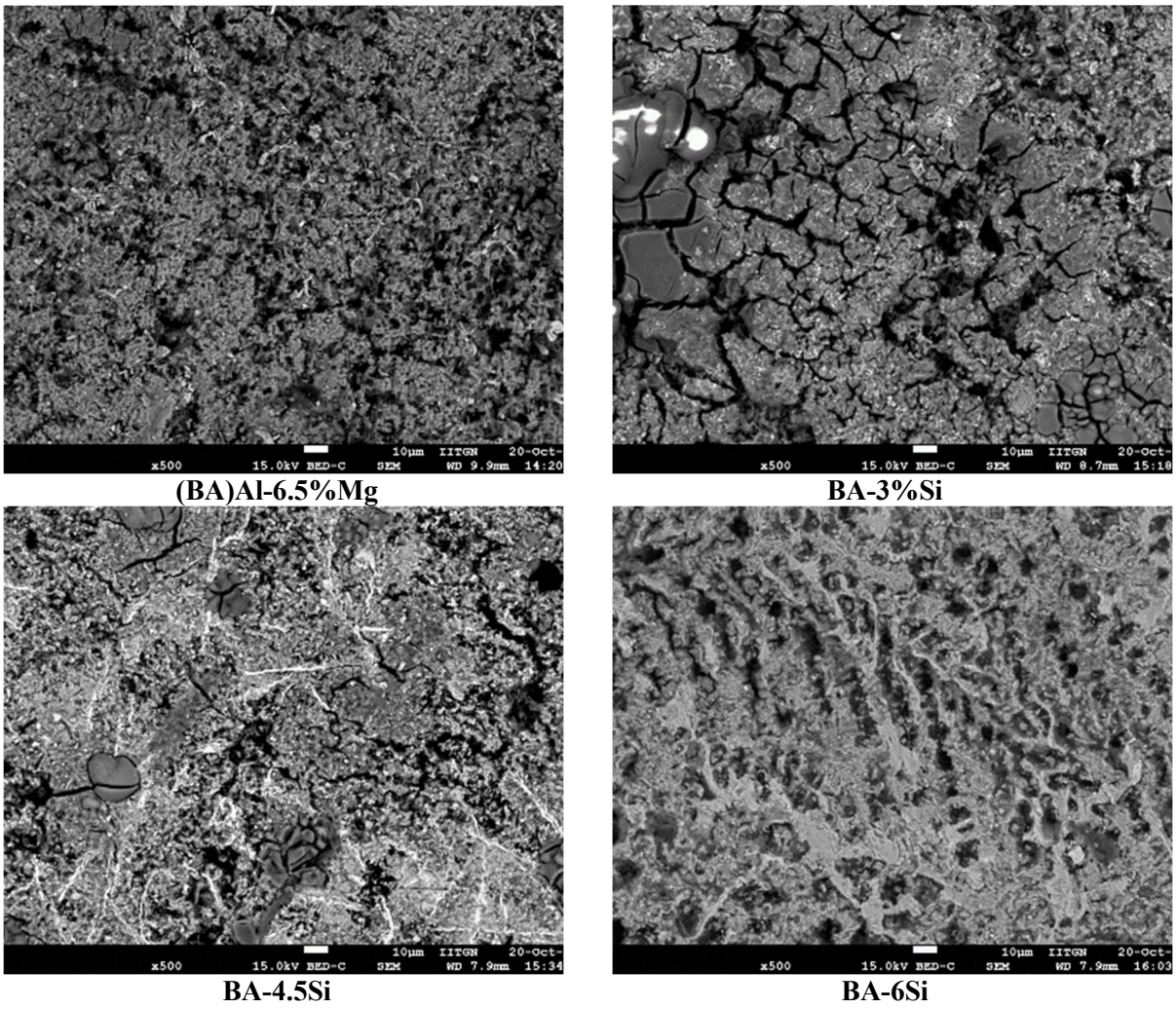

Figure 4.19 SEM images of Al-Mg-Si alloys after potentiodynamic polarization testing, showing corrosion morphology.

4.5.5 Effect of Heat Treatment (T6 Condition)

Following T6 heat treatment, all Si-containing alloys exhibit a pronounced shift in corrosion potential toward more negative values, indicating increased anodic activity. The *E*corr values shift to -955 mV, -858 mV, and -946 mV for the 1.5%, 3%, and 6% Si alloys, respectively. This shift reflects enhanced driving potential, which is beneficial for sacrificial anode performance. However, this increased activity is accompanied by higher corrosion current densities, particularly for the 1.5% Si alloy (7.51 μA/cm²) and the 6% Si alloy (4.64 μA/cm²).

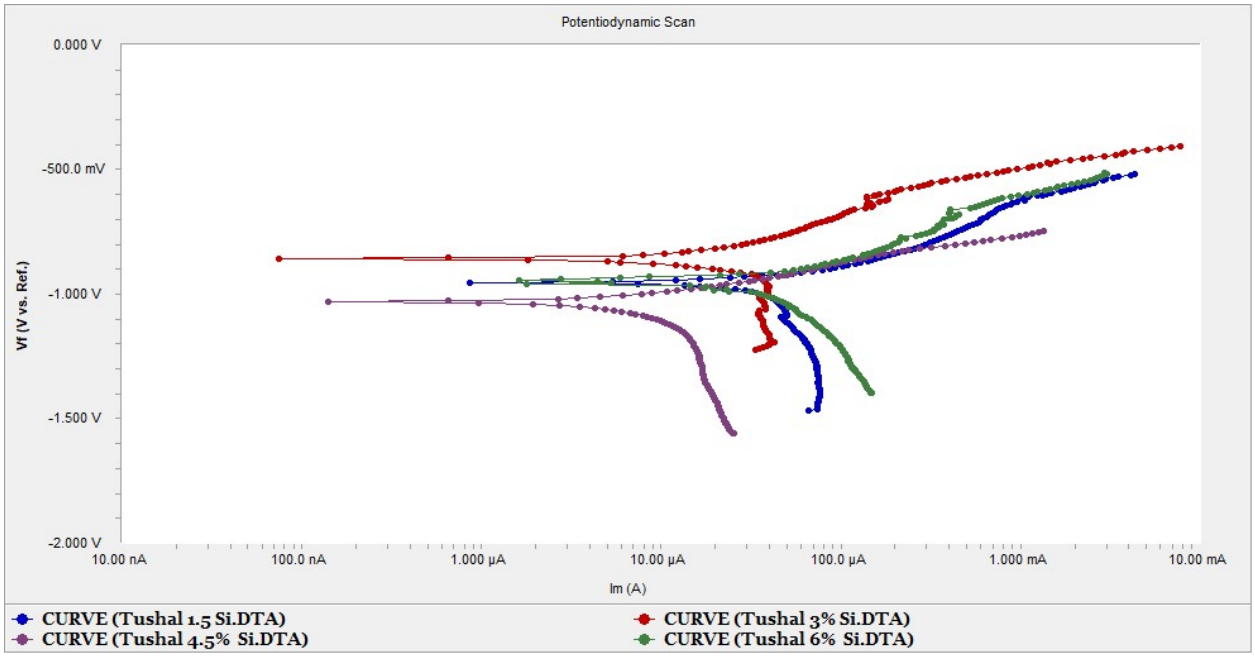

Figure 4.20 Potentiodynamic polarization curves of the developed Al-6.5Mg-xSi alloys in 3.5 % NaCl solution (T6 Heat treated).

The polarization curves obtained from these tests in the T6 heat treated condition are presented in Figure 4.20**,** while the corresponding electrochemical parameters are summarized in Table 4.8 for both the as-cast and T6 heat-treated conditions.

The increased *I*corr in the heat-treated condition is associated with microstructural refinement induced by solution treatment and aging. As discussed in Section 4.1, T6 treatment dissolves coarse Mg_2Si networks and reprecipitates them as fine, point-like, intermittently distributed particles. While this reduces the continuity of cathodic sites and promotes more uniform anodic dissolution[166], it also introduces solute-depleted zones adjacent to precipitates. These zones locally weaken passivation and contribute to more active *E*corr values and increased corrosion currents. [167–170]

4.5.6 Microstructure-Electrochemical Correlation

The electrochemical behavior observed from potentiodynamic polarization measurements shows a strong correlation with the microstructural features discussed earlier in Section 4.1 (Microstructural Evaluation) and is further supported by the weight-loss corrosion results presented in Section 4.4. Both corrosion assessment techniques consistently demonstrate that the

morphology, distribution, and continuity of the Mg_2Si phase play a decisive role in governing corrosion mechanisms in Al-6.5Mg-xSi alloys.

In the as-cast condition, coarse and morphologically heterogeneous Mg_2Si phases-appearing as flakes, rods, fibrous structures, or Chinese script networks-are distributed non-uniformly within the α-Al matrix, as shown in Section 4.1. These intermetallic phases behave first anodic and then after cathodic relative to the aluminum matrix, creating localized micro-galvanic cells at the Mg_2Si/α-Al interfaces. This localized galvanic coupling accelerates pit initiation and growth, which is reflected in both the higher corrosion current densities (*I*corr) obtained from polarization studies and the increased weight loss observed for alloys containing higher Si content. The weight-loss results further confirm that alloys with coarse and semi-continuous Mg_2Si networks exhibit higher corrosion rates and more pronounced pitting, particularly at elevated silicon levels.

In contrast, the T6 heat-treated condition exhibits a markedly refined microstructure due to the dissolution of coarse Mg_2Si during solution treatment and its subsequent reprecipitation as fine, point-like, and intermittently distributed particles during artificial aging, as detailed in Section 4.1. This refined and scatter precipitate distribution disrupts the continuity of Mg_2Si networks, thereby increase intense localized galvanic interactions. As a result, corrosion progresses in a comparatively more uniform manner across the alloy surface, which is evident from the more evenly distributed surface attack observed during post-corrosion examinations Figure 4.17.

However, despite improved corrosion uniformity, both polarization and weight-loss results indicate an increase in overall anodic activity in the heat-treated condition. The more negative *E*corr values and higher *I*corr values obtained after T6 treatment are attributed to the formation of solute-depleted zones adjacent to the reprecipitated Mg_2Si particles. These zones locally weaken the passive film and facilitate anodic dissolution over a larger surface area, leading to higher cumulative weight loss despite the absence of severe localized attack. [167]

The combined electrochemical and gravimetric corrosion results demonstrate that silicon content and heat-treatment-induced microstructural refinement jointly control the corrosion mechanism, anodic efficiency, and operational stability of Al-Mg-Si sacrificial anodes. An optimized balance between Mg_2Si morphology, distribution, and continuity is therefore essential to achieve controlled anodic dissolution without excessive localized corrosion. Similar microstructure-dependent electrochemical behavior has been widely reported in Al-Si alloy systems, where compositional

and precipitation effects govern *E*corr and *I*corr responses under chloride environments. [137,171,172].

4.5.7 Corrosion Mechanism in Al–Mg–Si Alloys

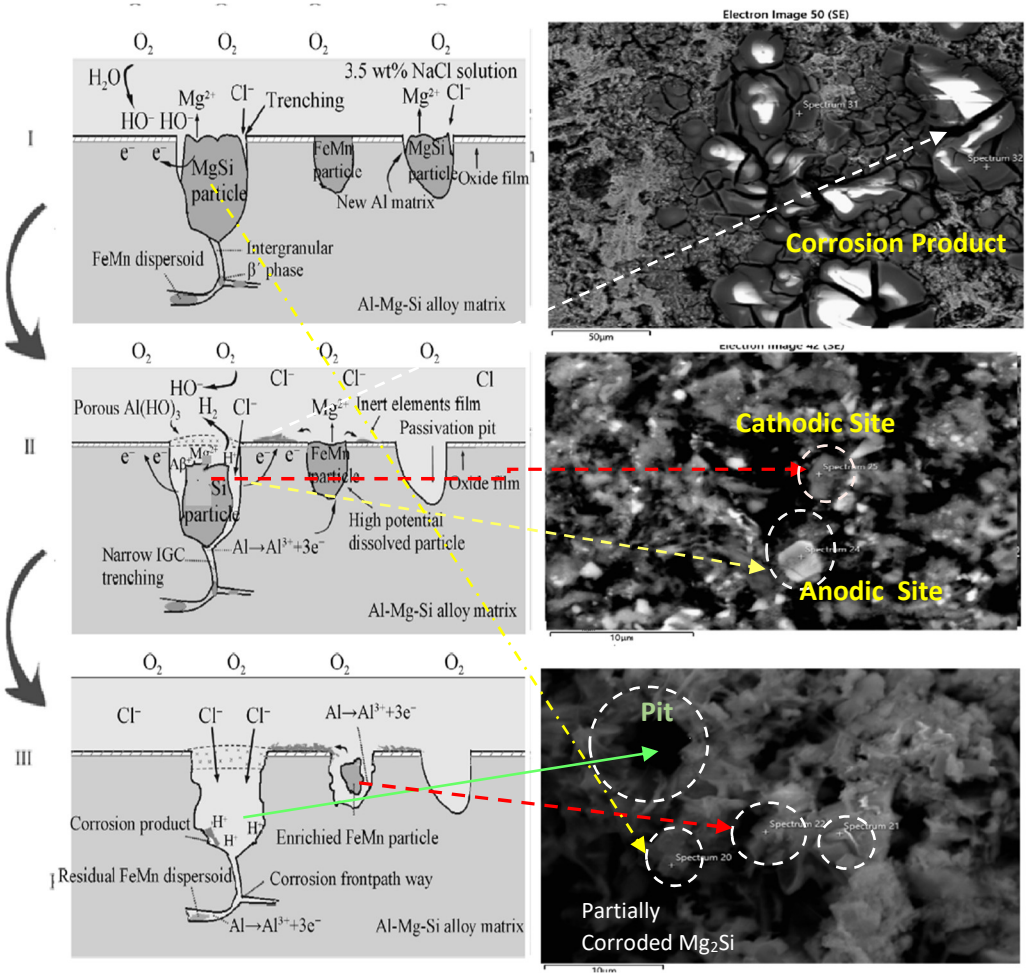

Figure 4.21 Schematic illustration of the corrosion mechanism in Al-Mg-Si alloys exposed to chloride solution. The yellow line marks initial anodic sites that later become cathodic regions (red line). Representative SEM images support the proposed mechanism. [173]

A proposed corrosion mechanism of Al–Mg–Si alloys in chloride-containing environments is schematically presented in Figure 4.21. The schematic represents a possible sequence of corrosion initiation and propagation based on the experimental observations obtained in the present study together with the corrosion mechanisms reported in the literature. It is intended to provide a conceptual interpretation rather than direct evidence of the cross-sectional corrosion morphology. The schematic suggests that corrosion may initiate at Mg_2Si particles, followed by propagation

into the surrounding α-Al matrix as a result of chloride ion penetration and localized breakdown of the protective oxide film. Since cross-sectional SEM observations were not performed in the present investigation, the proposed mechanism should be considered as a plausible interpretation based on surface morphological evidence and published literature. The mechanistic interpretation is further supported by EDS point analysis, presented in Figure 4.22, which identifies the presence of magnesium, silicon, oxygen, and associated corrosion products in the corroded regions. However, the EDS analysis alone does not directly verify the cross-sectional corrosion path depicted in the schematic.

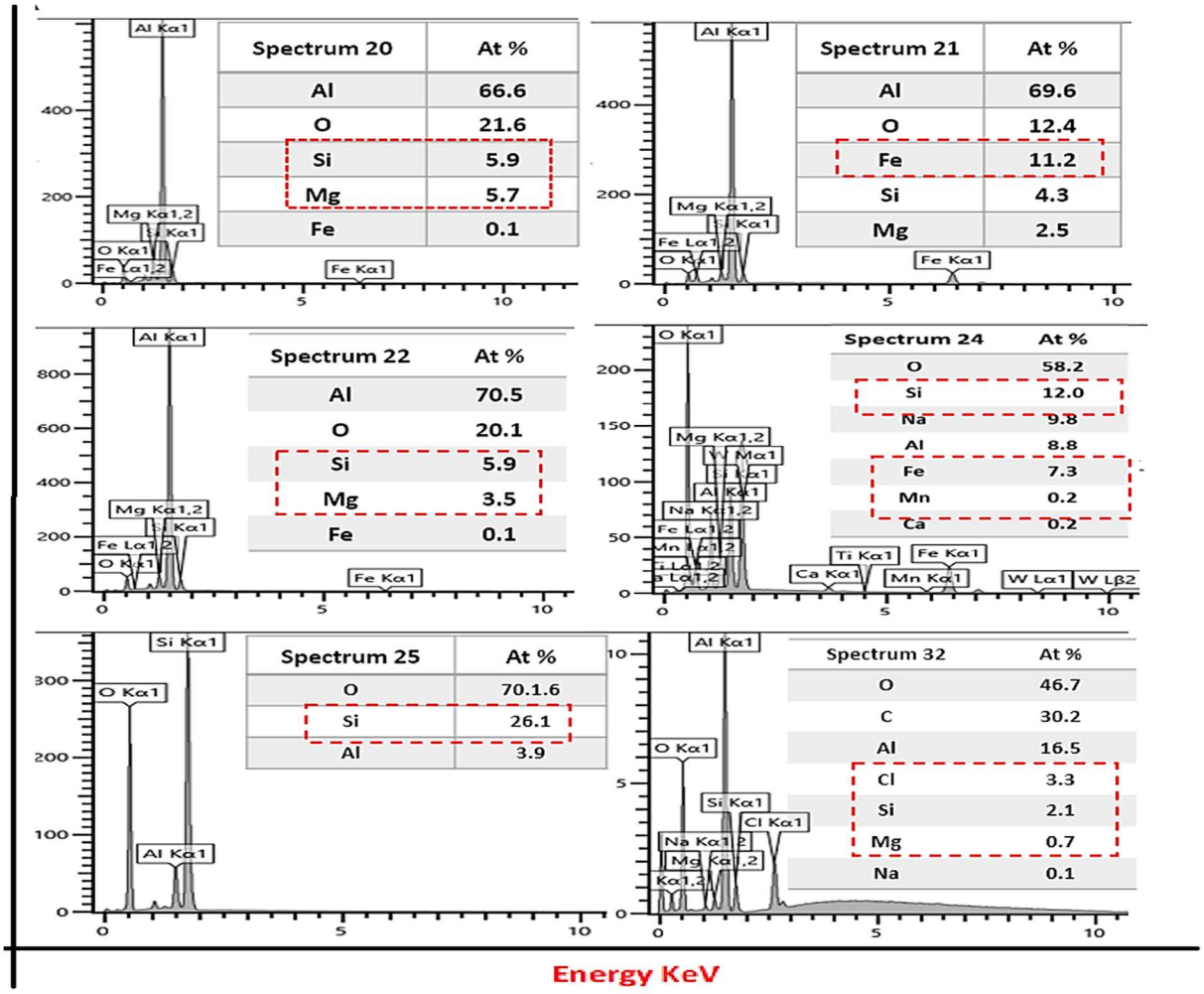

Figure 4.22 EDS point analysis of different particles in Al-Mg-Si alloys after potentiodynamic polarization testing, identifying elemental composition.

Corrosion in Al-Mg-Si alloys typically initiates when chloride ions infiltrate the alloy surface through microstructural heterogeneities such as surface defects, grain boundaries, or regions adjacent to intermetallic particles. This susceptibility arises primarily from variations in the size, morphology, and spatial distribution of Mg_2Si and Al-Fe-Si intermetallic phases, which create localized electrochemical potential differences within the matrix. [173] As observed in Figures 4.1 and 4.5**,** alloys containing fine, uniformly distributed, and relatively spheroidal Mg_2Si particles-typically associated with lower silicon content-exhibit delayed corrosion initiation and a more uniform corrosion pattern. In contrast, alloys with coarser or partially interconnected Mg_2Si networks, common at higher silicon contents, show earlier pit nucleation, faster propagation rates, and deeper localized attack. These observations suggest establish a clear mechanistic relationship between Mg_2Si morphology and corrosion behavior.

The corrosion process in Al-Mg-Si alloys generally progresses through two distinct stages: initiation and propagation. During the initiation stage, corrosion preferentially begins at the Mg_2Si particle–matrix interface, where localized galvanic coupling accelerates dissolution of the adjacent aluminum matrix. Initially, Mg_2Si particles may behave anodically relative to the α-Al matrix, as indicated by the yellow-marked regions in Figure 4.21**,** leading to selective magnesium leaching. This process alters the local electrochemical environment and shifts the Mg_2Si phase toward cathodic behavior, as marked by the red regions in the schematic. The increase in anodic driving potential during this transition accelerates localized corrosion; however, as the reactive Mg content within Mg_2Si diminishes, the overall corrosion rate may gradually decrease.

With continued exposure, the corrosion mechanism is proposed to transition from selective magnesium dissolution within Mg_2Si particles to anodic dissolution of the aluminum matrix surrounding silicon-enriched inclusions. [49,92] Insoluble corrosion products, such as $Mg(OH)_2$, accumulate near pit openings and contribute to the formation of occluded cells. These localized environments trap chloride ions, reduce local pH, and promote autocatalytic corrosion along grain boundaries, thereby sustaining pit growth. [49] Prolonged exposure may further result in positive shift in the electrochemical potential of Mg_2Si particles, transforming previously corroded precipitates into cathodic sites relative to the surrounding aluminum matrix. [173] Recent studies have confirmed the time-dependent electrochemical behavior of Mg_2Si, demonstrating that initially anodic precipitates become increasingly silicon-enriched as magnesium is leached,

emphasizing the dynamic and evolving nature of corrosion mechanisms in Al-Mg-Si alloys.[174–176]

To further elucidate the role of silicon in governing corrosion behavior, the developed alloys were systematically correlated in terms of Mg_2Si characteristics, hardness, and corrosion response. As summarized in Table 4.9**,** variations in silicon content directly influence the size, morphology, and distribution of Mg_2Si phases (Figure 4.5), which in turn affect both mechanical and electrochemical performance.

Table 4.9 Relationship between Mg_2Si characteristics, hardness, and corrosion behavior of developed Al-6.5%Mg-Si alloys in as-cast condition.

Alloy Composition	Hardness (BHN)	Mg_2Si Characteristics	Corrosion Initiation	Pit Morphology
BA-1.5Si	82 ± 1.9	Fine, uniformly distributed flake type Mg_2Si (Figure 4-5a)	Numerous anodic sites; rapid initiation	Shallow, widespread pits
BA-3Si	67 ± 1.7	Coarser, rod like Mg_2Si with moderate distribution (Figure 4-5b)	Preferential initiation at particle–matrix interfaces	Deep, isolated pits
BA-4.5Si	70 ± 1.7	Coarse, clustered fibrous Mg_2Si, partially interconnected (Figure 4-5c)	Multiple initiation sites but slower onset	Larger, semi-interconnected cavities
BA-6Si	83 ± 1.7	High density, clustered Chinese script type Mg_2Si (Figure 4-5d)	Rapid initiation across numerous sites	Interconnected corrosion cavities

The Brinell hardness values obtained in the present investigation reflect the combined influence of the α-Al matrix, solid-solution strengthening by magnesium, and the size, morphology, and distribution of the Mg_2Si and Al_3Mg_2 intermetallic phases. Therefore, the measured hardness represents the overall bulk mechanical response of the alloy rather than the hardness of individual constituent phases. Similar findings have been reported by Polmear et al. [156], Totten and MacKenzie [157], and Mondolfo [158], who demonstrated that the combined effects of matrix

strengthening and Mg_2Si precipitation govern the mechanical behaviour of Al–Mg–Si alloys. The present results further indicate that the evolution of Mg_2Si morphology strongly influences both the mechanical and electrochemical performance of the alloys. Fine and uniformly dispersed Mg_2Si particles in the 1.5 wt.% Si alloy produced higher hardness together with relatively rapid but shallow corrosion initiation. In contrast, alloys containing intermediate silicon contents (3 and 4.5 wt.% Si) exhibited coarser and partially clustered Mg_2Si morphologies, resulting in reduced hardness and increased susceptibility to deeper localized pitting due to enhanced galvanic interactions between the intermetallic phases and the surrounding α-Al matrix. At the highest silicon content (6 wt.% Si), hardness increased again owing to the higher volume fraction of Mg_2Si; however, prolonged exposure to chloride-containing environments promoted interconnected pit formation and the gradual anodic-to-cathodic transformation of Mg_2Si particles, thereby accelerating localized corrosion. Consequently, higher hardness did not necessarily correspond to superior sacrificial anode performance. Instead, the optimum alloy performance was governed by a balanced combination of mechanical strength and electrochemical activity, which depended primarily on the morphology, size, and distribution of Mg_2Si rather than hardness alone. Overall, the corrosion mechanism in Al–Mg–Si alloys is controlled by the complex interplay between microstructural evolution, intermetallic phase chemistry, and electrochemical interactions in chloride media. These findings are consistent with previous studies, which have established that optimization of Mg_2Si characteristics through appropriate alloy design and processing is essential for simultaneously achieving enhanced mechanical properties, controlled corrosion behaviour, and improved sacrificial anode performance in Al–Mg–Si alloys [49,117,155–158].

4.6 Anode Performance Measurement

The sacrificial anode performance of the Al-6.5Mg-xSi alloys was evaluated in accordance with DNV RP B401, using anode capacity and consumption rate as the primary performance indicators. These parameters provide a practical, application-oriented validation of the electrochemical behavior discussed in the previous section.

The trends observed in the potentiodynamic polarization and weight-loss corrosion studies are directly reflected in the anode performance results. Alloys exhibiting higher corrosion current densities and weaker passivation showed increased consumption rates, while compositions with

more stable electrochemical behavior demonstrated improved anode efficiency. The influence of Si content and T6 heat treatment on dissolution behavior is therefore critical in controlling both capacity and service life of the sacrificial anodes.

Table 4.10 summarizes the complete experimental data and calculated electrochemical performance parameters for both as-cast and T6 heat-treated Al-6.5Mg-xSi alloys, highlighting the role of microstructural modification on anode efficiency and consumption characteristics under simulated service conditions.

T6 heat-treated alloys exhibit slightly lower anode capacities and marginally higher consumption rates compared to their as-cast counterparts, indicating that microstructural refinement and precipitation hardening promote more uniform but accelerated dissolution. This behavior is consistent with the reduced passivation stability and enhanced electrochemical activity observed in the polarization studies.

A clear correlation is observed between the weight-loss corrosion data (Tables 4.6 and 4.7), the electrochemical parameters obtained from potentiodynamic polarization (Table 4.8), and the sacrificial anode performance characteristics (Table 4.10). Alloys exhibiting higher corrosion current densities (*I*corr) and higher long-term corrosion rates during immersion testing consistently show increased anode consumption rates during galvanostatic evaluation, confirming coherence between short-term electrochemical response and cumulative material loss.

Table 4.10 Experimental data and electrochemical performance parameters for as-cast and T6 heat treated Al-6.5Mg-Si sacrificial anodes

Sr. No	Alloy Name	Surface Area (mm^2)	Anode sample			Wt. of copper coulometers in gm			Anode capacity (Amp.hr /kg)	Consu-mption Rate kg/Amp*year
			Initial Wt (gm)	Final Wt (gm)	Wt loss (gm/ cm^2)	Initial Wt (gm)	Final wt (gm)	Difference (gm)		
as -cast										
1	BA	16.010 ± 0.061	15.667 ± 0.060	14.265 ± 0.058	8.757 ± 0.050	0.321 ± 0.001	4.811 ± 0.025	4.490 ± 0.024	2701.5 ± 19.5	3.24 ± 0.03

2	BA-1.5Si	16.170 ± 0.108	16.837 ± 0.057	15.932 ± 0.061	5.597 ± 0.033	0.300 ± 0.001	2.593 ± 0.008	2.293 ± 0.008	2136.7 ± 20.5	4.09 ± 0.04
3	BA-3Si	15.860 ± 0.114	16.661 ± 0.071	15.608 ± 0.064	6.639 ± 0.033	0.310 ± 0.001	2.496 ± 0.017	2.186 ± 0.017	1750.0 ± 16.0	5.00 ± 0.05
4	BA-4.5Si	15.860 ± 0.056	17.115 ± 0.042	15.373 ± 0.039	10.984 ± 0.082	0.313 ± 0.001	3.666 ± 0.012	3.353 ± 0.011	1623.9 ± 7.6	5.39 ± 0.04
5	BA-6Si	15.860 ± 0.056	15.801 ± 0.073	14.666 ± 0.078	7.156 ± 0.049	0.319 ± 0.001	4.063 ± 0.024	3.744 ± 0.024	2781.5 ± 24.1	3.14 ± 0.02
T6 heat treated										
6	BA-1.5Si-T6	15.86 ± 0.101	12.843 ± 0.06	11.460 ± 0.05	8.720 ± 0.03	0.329 ± 0.001	3.832 ± 0.018	3.503 ± 0.018	2135.8 ± 25.7	4.10 ± 0.04
7	BA-3Si-T6	15.56 ± 0.102	14.096 ± 0.06	12.810 ± 0.07	8.265 ± 0.03	0.325 ± 0.002	3.022 ± 0.010	2.697 ± 0.011	1769.3 ± 12.5	4.95 ± 0.05
8	BA-4.5Si-T6	16.01 ± 0.123	15.758 ± 0.06	14.036 ± 0.07	10.756 ± 0.09	0.316 ± 0.001	3.741 ± 0.021	3.425 ± 0.022	1677.4 ± 7.9	5.22 ± 0.03
9	BA-6Si-T6	16.01 ± 0.12	16.681 ± 0.04	14.972 ± 0.04	10.675 ± 0.08	0.313 ± 0.001	3.718 ± 0.025	3.405 ± 0.025	1680.1 ± 8.2	5.21 ± 0.04

Among the as-cast alloys, the Al-6.5Mg-3Si and Al-6.5Mg-4.5Si compositions display progressively higher *I*corr values (1.69 and 2.58 μA/cm², respectively) and elevated corrosion rates after prolonged exposure (up to ~0.30 MPY), which directly correspond to their higher consumption rates (5.00 and 5.39 kg/A·year) and lower anode capacities (Table 4.10). In contrast, the Al-6.5Mg-1.5Si alloy exhibits the lowest *I*corr (0.41 μA/cm²), relatively moderate corrosion rates, and a comparatively lower consumption rate (4.09 kg/A·year), indicating more controlled anodic dissolution and improved charge efficiency. The Al-6.5Mg-6Si alloy shows a distinct behavior, where a high *I*corr (3.62 μA/cm²) and elevated weight-loss corrosion rates are accompanied by a high anode capacity but a reduced consumption rate, reflecting intense but partially self-limiting anodic activity associated with dense Mg_2Si networks.

Heat treatment further intensifies these trends. T6-treated alloys exhibit markedly more negative corrosion potentials and substantially higher *I*corr values, particularly for the 1.5% Si and 6% Si alloys (7.51 and 4.64 μA/cm², respectively), which is consistent with their increased corrosion

rates during immersion and higher consumption rates during anode testing. This behavior is attributed to microstructural modification during solution treatment and aging, including Mg redistribution and refinement or reconfiguration of Mg_2Si phases, which weakens local passivation and promotes more uniform but accelerated anodic dissolution.

The combined weight-loss, polarization, and anode performance data establish a strong microstructure-electrochemical performance relationship. Silicon content governs Mg_2Si morphology and electrochemical stability, which in turn controls corrosion kinetics and sacrificial efficiency. These findings confirm that optimal sacrificial anode performance in Al-Mg-Si alloys requires a balance between sufficient anodic activity and controlled dissolution, rather than simply maximizing corrosion current density.

4.6.1 Evaluation of Anode Capacity and Consumption Rate

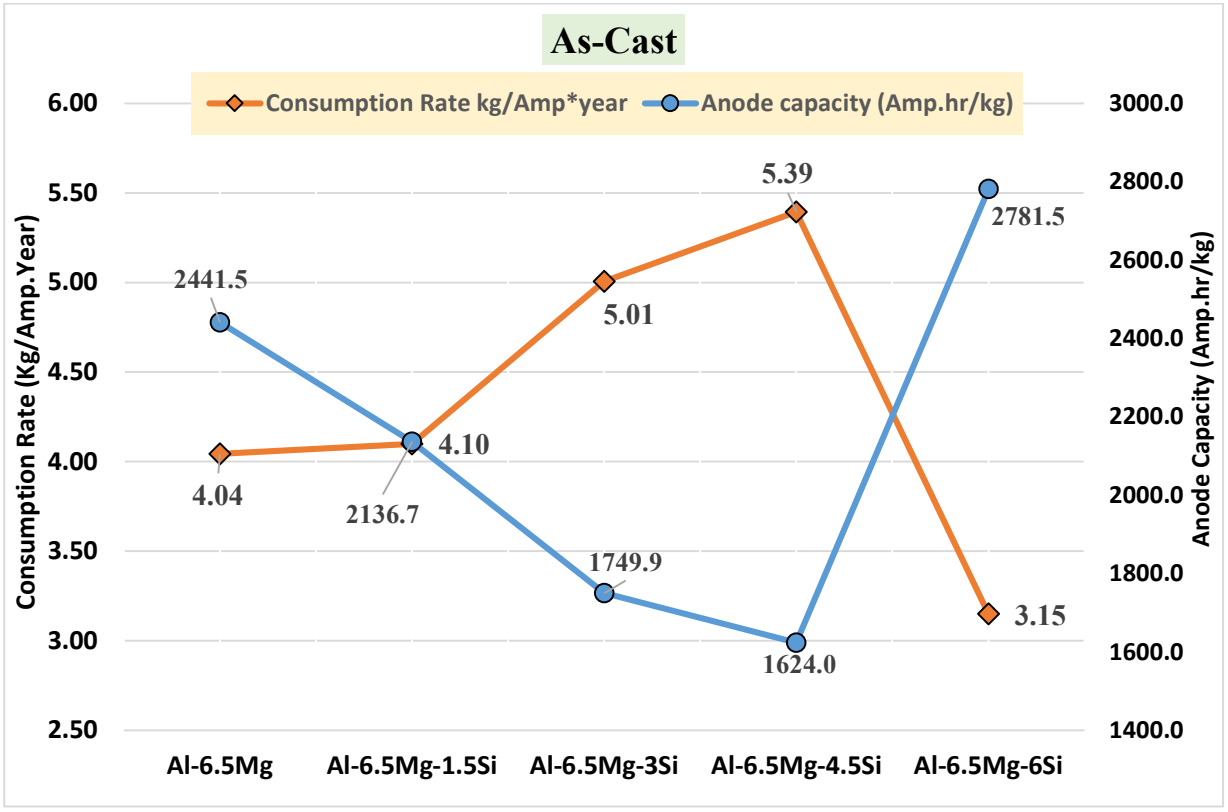

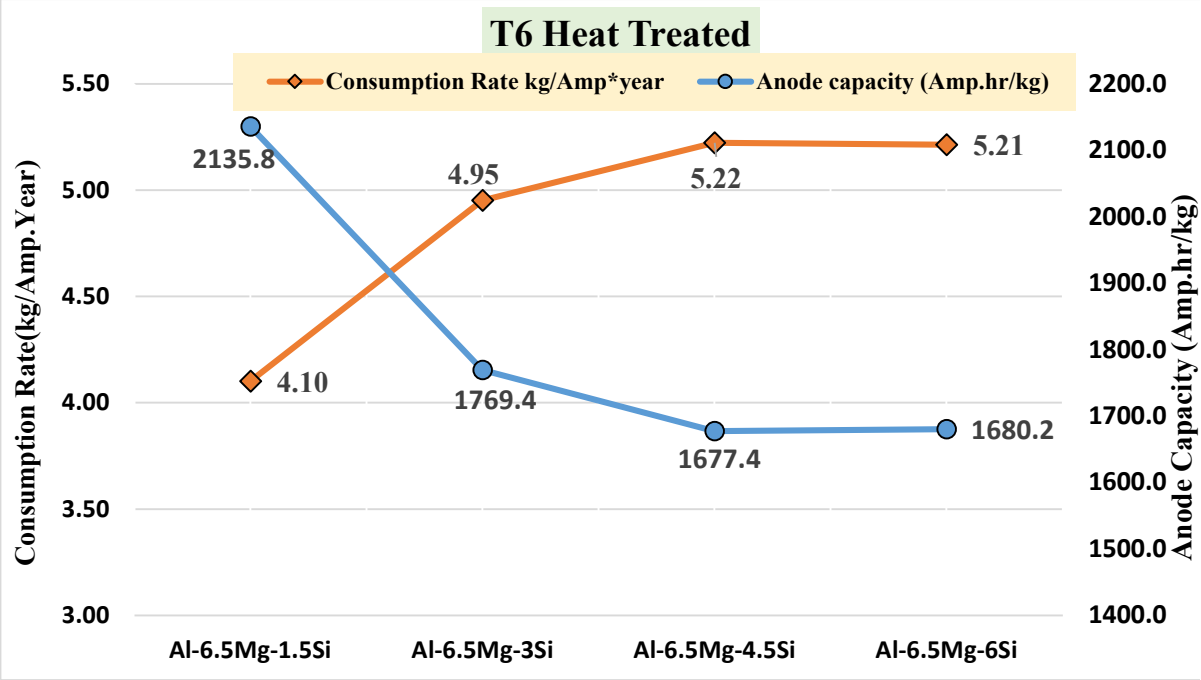

Figure 4.23 Comparison of consumption rate and anode capacity for "as-cast" and “heat treated” Al-6.5Mg-xSi alloys with varying silicon content.

The sacrificial anode performance of the Al-6.5Mg-xSi alloys exhibits a distinctly non-linear dependence on silicon content, as summarized in Table 4.10 and illustrated in Figure 4.23. In the as-cast condition, increasing Si content from 1.5% to 3% results in a marked decline in anode capacity from 2136.7 to 1749.9 A·h/kg, accompanied by an increase in consumption rate from 4.09 to 5.00 kg/A·year. This degradation becomes more pronounced at 4.5% Si, where the anode capacity further decreases to 1623.9 A·h/kg and the consumption rate reaches a maximum value of 5.39 kg/A·year, indicating the least efficient utilization of material within the investigated compositional range.

The inferior performance of the intermediate-Si alloys (3% and 4.5% Si) is attributed to their characteristic microstructural features, where Mg_2Si precipitates form coarse, partially continuous lamellar and rod-like morphologies (Figure 4.1). Such interconnected intermetallic networks promote localized galvanic coupling with the α-Al matrix, leading to non-uniform dissolution and premature material loss. Similar observations have been reported by Feng-li Zeng et al., who demonstrated that coarse Mg_2Si morphologies reduce current efficiency by concentrating anodic dissolution at discrete sites rather than enabling uniform sacrificial behavior.[92] In this

compositional regime, silicon effectively behaves as a performance-degrading element by reducing the availability of electrochemically active magnesium and promoting localized corrosion.

A notable reversal of this trend is observed at the highest silicon content. The as-cast Al-6.5Mg-6Si alloy demonstrates an exceptionally high anode capacity of 2781.5 A·h/kg, significantly exceeding both the intermediate-Si alloys and the typical performance range of conventional Al-Mg sacrificial anodes (generally ≤2500 A·h/kg). Simultaneously, this alloy exhibits the lowest consumption rate among the as-cast series (3.14 kg/A·year), indicating superior anodic efficiency and extended service life potential. This unique behavior highlights that silicon content alone does not govern anode performance; rather, the specific Mg_2Si morphology and its distribution play a decisive role in determining sacrificial efficiency.

4.6.2 Influence of Heat Treatment on Anode Performance

The effect of T6 heat treatment on anode performance is strongly composition-dependent and reflects the sensitivity of Mg_2Si morphology to thermal processing. For the low-Si alloy (1.5% Si), heat treatment produces only a marginal change in anode capacity (2136.7 to 2135.8 A·h/kg) and consumption rate (4.09 to 4.10 kg/A·year), indicating that the sacrificial behavior remains largely unaffected. A similar trend is observed for the 3% Si alloy, where the consumption rate shows a slight reduction from 5.00 to 4.95 kg/A·year, suggesting limited microstructural benefit from the T6 cycle.

In contrast, the 4.5% Si alloy maintains a high consumption rate after heat treatment (5.22 kg/A·year), closely comparable to its as-cast value, confirming that the coarse Mg_2Si networks responsible for accelerated dissolution are not effectively mitigated by T6 processing. This persistence of high consumption highlights the inherent instability of intermediate-Si microstructures for sacrificial applications.

The most pronounced heat-treatment effect is observed for the Al-6.5Mg-6Si alloy. While this alloy exhibits outstanding efficiency in the as-cast condition, T6 heat treatment results in a sharp increase in consumption rate from 3.14 to 5.21 kg/A·year, representing a performance degradation of approximately 65%. This deterioration is accompanied by a substantial reduction in effective

anodic efficiency, demonstrating that the superior sacrificial behavior of the 6% Si alloy is intrinsically linked to its as-cast microstructural state. This behaviour can be attributed to the microstructural evolution occurring during solution treatment and artificial ageing. T6 heat treatment promotes the dissolution of coarse Mg_2Si particles during solution treatment, followed by the precipitation of finer Mg_2Si phases during ageing. Although these precipitates contribute to precipitation hardening and significantly improve hardness, they also increase the electrochemical heterogeneity of the alloy. The increased number of finely dispersed Mg_2Si precipitates enhances localized micro-galvanic coupling with the surrounding α-Al matrix, thereby accelerating preferential anodic dissolution and reducing current efficiency. Consequently, despite the improvement in mechanical properties, the electrochemical performance of the alloy as a sacrificial anode deteriorates. Similar observations have been reported in previous studies, which demonstrated that precipitation hardening in Al–Mg–Si alloys improve hardness but may adversely affect corrosion behaviour and anodic performance due to changes in precipitate distribution and galvanic interactions. [92, 117, 173–175] Phase redistribution and Mg_2Si fragmentation during solution treatment and aging disrupt the beneficial interconnected morphology, leading to accelerated and less controlled dissolution.

4.6.3 Correlation with Microstructure and Potentiodynamic Polarization Behavior

The observed trends in anode capacity and consumption rate are strongly correlated with both microstructural characteristics and electrochemical parameters. The superior performance of the as-cast Al-6.5Mg-6Si alloy is associated with the presence of a fine, interconnected “Chinese-script” Mg_2Si morphology, which promotes more uniform anodic dissolution compared to the coarse flakes and rods characteristic of the 3% and 4.5% Si alloys.[169] This morphology effectively distributes anodic sites throughout the matrix, minimizing localized attack and improving current utilization efficiency.

Potentiodynamic polarization results further substantiate this relationship. In the as-cast condition, the 6% Si alloy exhibits a relatively high corrosion current density (Icorr = 3.62 μA/cm²), indicative of strong anodic activity, yet without excessive material wastage due to its uniform dissolution mode. Conversely, the intermediate-Si alloys display elevated Icorr values combined with poor anode efficiency, reflecting aggressive but localized corrosion behavior.

Following T6 heat treatment, although the corrosion potential of the 6% Si alloy shifts to a more active value (Ecorr ≈ −946 mV), the corresponding increase in Icorr to 4.64 μA/cm² directly correlates with the observed rise in consumption rate. This confirms that enhanced electrochemical activity alone does not guarantee superior sacrificial performance; rather, it must be accompanied by a favorable dissolution morphology. The combined microstructural, electrochemical, and anode performance data conclusively demonstrate that optimal sacrificial behavior in Al-Mg-Si alloys arises from a synergistic balance between Si content, Mg_2Si morphology, and thermal history.

4.6.4 Surface Examination after Anode Performance Testing

The macroscopic surface examination of the anode performance–tested specimens provides direct visual confirmation of the electrochemical and gravimetric trends discussed in the preceding sections. As illustrated in Figure 4.24, the as-cast alloys exhibit pronounced non-uniform corrosion characterized by localized pitting, deep crevice formation, and uneven material removal. Among these, the Al-6.5Mg-3Si alloy shows the most severe localized attack, with deep pits and irregular dissolution features. This observation directly correlates with its highest consumption rate (5.0 kg/Amp·year) and reduced anode capacity listed in Table 4.10, confirming inefficient current utilization due to localized micro-galvanic activity associated with coarse and partially continuous Mg_2Si networks.

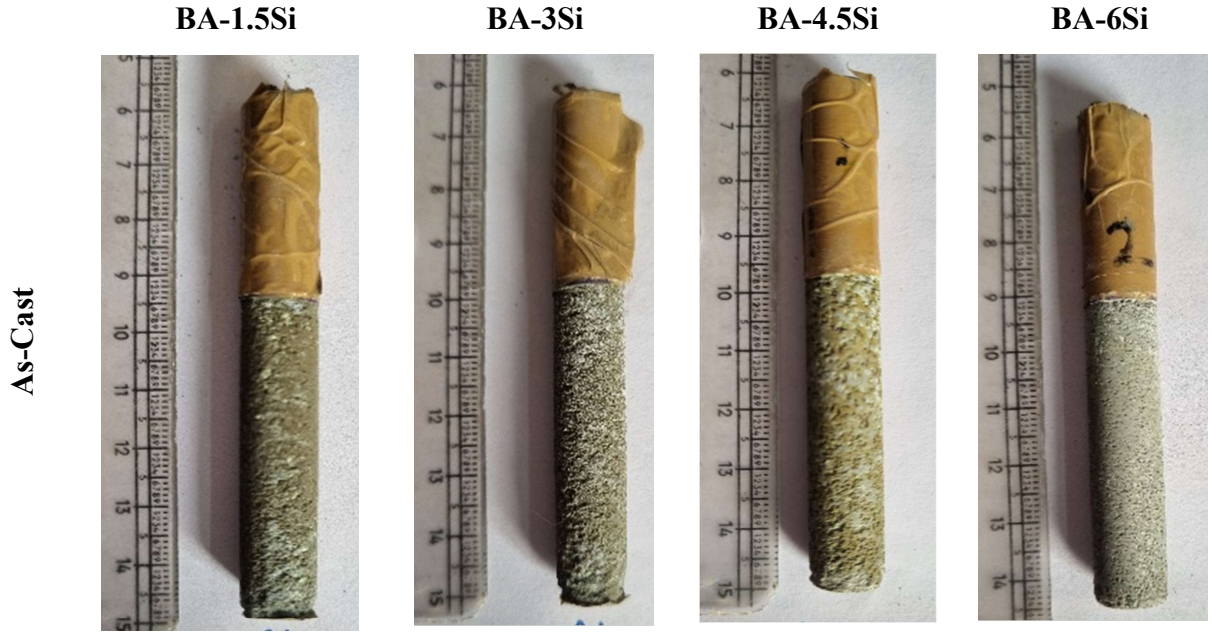

Figure 4.24 Surface morphology of Al-6.5Mg-xSi sacrificial anode specimens after Anode performance measurement in both as-cast and T6 heat treated conditions.

The Al-6.5Mg-1.5Si alloy displays comparatively shallower pits and more dispersed corrosion sites, consistent with its lower corrosion current density and moderate consumption rate. In contrast, the 4.5% Si alloy shows mixed corrosion behavior, with regions of uniform dissolution interspersed with localized attack, reflecting its intermediate electrochemical response and relatively high consumption rate. These observations reinforce the conclusion that increasing Si content in the as-cast condition promotes microstructural heterogeneity, leading to unstable and localized anodic dissolution.

In comparison, the T6 heat-treated specimens demonstrate a markedly different surface morphology. All heat-treated alloys exhibit more uniform surface recession with significantly reduced pit depth, indicating a transition from localized to generalized anodic dissolution. This behavior is attributed to the redistribution and refinement of the Mg_2Si phase during solution treatment and aging, as evidenced by the corresponding shifts in *E*corr and *I*corr values (Table 4.8). The homogenization of cathodic sites minimizes localized galvanic coupling, thereby promoting steadier material consumption.

This uniform dissolution is particularly evident in the T6-treated Al-6.5Mg-6Si alloy, which exhibits smooth and evenly recessed surfaces with minimal deep pitting. Despite its increased anodic activity after heat treatment, the absence of severe localized attack allows for sustained

current output, resulting in a high anode capacity of 2781.5 Amp·hr/kg. The reduced pitting tendency in heat-treated alloys helps preserve the geometric integrity of the anode throughout service exposure, ensuring predictable consumption behavior and stable cathodic protection performance.

4.7 Summary

This chapter systematically established the interrelationship between silicon content, microstructural evolution, electrochemical behavior, and sacrificial anode performance of Al-6.5Mg-xSi alloys. Microstructural analysis demonstrated that variations in Si content govern the morphology and distribution of Mg_2Si phases, which in turn control corrosion initiation, propagation, and dissolution uniformity in chloride environments. Weight-loss immersion tests and potentiodynamic polarization studies revealed consistent trends, confirming that alloys exhibiting higher anodic activity and localized micro-galvanic effects experience accelerated material loss. Anode performance evaluation further validated these findings, showing that intermediate Si contents (3–4.5%) lead to inefficient consumption due to coarse Mg_2Si networks, while the as-cast 6% Si alloy achieves superior anode capacity and lowest consumption rate owing to its favorable "Chinese-script" Mg_2Si morphology. Heat treatment, although beneficial for mechanical properties, was shown to adversely affect sacrificial efficiency by disrupting this morphology and increasing dissolution rates. Collectively, the results demonstrate that optimal sacrificial performance in Al–Mg–Si alloys is governed by a delicate balance between composition and microstructure, with the as-cast Al–6.5Mg–6Si alloy emerging as the most promising candidate for cathodic protection applications.

CHAPTER 5
MAJOR CONTRIBUTIONS AND HYPOTHESIS DEVELOPED

5.1 Introduction

Chapter 4 established the interrelationships among composition, microstructure, electrochemical behavior, and sacrificial performance through systematic experimentation, a generalized scientific understanding requires these observations to be articulated as testable and predictive propositions. Accordingly, Chapter 5 synthesizes the key outcomes of Chapter 4 into two complementary elements: (1) A concise statement of the original research contributions derived from this investigation; and (2) A structured set of research hypotheses that integrate microstructural, electrochemical, and performance-based evidence. Together, these hypotheses provide a mechanistic and predictive framework for interpreting the sacrificial behavior of Al-Mg-Si alloys and for guiding the design and optimization of aluminum-based anodes for cathodic protection applications.

5.2 Research Contributions

This thesis presents a systematic investigation into the role of silicon addition and heat treatment on the microstructure, electrochemical behavior, corrosion response, and sacrificial anode performance of Al-6.5Mg-xSi alloys. The key original contributions of this research are summarized below, with direct reference to the experimental evidence presented in Chapter 4.

1. Establishment of a Microstructure -Electrochemical Performance Relationship

A comprehensive framework is developed linking Mg_2Si morphology to corrosion kinetics and sacrificial anode efficiency. By correlating SEM/EDS microstructural observations (Figures 4.1, 4.6), polarization parameters (Table 4.8), weight-loss corrosion behavior (Tables 4.6 and 4.7), and anode performance data (Table 4.10), this work demonstrates that sacrificial behavior is governed by microstructural continuity and phase distribution rather than composition alone.

2. Identification of a Non-Linear Effect of Silicon Content on Sacrificial Anode Performance

This study establishes a non-linear dependence of anode capacity and consumption rate on silicon content. Intermediate Si levels (1.5-4.5%) result in reduced anode capacity and increased consumption due to coarse or partially continuous Mg_2Si networks (Figures 4.1c–d, Table 4.10). In contrast, the as-cast Al-6.5Mg-6Si alloy exhibits an exceptionally high anode capacity of 2781.5 A·h/kg and the lowest consumption rate (3.14 kg/A·year), exceeding conventional Al-Mg anode performance (Table 4.10).

3. Demonstration of the Dominant Role of Mg_2Si Morphology in Corrosion Mechanisms

The work demonstrates that Mg_2Si morphology critically controls corrosion initiation and propagation. Fine and uniformly distributed Mg_2Si particles promote shallow, uniform dissolution (Figures 4.14 and 4.15), while coarse or interconnected Mg_2Si networks act as micro-galvanic cathodes, accelerating localized pitting and pit coalescence (Figures 4.18 and 4.19). This mechanistic understanding is supported by both weight-loss trends (Tables 4.6, 4.7) and electrochemical current densities (Table 4.8).

4. Clarification of the Dual Influence of T6 Heat Treatment

This research clarifies the dual role of T6 heat treatment in sacrificial anode systems. Heat treatment consistently shifts corrosion potential toward more active values (Ecorr ≈ –946 to –955 mV; Table 4.8), enhancing driving potential. However, it also increases corrosion current density and consumption rate by disrupting favorable as-cast Mg_2Si morphologies (Figures 4.6 and 4.18), particularly in high-Si alloys (Table 4.10).

5. Validation of Long-Term Corrosion Behavior Through Multi-Method Consistency

A strong consistency is demonstrated between short-term electrochemical testing and long-term immersion behavior. Alloys exhibiting higher Icorr values in polarization studies (Table 4-8) show correspondingly higher corrosion rates in weight-loss testing (Tables 4-6 and 4-7) and increased consumption rates during anode performance evaluation (Table 4-10), validating the reliability of the proposed evaluation methodology.

6. Development of a Mechanism-Based Sacrificial Anode Design Strategy

Based on integrated microstructural, electrochemical, and performance data, this thesis proposes a mechanism-based strategy for optimizing Al-Mg-Si sacrificial anodes. The results identify the as-cast Al-6.5Mg-6Si alloy as an optimal composition, microstructure combination for high-capacity anode applications, while demonstrating that heat treatment must be carefully controlled to avoid degradation of sacrificial efficiency.

The relationships between the identified research contributions, the corresponding hypotheses, and the supporting experimental evidence are summarized in Table 5.1. This structured linkage establishes the experimental basis for the hypothesis development presented in the subsequent section.

Table 5.1 Contribution–Hypothesis–Evidence Linkage for the Present Study

No.	Research Contribution of This Study	Linked Research Hypothesis	Key Supporting Experimental Evidence
1	Established a clear microstructure–electrochemical–performance relationship governing sacrificial behavior of Al–6.5Mg–xSi alloys.	**H6:** Sacrificial behavior is governed by a coupled interaction between microstructure, electrochemical response, and dissolution morphology.	Correlation of Mg_2Si morphology (Figures. 4.5, 4.6), *E*corr and *I*corr (Table 4-8), weight-loss corrosion (Tables 4-6, 4-7), and anode performance (Table 4-10).
2	Demonstrated a non-linear dependence of sacrificial anode performance on silicon content.	**H3:** Silicon content affects anode performance non-monotonically, with intermediate Si reducing efficiency and high Si restoring performance under favorable microstructures.	Decline in anode capacity from 1.5–4.5% Si and sharp improvement at 6% Si (Table 4-10; Figure 4.23).
3	Identified Mg_2Si morphology as the dominant factor controlling corrosion	**H1:** Silicon content governs corrosion initiation through its control of Mg_2Si	Delayed corrosion initiation for fine Mg_2Si (1.5% Si) vs. early pitting for coarse/interconnected

	initiation and propagation.	morphology and spatial distribution.	Mg_2Si (Tables 4-6, 4-7; Figure. 4.14, 4.19).
4	Demonstrated the role of Mg_2Si continuity in intensifying micro-galvanic corrosion.	**H2:** Increased continuity of Mg_2Si enhances micro-galvanic coupling and increases corrosion current density.	Progressive increase in *I*corr with increasing Si content in as-cast alloys (Table 4-8) correlated with Mg_2Si connectivity (Figure 4.6).
5	Clarified the dual and composition-dependent influence of T6 heat treatment on sacrificial efficiency.	**H4:** Heat treatment enhances anodic activity but reduces efficiency at high Si by disrupting favorable Mg_2Si morphologies.	Negative shift in *E*corr after T6 (Table 4-8) coupled with increased consumption rate for high-Si alloys (Table 4-10; Figure 4.23).
6	Established uniform anodic dissolution as the governing factor for long-term anode efficiency.	**H5:** Uniform dissolution governs anode efficiency more strongly than corrosion rate or anodic activity alone.	Surface recession vs. localized pitting trends correlated with anode capacity and consumption rate (Figure 4.24; Table 4-10).
7	Identified the as-cast Al–6.5Mg–6Si alloy as an optimized sacrificial anode composition–microstructure combination.	**H3 & H6:** Superior performance arises from favorable as-cast Mg_2Si morphology and coupled electrochemical response.	Highest anode capacity (2781.5 A·h/kg) and lowest consumption rate (3.14 kg/A·year) for as-cast 6% Si alloy (Table 4-10; Figure 4.6d).

5.3 Hypothesis Development

5.3.1 Basis for Hypothesis Formulation

The hypotheses proposed in this chapter are derived from the following key experimental findings:

- The morphology, continuity, and spatial distribution of the Mg_2Si phase vary significantly with silicon content and heat treatment condition.
- Corrosion behavior shows strong dependence on micro-galvanic interactions between α-Al matrix and Mg_2Si particles.
- Electrochemical parameters (*E*corr, *I*corr) correlate consistently with long-term weight-loss corrosion rates and anode consumption behavior.

- As-cast high-silicon alloys exhibit superior sacrificial efficiency compared to intermediate-silicon compositions and heat-treated counterparts.

These observations indicate that microstructure-mediated electrochemical mechanisms dominate sacrificial performance, thereby justifying the development of hypotheses that explicitly link phase evolution to corrosion and anode efficiency.

To provide a consolidated visual representation of the relationships between silicon content, microstructural evolution, electrochemical behavior, and sacrificial anode performance identified in Chapter 4, a graphical abstract summarizing the basis of the proposed hypotheses is presented in Figure 5.1.

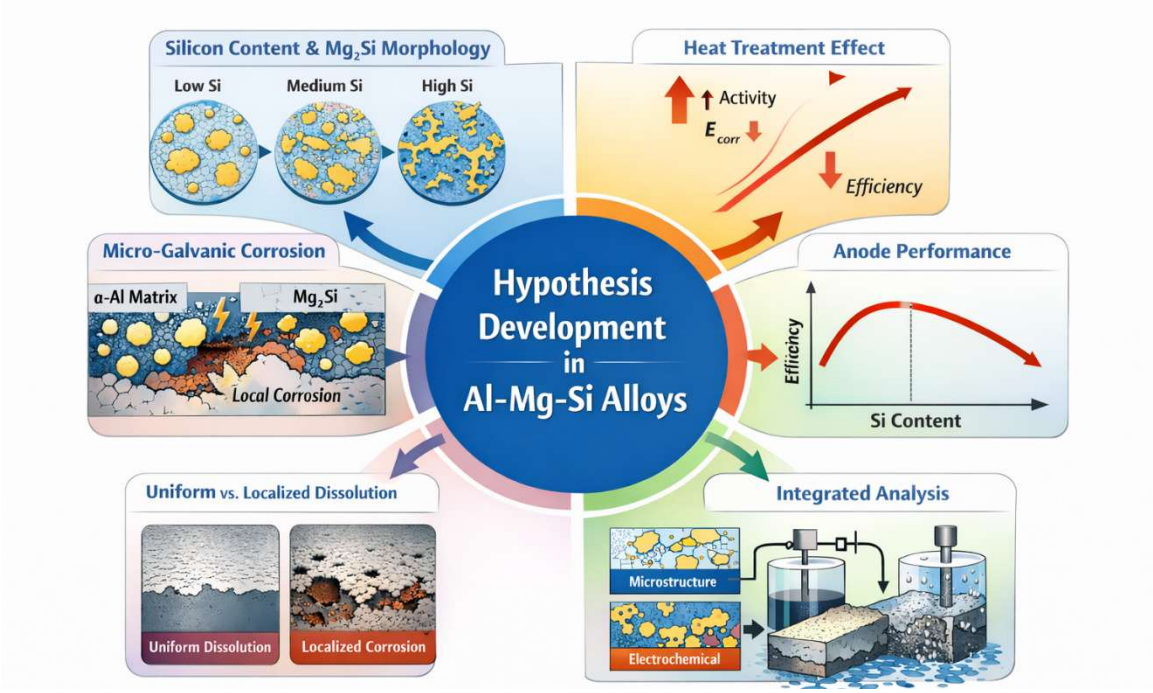

Figure 5.1 Graphical abstract illustrating the hypothesis development framework for Al–6.5Mg–xSi sacrificial anode alloys, highlighting the influence of silicon content on Mg_2Si morphology, micro-galvanic interactions, electrochemical response, and resulting anode efficiency.

5.3.2 Hypothesis H1: Influence of Silicon Content on Mg_2Si Morphology and Corrosion Initiation

"Increasing silicon content in Al-6.5Mg alloys alters the morphology and spatial distribution of the Mg_2Si phase, which directly controls corrosion initiation behavior in chloride environments".

Chapter 4 established that silicon addition exerts a dominant influence on Mg_2Si precipitation behavior. At low silicon content (1.5% Si), Mg_2Si forms as fine, discrete, and uniformly distributed particles within the α-Al matrix, as observed in the microstructural analysis (Figures 4.2 and 4.6). In contrast, increasing silicon content to 3-4.5% promotes the development of coarser, elongated, and partially continuous Mg_2Si networks, while the highest silicon level (6% Si) results in a high volume fraction of interconnected Mg_2Si with complex morphologies. These microstructural transitions significantly modify local electrochemical heterogeneity at the Mg_2Si/Al interface.

The influence of Mg_2Si morphology on corrosion initiation is reflected in the weight-loss corrosion results (Tables 4.6 and 4.7), where low-Si alloys exhibit delayed corrosion onset and comparatively stable corrosion rates over extended immersion periods. Conversely, alloys containing coarser or interconnected Mg_2Si phases show earlier pit nucleation and higher initial corrosion rates, indicating increased susceptibility to localized attack. SEM surface examinations after electrochemical testing (Figures 4.19) further confirm that corrosion preferentially initiates at Mg_2Si matrix interfaces, particularly where Mg_2Si exists as coarse or continuous phases that promote micro-galvanic coupling.

Accordingly, this hypothesis proposes that silicon does not merely act as a compositional modifier, but fundamentally controls corrosion initiation by regulating Mg_2Si morphology and phase connectivity. The spatial continuity and electrochemical role of Mg_2Si are therefore hypothesized to be the primary microstructural parameters governing early-stage corrosion behavior in Al-Mg-Si sacrificial anode alloys.

5.3.3 Hypothesis H2: Role of Mg_2Si Continuity in Micro-Galvanic Corrosion

"The continuity and spatial connectivity of Mg_2Si phases increase micro-galvanic coupling with the α-Al matrix, thereby accelerating localized corrosion and increasing corrosion current density."

Potentiodynamic polarization results in Chapter 4 reveal a systematic increase in corrosion current density (*I*corr) with increasing silicon content in the as-cast condition (Table 4.8). The Al-6.5Mg-3Si, 4.5Si, and 6Si alloys exhibit significantly higher *I*corr values compared to the 1.5Si alloy, despite similar base compositions.

Microstructural analysis indicates that these alloys contain coarser and partially interconnected Mg_2Si phases, which act as effective cathodic regions relative to the α-Al matrix. This spatial continuity enhances micro-galvanic coupling, promoting localized anodic dissolution and non-uniform corrosion attack. In contrast, discontinuous Mg_2Si particles limit galvanic intensity and reduce localized corrosion severity.

This hypothesis states that corrosion kinetics are governed not merely by Mg_2Si presence, but by its continuity and connectivity within the matrix.

This hypothesis may be tested by comparing *I*corr values and localized corrosion morphology across alloys with equivalent Mg_2Si volume fraction but differing degrees of phase continuity.

5.3.4 Hypothesis H3: Non-Linear Relationship Between Silicon Content and Anode Performance

"The relationship between silicon content and sacrificial anode performance in Al–6.5Mg–xSi alloys are non-linear, with intermediate silicon levels reducing efficiency and high silicon levels restoring or enhancing anode capacity under favorable microstructural conditions." Anode performance results (Table 4.10) demonstrate a clear non-monotonic trend. Increasing silicon content from 1.5% to 3% leads to reduced anode capacity and increased consumption rate, with the 3% Si alloy exhibiting the poorest efficiency. However, further increasing silicon content to 6% results in a substantial improvement in anode capacity and the lowest consumption rate in the as-cast condition.

Microstructural observations reveal that intermediate silicon levels promote coarse, lamellar Mg_2Si morphologies that favor localized attack, whereas the as-cast 6% Si alloy develops a fine Chinese-script Mg_2Si structure that supports more uniform dissolution. This finding contradicts the assumption of a linear degradation in performance with increasing silicon content.

The hypothesis proposes that sacrificial efficiency depends on silicon-induced microstructural state rather than silicon concentration alone.

This hypothesis can be validated by comparing anode capacity and consumption rate as functions of both silicon content and quantified Mg_2Si morphology descriptors.

5.3.5 Hypothesis H4: Heat Treatment Enhances Anodic Activity but Reduces Anode Efficiency at High Silicon Levels

"T6 heat treatment enhances anodic activity by shifting corrosion potential to more negative values; however, at high silicon contents, it increases anode consumption rate by disrupting favorable as-cast Mg_2Si morphologies."

Potentiodynamic polarization results indicate that T6 heat treatment shifts corrosion potential (*E*corr) to more negative values for all alloys, enhancing anodic driving force (Table 4.8). Despite this increased activity, anode performance data (Table 4.10) reveal that efficiency does not uniformly improve.

The Al-6.5Mg-6Si alloy exhibits the most pronounced degradation, with consumption rate increasing from 3.14 to 5.21 kg/Amp·year after T6 treatment. Microstructural analysis shows that heat treatment dissolves the beneficial Chinese-script Mg_2Si network and reprecipitates it as fine β″ particles, increasing electrochemical homogeneity but weakening local passivation.

This hypothesis states that excessive anodic activation without preservation of favorable microstructure leads to accelerated but inefficient dissolution.

5.3.6 Hypothesis H5: Uniform Anodic Dissolution Governs Long-Term Anode Efficiency

"Uniform anodic dissolution, rather than minimum corrosion rate or maximum anodic activity, is the primary determinant of long-term sacrificial anode efficiency."

Surface examinations of tested anodes reveal that alloys exhibiting uniform surface recession achieve higher anode capacities and more stable consumption behavior (Figure 4.24). In contrast, alloys experiencing localized pitting and deep crevice formation show rapid mass loss and reduced current efficiency.

This explains why certain alloys with relatively high corrosion current densities such as the as-cast 6% Si alloy, outperform intermediate-Si alloys in practical anode tests. Uniform dissolution ensures sustained current delivery and preserves structural integrity over service life.

The hypothesis emphasizes that dissolution morphology is a more critical performance parameter than instantaneous electrochemical metrics alone.

5.3.7 Hypothesis H6: Coupled Microstructure–Electrochemical Performance Relationship

"The sacrificial behavior of Al-Mg-Si alloys is governed by a coupled interaction between microstructural state, electrochemical response, and dissolution morphology, rather than by individual parameters such as silicon content or corrosion current density alone."

Integrated analysis of weight-loss corrosion data (Tables 4.6 and 4.7), polarization results (Table 4.8), anode performance testing (Table 4.10), and surface examination confirms that no single parameter independently predicts sacrificial performance.

Instead, performance emerges from the interaction between Mg_2Si morphology, electrochemical characteristics (Ecorr and Icorr), and long-term dissolution uniformity. This hypothesis formalizes the multi-parameter mechanism governing sacrificial behavior and provides a predictive framework for rational alloy optimization.

To consolidate the hypothesis development presented in above, Table 5.1 summarizes the clear linkages between the research contributions, the formulated hypotheses, and the corresponding

experimental evidence derived from Chapter 4. This integrated overview reinforces the data-driven nature of the proposed hypotheses.

5.4 Summary

This chapter consolidated the experimental outcomes of Chapter 4 into a coherent contribution–hypothesis framework. Key research contributions were identified, emphasizing the dominant role of silicon-controlled Mg_2Si morphology in governing corrosion behavior and sacrificial anode efficiency of Al-6.5Mg-xSi alloys. Based on these findings, six interrelated hypotheses (H1–H6) were formulated to explain the effects of silicon content, Mg_2Si continuity, micro-galvanic interactions, heat treatment, and dissolution morphology on electrochemical response and anode performance.

The hypotheses collectively establish that sacrificial behavior arises from a coupled interaction between microstructural state and electrochemical mechanisms rather than from alloy composition alone. This chapter thus provides a mechanistic and predictive framework for alloy optimization, forming a logical transition to the subsequent chapter focused on validation and interpretation of these hypotheses.

CHAPTER 6
CONCLUSIONS AND SCOPE FOR FUTURE WORK

6.1 Conclusions

Based on the experimental results and analysis presented in this thesis, the following major conclusions are drawn:

- Increasing silicon content significantly modifies the as-cast microstructure of Al–6.5Mg alloys, promoting a transformation from fine, flake-like intermetallic morphologies at low silicon levels to a refined Chinese-script Mg_2Si eutectic structure at 6 wt% Si. XRD and EDS analyses confirm the presence of α-Al and Mg_2Si as the dominant phases across all compositions. Increasing silicon content reduces the α-Al volume fraction while increasing the Mg_2Si fraction and phase continuity.
- T6 heat treatment effectively dissolves coarse as-cast Mg_2Si structures and reprecipitates them as a high density of fine, intermittent β″ precipitates. While this treatment enhances microstructural homogeneity and precipitation strengthening, it disrupts favorable as-cast Mg_2Si morphologies that are beneficial for sacrificial anode performance.
- Alloy hardness increases systematically with silicon addition and artificial aging. The Al-6.5Mg-6Si alloy achieves a peak hardness of approximately 107 HV after T6 treatment, compared to 83 HV in the as-cast condition. This strengthening is attributed to combined solid-solution strengthening and the formation of fine, coherent β″ precipitates that effectively impede dislocation motion.
- Potentiodynamic polarization studies reveal that T6 heat treatment shifts the corrosion potential (*E*corr) toward more active values, enhancing anodic driving force. The most negative *E*corr value (~ −946 mV) is observed for the 6 wt% Si alloy. However, this increased anodic activity is accompanied by higher corrosion current densities (*I*corr), indicating accelerated dissolution rates in the heat-treated condition.
- Corrosion preferentially initiates at Mg_2Si particles due to selective magnesium dissolution, followed by localized attack on the surrounding aluminum matrix. Increasing silicon content

promotes deeper, more irregular pitting through enhanced micro-galvanic coupling, passive film breakdown, and occluded cell formation. The electrochemical role of Mg_2Si evolves during exposure, contributing to dynamic corrosion behavior.

- Intermediate silicon additions reduce anode efficiency due to unfavorable Mg_2Si morphologies and localized corrosion. In contrast, the as-cast Al-6.5Mg-6Si alloy demonstrates exceptional sacrificial performance, achieving a very high anode capacity of 2781.49 Ah/kg-significantly exceeding conventional Al-Mg anodes and the lowest consumption rate of 3.15 kg/Amp·year.
- Although T6 heat treatment maximizes hardness, it significantly degrades anodic efficiency in high-silicon alloys. For the 6 wt% Si alloy, heat treatment increases the consumption rate from 3.15 to 5.21 kg/Amp·year, corresponding to an approximate 65% reduction in sacrificial performance.
- The as-cast Al-6.5Mg-6Si alloy is identified as the optimal composition for cathodic protection applications requiring high anode capacity, low consumption rate, and long service life. Conversely, the T6-treated Al–6.5Mg–6Si alloy is better suited for structural applications where high mechanical strength is the primary requirement.

6.2 Future Scope of The Study

While the present investigation establishes clear relationships between silicon content, Mg_2Si morphology, electrochemical behavior, and sacrificial anode performance of Al–6.5Mg–xSi alloys, several research directions emerge for extending and strengthening the proposed mechanistic framework.

6.2.1 Effect of Cold Working on Microstructure–Electrochemical Coupling

Chapter 5 proposed that sacrificial anode performance is governed by coupled interactions between microstructure, electrochemical response, and dissolution morphology (Hypothesis 6). Cold working introduces high dislocation density, residual stresses, and sub-grain refinement within the α-Al matrix, which are expected to modify Mg_2Si particle distribution, phase continuity, and local electrochemical homogeneity. Future studies may systematically investigate the influence of varying degrees of cold deformation (e.g., 10–40% thickness reduction) on corrosion potential (*E*corr), corrosion current density (*I*corr), and anodic dissolution uniformity. Such work would

clarify the role of deformation-induced microstructural features in controlling micro-galvanic interactions and long-term sacrificial efficiency.

6.2.2 Combined Effects of Cold Working and Heat Treatment

Hypothesis 4 highlighted that T6 heat treatment, although beneficial for anodic activation, can adversely affect sacrificial efficiency at high silicon levels due to disruption of favorable as-cast Mg_2Si morphologies. Future research may explore controlled thermo-mechanical processing routes, such as cold working followed by partial or modified aging treatments, to balance mechanical strengthening with anodic efficiency. This approach could provide insight into optimizing processing parameters that preserve beneficial Mg_2Si morphologies while maintaining sufficient anodic driving potential.

6.2.3 Interaction Between Cold Work and Mg_2Si Morphology

Hypotheses 1 and 2 emphasized the dominant influence of Mg_2Si morphology and phase continuity on corrosion initiation and micro-galvanic behavior. Cold working may fragment coarse Mg_2Si networks or induce preferential particle alignment, thereby modifying micro-galvanic coupling intensity at the Mg_2Si/α-Al interface. Detailed microstructural characterization using SEM and EBSD, combined with localized electrochemical techniques, could elucidate how deformation-induced changes in Mg_2Si morphology influence corrosion initiation sites and localized dissolution behavior.

6.2.4 Advanced Electrochemical and Modeling Approaches

The hypotheses formulated in Chapter 5 may be further validated using electrochemical impedance spectroscopy (EIS), scanning Kelvin probe force microscopy (SKPFM), and computational modeling to quantify the influence of deformation-induced microstructural heterogeneity on galvanic interactions.

6.2.5 Three-Dimensional Corrosion Evolution and Cross-Sectional Characterization

Although the present study successfully correlates surface corrosion morphology with electrochemical behaviour, the subsurface evolution of localized corrosion and pit propagation

through the Mg_2Si/α-Al interface remains unexplored. Future investigations employing cross-sectional scanning electron microscopy (SEM), focused ion beam (FIB-SEM) sectioning, or X-ray computed tomography (micro-CT) could provide three-dimensional insight into pit initiation, propagation pathways, and the role of intermetallic phases during long-term exposure. Such studies would further validate the corrosion mechanisms proposed in the present investigation.

6.2.6 Time-Dependent Electrochemical Transformation of Mg_2Si

The present work indicates that Mg_2Si morphology strongly influences sacrificial anode performance; however, the electrochemical transformation of Mg_2Si from anodic to cathodic behaviour during prolonged chloride exposure has been inferred primarily from published literature. Future studies employing localized electrochemical techniques such as Scanning Kelvin Probe Force Microscopy (SKPFM), Scanning Vibrating Electrode Technique (SVET), or Localized Electrochemical Impedance Spectroscopy (LEIS) could quantify the temporal evolution of Mg_2Si electrochemical activity and validate the proposed corrosion mechanism.

REFERENCES

[1] R. W. Revie and H. H. Uhlig, *Corrosion and Corrosion Control: An Introduction to Corrosion Science and Engineering*, 4th ed. Hoboken, NJ: John Wiley & Sons, 2011.

[2] M. G. Fontana, *Corrosion Engineering*, 3rd ed. New Delhi: Tata McGraw-Hill, 2005.

[3] E. McCafferty, *Introduction to Corrosion Science*. New York: Springer, 2010.

[4] L. L. Shreir, R. A. Jarman, and G. T. Burstein, *Corrosion: Metal/Environment Reactions*, 3rd ed. Elsevier, 2013.

[5] "India loses 2-3% of GDP annually due to corrosion," *The Times of India*, Feb. 11, 2025. [Online]. Available: https://timesofindia.indiatimes.com/city/ranchi/india-loses-2-3-of-gdp-annually-due-to-corrosion/articleshow/117990574.cms. [Accessed: Feb. 11, 2026].

[6] NACE International, "Corrosion Costs and Preventive Strategies in the United States," FHWA-RD-01-156, .

[7] F. Mansfeld and P. Marcus, *Analytical Methods in Corrosion Science and Engineering*, 1st ed. CRC Press, 2005.

[8] P. R. Roberge, *Corrosion Engineering: Principles and Practice*. McGraw-Hill Education, 2008.

[09] I. Gurrappa, "Cathodic protection of cooling water systems and selection of appropriate materials," *J. Mater. Process. Technol.*, vol. 66, pp. 256–267, 2005.

[10] L. Dube, "Effectiveness of impressed current cathodic protection system on underground steel Engen refinery transfer lines system," Doctoral dissertation, 2022.

[11] R. Bender et al., "Corrosion challenges towards a sustainable society," *Materials and Corrosion*, vol. 73, pp. 1730–1751, 2022. doi: 10.1002/maco.202213140.

[12] H. H. Uhlig and R. W. Revie, *Corrosion and Corrosion Control: An Introduction to Corrosion Science and Engineering*. John Wiley & Sons, Inc., 2008.

[13] "Galvanic (Sacrificial) Anode Material Selection and Design Considerations and Example Calculations (Non-Mandatory)," Standard Report, 2017.

[14] Total Materia, "Sacrificial Anodes," [Online]. Available: https://www.totalmateria.com/en-us/articles/sacrificial-anodes-2/.

[15] The Marine King, "Comparing Zinc, Aluminum, and Magnesium Anodes," [Online]. Available: https://themarineking.com/blogs/news/comparing-zinc-aluminum-and-magnesium-anodes.

[16] Cathodic Protection Co. Ltd., "Standard Anode Types and Weights - D Shape Magnesium Anodes," [Online]. Available: www.cathodic.co.uk.

[17] R. Baboian, *Corrosion Tests and Standards: Application and Interpretation*. ASTM International, 2005.

[18] D. A. Jones, *Principles and Prevention of Corrosion*, 2nd ed. Pearson, 2013.

[19] Nwanonenyi, S. C., Daniyan, A. A., Idris, M. B., & Ige, O. O. (2025). Corrosion control through sacrificial anodes: A review of aluminium alloys in oil and gas applications. Hybrid Advances, 11, 100571. https://doi.org/10.1016/j.hybadv.2025.100571

[20] Y. L. Shuaib-Babata et al., "The effect of Magnesium addition on the performance of Aluminium-Zinc-Copper alloy as a sacrificial anode in seawater," *J. Mater. Environ. Sci.*, vol. 11, no. 6, pp. 963–976, 2020.

[21] T. M. Tsai, "Protection of Steel Using Aluminum Sacrificial Anodes in Artificial Seawater," *J. Mar. Sci. Technol.*, vol. 4, 1996. doi: 10.51400/2709-6998.2545.

[22] J. C. Benedyk, "Aluminum alloys for lightweight automotive structures," in *Materials, Design and Manufacturing for Lightweight Vehicles*, Elsevier, 2010, pp. 79–113.

[23] T. K. Kyada, I. B. Dave, and S. M. Patel, "An Extensive Overview of Al-Mg-Si Alloy's Electrochemical Behavior," *International Journal of Metallurgy and Alloys*, 2023. doi: 10.37628/IJMA.

[24] V. A. Mistry, M. S. Dani, and I. B. Dave, "A Review on Effect of Alloying Element on Aluminium Anode," in *Proc. 14th International Conference on Recent Progress in Material Science and Mechanical Engineering*, 2022.

[25] C. Dehchar, D. Charif, L. Abdellatif, and Y. B. Walid, "Electrochemical behavior of pure aluminum and aluminum alloy sacrificial anodes in seawater solution," ResearchGate, 2018.

[26] A. J. Bard and L. R. Faulkner, *Electrochemical Methods: Fundamentals and Applications*, 2nd ed. Wiley, 2000.

[27] M. Pourbaix, *Atlas of Electrochemical Equilibria in Aqueous Solutions*, 2nd ed. National Association of Corrosion Engineers, 1974.

[28] J. R. Davis, *ASM Specialty Handbook: Aluminum and Aluminum Alloys*. ASM International.

[29] J. R. Scully and K. Lutton, "3.1 Polarization Behavior of Active Passive Metals and Alloys," Reference Module,

[30] N. K. Prasad et al., "On the novel approach of sacrificial cathodic protection of mild steel in simulated concrete pore solution and concrete mortar by high phosphorus pig iron anodes," *J. Mater. Res. Technol.*, vol. 14, pp. 582–608, 2021.

[31] A. N. Anang and R. Olabiyi, "Enhancing Corrosion Resistance in High-Performance Metal Alloys," *Int. Res. J. Modernization Eng. Technol.*, 2024. doi: 10.56726/IRJMETS62327.

[32] H. Böhni and H. H. Uhlig, "Environmental Factors Affecting the Critical Pitting Potential of Aluminum," *J. Electrochem. Soc.*

[33] C. H. Caceres and D. M. Rovera, "Solid solution strengthening in concentrated Mg-Al alloys," *J. Light Metals*, vol. 1, no. 3, pp. 151-156,

[34] A. Yaro and A. Muazu, "Effects of Zinc Addition on the Performance of Aluminium as Sacrificial Anode in Seawater," 2011.

[35] S. H. Avner, *Introduction to Physical Metallurgy*, 2nd ed. McGraw-Hill,

[36] "Aluminum and Aluminum Alloys Introduction and Overview," *ASM International*, 2001. doi: 10.1361/autb2001p351.

[37] S. Lameche-Djeghaba et al., "Electrochemical Behaviour of Pure Aluminium and Al-5%Zn Alloy in 3% NaCl Solution," *Arab. J. Sci. Eng.*, vol. 39, pp. 113–122, 2014.

[38] L. E. Umoru and O. O. Ige, "Effects of Tin on Aluminum-Zinc-Magnesium Alloy as Sacrificial Anode in Seawater," *J. Minerals Mater. Charact. Eng.*, 2007.

[39] K. Cheng et al., "Effect of Ti on microstructure and properties of aluminum sacrificial anode containing rare earth elements," in *Proc. MEITA*, 2015, pp. 941–944.

[40] J. Ma et al., "Influence of Mg and Ti on the microstructure and electrochemical performance of aluminum alloy sacrificial anodes," *Rare Metals*, vol. 28, pp. 187–192, 2009.

[41] J. Wen, J. He, and X. Lu, "Influence of silicon on the corrosion behaviour of Al-Zn-In-Mg-Ti sacrificial anode," *Corros. Sci.*, vol. 53, pp. 3861–3865, 2011.

[42] J. G. He et al., "Influence of Ga and Bi on electrochemical performance of Al-Zn-Sn sacrificial anodes," *Trans. Nonferrous Met. Soc. China*, vol. 21, pp. 1580–1586, 2011.

[43] H. Sina et al., "The influence of Ti and Zr on electrochemical properties of aluminum sacrificial anodes," *Mater. Sci. Eng. A*, vol. 431, pp. 263–276, 2006.

[44] R. Correa, H. Sánchez, and J. A. Calderón, "Improvement of micro-hardness and electrochemical properties of Al-4%Cu-0.5%Mg alloy by Ag addition," *Rev. Fac. Ing. Univ. Antioquia*, pp. 19–28, 2011.

[45] S. M. A. Shibli and V. S. Gireesh, "Activation of aluminium alloy sacrificial anodes by selenium," *Corros. Sci.*, vol. 47, pp. 2091–2097, 2005.

[46] E. Aragon et al., "Influence of alloying elements on electrochemical behaviour of ternary Al-Zn-Ga alloys for sacrificial anodes," *Br. Corros. J.*, vol. 32, pp. 263–268, 1997.

[47] V. Singh, *Physical Metallurgy*. Standard Publishers Distributors, 2020.

[48] G. E. Totten and D. S. MacKenzie, *Handbook of Aluminum Vol. 1: Physical Metallurgy and Processes*. CRC Press, 2003.

[49] Y. Zheng et al., "Study of the precipitation hardening behaviour and intergranular corrosion of Al-Mg-Si alloys with differing Si contents," *Metals*, vol. 7, no. 10, 2017. doi: 10.3390/met7100387.

[50] S. M. A. Shibli and K. K. Binoj, "Development of MnO2-incorporated high performance aluminum alloy matrix sacrificial anodes," *J. Appl. Electrochem.*, vol. 39, pp. 159–166, 2009.

[51] X. Liu et al., "Effect of Alloy Elements on the Performance of Al Sacrificial Anode," *J. Phys. Conf. Ser.*, vol. 2679, no. 1, 2024. doi: 10.1088/1742-6596/2679/1/012036.

[52] K. Worasaen and P. Mungsantisuk, "Influence of Ti on the electrochemical behavior of Al-Zn-In-Si sacrificial anodes," *Key Eng. Mater.*, vol. 728, pp. 15–19, 2017.

[53] X. Liu et al., "Effect of Bi on the Performance of Al-Ga-In Sacrificial Anodes," *Materials*, vol. 17, no. 4, 2024. doi: 10.3390/ma17040811.

[54] M. Saremi, H. Sina, A. Keyvani, and M. Emamy, "The Influence of Ti and Sr Alloying Elements on Electrochemical Properties of Aluminum Sacrificial Anodes,"

[55] M. S. Ahmed et al., "Experimental study on the effects of three alloying elements on the properties of aluminum alloys," *Results in Materials*, vol. 20, p. 100485, 2023.

[56] A. Korjenic, E. Romanovskaia, and J. R. Scully, "Analysis of Al-Zn, Mg, and Mg/Al-Zn Metal Rich Primers Applied to AA 7075-T651," *J. Electrochem. Soc.*, 2024.

[57] R. Orozco-Cruz, J. Genesca, and J. A. Juarez-Islas, "Electrochemical behavior of new ternary aluminum alloys as sacrificial anodes," in *Corrosion Behaviour and Protection of Copper and Aluminium Alloys in Seawater*, 2007, pp. 159–172.

[58] I. Polmear, D. StJohn, J. F. Nie, and M. Qian, *Light Alloys: Metallurgy of the Light Metals*. Butterworth-Heinemann, 2017.

[59] G. Gao et al., "Effects of the quenching rate on the paint bake-hardening response of Al-Mg-Si automotive sheets," *Materials*, vol. 12, no. 21, 2019.

[60] C. D. Marioara et al., "The influence of temperature and storage time at RT on nucleation of the beta phase in a 6082 Al-Mg-Si alloy," *Acta Mater.*, vol. 51, pp. 789–796, 2003.

[61] A. Deschamps and Y. Brechet, "Influence of predeformation and ageing of an Al-Zn-Mg alloy," *Acta Mater.*, vol. 47, pp. 293–305, 1998.

[62] W. Smith and J. Hashemi, *Foundations of Materials Science and Engineering*, 7th ed., 2023.

[63] F. E. El Garchani et al., "Effects of heat treatment on the corrosion behavior and mechanical properties of aluminum alloy 2024," *J. Mater. Res. Technol.*, vol. 25, pp. 1355–1363, 2023.

[64] N. Z. Nasir et al., "The Effect of Heat Treatment on Fatigue and Mechanical Properties of 6061 Aluminium Alloy," *Appl. Mech. Mater.*, vol. 699, pp. 227–232, 2014.

[65] Q. Qi et al., "Effect of Solution Heat Treatment on the Microstructure and Microhardness of 7050 Aluminum Alloy," *Metals*, vol. 13, 2023.

[66] J. Pezda, "Optimization of heat treatment parameters of AlSi7Mg alloy," *Materials*, vol. 15, p. 1163, 2022.

[67] M. Beder et al., "The Effect of Heat Treatment on the Mechanical Properties and Oxidation Resistance of AlSi10Mg Alloy," *Arab. J. Sci. Eng.*, 2024.

[68] A. Jarco and J. Pezda, "Effect of heat treatment process and optimization of its parameters on AlSi11(Fe) alloy," *Materials*, vol. 14, 2021.

[69] J. M. Li et al., "Anisotropic behavior of TiB2 nanoparticles reinforced 2024Al composites rolling sheet," *Mater. Charact.*, vol. 162, p. 110196, 2020.

[70] W. D. Callister Jr. and D. G. Rethwisch, *Materials Science and Engineering: An Introduction*. John Wiley & Sons, 2020.

[71] ASM International, *The Materials Information Company*.

[72] S. A. Zakaria et al., "Characterization of mechanical and corrosion properties of cryorolled Al 1100 alloy," *Trans. Nonferrous Met. Soc. China*, vol. 31, pp. 2949–2961, 2021.

[73] J. Grasserbauer et al., "Evolution of microstructure and texture in production of automotive Al-sheets," *Materials*, vol. 13, no. 2, 2020.

[74] H. Zhao et al., "Segregation assisted grain boundary precipitation in a model Al-Zn-Mg-Cu alloy," *Acta Mater.*, vol. 156, pp. 318–329, 2018.

[75] C. N. Panagopoulos and E. P. Georgiou, "The Effect of Cold Rolling on the Corrosion Behaviour of 5083 Aluminium Alloys," *Metals*, vol. 14, no. 2, 2024.

[76] M. Q. Lobato et al., "Influence of Cold Working on Mechanical Properties of Al-Zr and Al-Zr-Mg Alloys," Technical Report, 2017.

[77] W. Taktak et al., "Study of the influence of cold working on mechanical behavior of 5754 aluminum alloy," *J. Theor. Appl. Mech.*, vol. 55, no. 3, pp. 923–935, 2017.

[78] Y. P. Asmara et al., "Improving Efficiency of Aluminium Sacrificial Anode Using Cold Work Process," *IOP Conf. Ser. Mater. Sci. Eng.*, vol. 114, 2016.

[79] N. Afnan and M. Nordin, "Effect of Deformation to the Performance of Aluminium Sacrificial Anode," Final Year Project Report, 2008.

[80] R. K. Harchegani and A. R. Riahi, "Effect of Cold-Working on the Discharge Performance of AA7050 Alloy Anodes," *J. Electrochem. Soc.*, vol. 169, p. 120525, 2022.

[81] B. S. Boroujeny et al., "Effects of SIMA on microstructure and electrochemical behavior of Al-Zn-In sacrificial anodes," *J. Alloys Compd.*, vol. 731, pp. 354–363, 2018.

[82] V. A. Mistry and U. Vala, "Improving Performance of Al-Mg Sacrificial Anode Through Forging," .

[83] I. V. Dubova et al., "Electrochemical behavior of 6xxx series aluminium alloys in electrolytes containing chloride ions," *J. Phys. Conf. Ser.*, vol. 1679, no. 4, 2020.

[84] J. E. Hatch, *Aluminum: Properties and Physical Metallurgy*. American Society for Metals, 1984.

[85] M. Baruah and A. Borah, "Processing and precipitation strengthening of 6xxx series aluminium alloys: A review," *Int. J. Mater. Sci.*, vol. 1, no. 1, pp. 40–48, 2020.

[86] M. H. Larsen et al., "Intergranular Corrosion of Copper-Containing AA6xxx AlMgSi Aluminum Alloys," *J. Electrochem. Soc.*, vol. 155, no. 12, p. C550, 2008.

[87] K. Pal and S. Chauhan, "Influence of Heat Treatment on the Mechanical Properties of Aluminium Alloys (6xxx Series)," *IJERT*.

[88] W. S. Miller et al., "Recent development in aluminium alloys for the automotive industry," *Mater. Sci. Eng. A*, vol. 280, pp. 37–49, 2000.

[89] Hariyanti et al., "Effect of corrosion product on the electrochemical behavior of Al-Mg-Si alloy coated steel," *Electrochemistry*, vol. 80, no. 4, pp. 218–221, 2012.

[90] M. Enokida et al., "Effect of Mg and Si Content on the Electrochemical Behavior of Al-Mg-Si Alloy,"

[91] P. P. Seth, O. Parkash, and D. Kumar, "Mechanical and electrochemical behavior of Mg-Al-Si alloys," *Proc. Inst. Mech. Eng. C J. Mech. Eng. Sci.*, vol. 235, pp. 4129–4142, 2021.

[92] F. L. Zeng et al., "Corrosion mechanism associated with Mg_2Si and Si particles in Al-Mg-Si alloys," *Trans. Nonferrous Met. Soc. China*, vol. 21, pp. 2559–2567, 2011.

[93] C. Kruehong et al., "Influence of second phases on the electrochemical behavior of hot dipped Al-Mg-Si coated steel," *Corros. Sci.*, vol. 52, pp. 2379–2386, 2010.

[94] L. L. Li et al., "SVET Study of Galvanic Corrosion of Al/Mg_2Si Couple in Aqueous Solutions," *J. Electrochem. Soc.*, vol. 164, no. 5, pp. C240–C249, 2017.

[95] N. Birbilis and R. G. Buchheit, "Electrochemical Characteristics of Intermetallic Phases in Aluminum Alloys," *J. Electrochem. Soc.*, vol. 152, no. 4, p. B140, 2005.

[96] J. Zhang et al., "Microstructural development of Al-15wt.%Mg_2Si in situ composite with mischmetal addition," *Mater. Sci. Eng. A*, 2000.

[97] J. Zhang et al., "Equilibrium pseudobinary Al-Mg_2Si phase diagram,"

[98] S. P. Li et al., "Eutectic reaction and microstructural characteristics of Al(Li)-Mg_2Si alloys," *J. Mater. Sci.*, 2001.

[99] C. Li et al., "Morphological evolution and growth mechanism of primary Mg_2Si phase in Al-Mg_2Si alloys," *Acta Mater.*, vol. 59, pp. 1058–1067, 2011.

[100] M. R. S. Ganesh et al., "Strontium in Al-Si-Mg Alloy: A Review," *Met. Mater. Int.*, vol. 28, 2022.

[101] X. Zhu et al., "The effects of varying Mg and Si levels on eutectic Mg_2Si morphology in die-cast Al-Mg-Si alloys," *J. Mater. Sci.*, vol. 54, pp. 5773–5787, 2019.

[102] D. Shimosaka et al., "Effect of cooling rates on Al-Mg_2Si pseudo-binary alloys," *Mater. Trans.*, pp. 920–927, 2011.

[103] S. Li et al., "Solidification and Structural Characteristics of alpha(Al)-Mg_2Si Eutectic," *Mater. Trans.*, vol. 38, no. 6, pp. 553–559, 1997.

[104] M. Tebib et al., "Effect of P and Sr additions on hypereutectic Al-15Si-14Mg-4Cu alloy," *Mater. Charact.*, vol. 89, pp. 112–123, 2014.

[105] S. Farahany et al., "Effect of Primary and Eutectic Mg_2Si Crystal Modifications on Al-20Mg_2Si-2Cu-xBi Composite," *J. Mater. Sci. Technol.*, vol. 32, pp. 1083–1097, 2016.

[106] S. G. Shabestari et al., "Effect of magnesium and artificial aging on Al-Si-Mn-Mg alloys," *Adv. Mater. Res.*, pp. 415–420, 2010.

[107] M. Yildirim and D. Özyürek, "The effects of Mg amount on the properties of Al-Si-Mg alloys," *Mater. Des.*, vol. 51, pp. 767–774, 2013.

[108] T. Hosch and R. E. Napolitano, "The effect of silicon morphology on tensile properties of Al-Si eutectic alloys," *Mater. Sci. Eng. A*, vol. 528, pp. 226–232, 2010.

[109] M. C. Flemings, "Solidification Processing," *Metall. Trans. A*, vol. 5, no. 10, pp. 2121-2134,

[110] N. A. Nordin et al., "Refinement of Mg_2Si reinforcement in Al-20%Mg_2Si in-situ composite," *Mater. Charact.*, vol. 86, pp. 97–107, 2013.

[111] S. Ji et al., "Microstructural evolution of Al-Mg-Si alloy in high-pressure die casting," *Metall. Mater. Trans. A*, vol. 44, pp. 3185–3197, 2013.

[112] S. K. Kairy et al., "The influence of copper additions and ageing on Al-Mg-Si alloy,"

[113] A. P. Sekhar et al., "Influence of Ageing on the Intergranular Corrosion of an Al-Mg-Si Alloy," *Met. Mater. Int.*, vol. 27, pp. 5059–5073, 2021.

[114] A. K. Bhattamishra and K. Lal, "Microstructural studies on the effect of Si and Cr on Al-Mg-Si alloys," *Elsevier*, 1997.

[115] W. Li et al., "Effect of aging on the corrosion behavior of 6005 Al alloys," *J. Mater. Res.*, vol. 33, pp. 1830–1838, 2018.

[116] E. Cevik et al., "Effect of peak-aged heat treatment on AA6063 alloy containing Al3Ti," *Arch. Metall. Mater.*, vol. 57, pp. 469–477, 2012.

[117] G. A. Edwards et al., "The Precipitation Sequence in Al-Mg-Si Alloys," *Phys. Status Solidi A*,

[118] C. D. Marioara et al., "Atomic model for GP-zones in a 6082 Al-Mg-Si system," *Acta Mater.*, vol. 49, pp. 321–328, 2001.

[119] S. J. Andersen et al., "The Crystal Structure of the beta' phase in Al-Mg-Si Alloys,"

[120] R. Vissers et al., "The crystal structure of the beta' phase in Al-Mg-Si alloys," *Acta Mater.*, vol. 55, pp. 3815–3823, 2007.

[121] G. Svenningsen et al., "Effect of high temperature heat treatment on intergranular corrosion of AlMgSi(Cu) model alloy," *Corros. Sci.*, vol. 48, pp. 258–272, 2006.

[122] C. I. Chang et al., "Influence of Si/Mg, Cu Content and Aging Condition on Al-Mg-Si Alloy,"

[123] B. Wang et al., "Experimental study of AA6061-T6 aluminum alloy under repeated impacts," *Int. J. Fatigue*, vol. 183, p. 108213, 2024.

[124] M. El-Shennawy et al., "Metallurgical and Mechanical Properties of AA6082 Welds," *Int. J. Eng. Res. Dev.*, 2017.

[125] S. Pogatscher et al., "Mechanisms controlling the artificial aging of Al-Mg-Si Alloys," *Acta Mater.*, vol. 59, pp. 3352–3363, 2011.

[126] Y. Chen et al., "The effect of interrupted aging on yield strength of Al alloys," *Acta Mater.*, vol. 61, pp. 5877–5894, 2013.

[127] S. K. Shaha et al., "Ageing characteristics of Al-Si-Cu-Mg alloys with additions of Mo and Mn," *Mater. Sci. Eng. A*, vol. 684, pp. 726–736, 2017.

[128] H. Pratikno, "Aging Treatment to Increase the Erosion-Corrosion Resistance of AA6063 Alloys," *Procedia Earth Planet. Sci.*, vol. 14, pp. 41–46, 2015.

[129] H. Jangid et al., "Process Parameters and Heat-Treatment Optimization for AA6082-T651," *Processes*, vol. 13, p. 637, 2025.

[130] Z. Yin et al., "Enhancing strength-ductility synergy in age-hardened Al-Mg-Si alloy," *J. Alloys Compd.*, vol. 1010, p. 178264, 2025.

[131] X. Yan et al., "Effect of Solid Solution System on Al-6.5Si-5.5Cu Alloy," *J. Mater. Eng. Perform.*, vol. 33, pp. 5881–5894, 2024.

[132] M. Vlach et al., "Microstructure and mechanical properties of AA6082 with Sc and Zr," *Int. J. Mater. Res.*, vol. 100, pp. 420–423, 2009.

[133] F. Meng et al., "Effect of Si addition on microstructure of Al-Mg-Si-Zn alloy," *China Foundry*, vol. 17, pp. 15–20, 2020.

[134] D. Dwivedi et al., "Influence of silicon content on cast Al-Si-Mg alloys," *Int. J. Cast Met. Res.*, vol. 19, pp. 275–282, 2006.

[135] N. Maruyama et al., "Effect of silicon addition on precipitates in Al-Mg-Si alloys," *Scr. Mater.*, vol. 36, pp. 89–93, 1997.

[136] Y. Kaygisiz and D. B. Kayan, "Effect of Heat Treatment on Al-Si-Mg Alloy Systems," *Phys. Met. Metallogr.*, vol. 123, pp. 1499–1508, 2022.

[137] K. S. Jang et al., "Effect of Heat Treatment on Corrosion Resistance of A356 Casting Alloy," *Materials*, vol. 18, p. 1056, 2025.

[138] W. Jurczak, "The effect of heat treatment on corrosion resistance of Al-Zn-Mg alloys," *Pol. Marit. Res.*, vol. 15, pp. 66–71, 2008.

[139] ASTM Standard, "Standard Test Method for Analysis of Aluminum and Aluminum Alloys by Spark Atomic Emission Spectrometry," ASTM E1251, 2017.

[140] ASTM Standard, "Standard Test Method for Brinell Hardness of Metallic Materials," ASTM E10-00a, 2000.

[141] DNV, "RP-B401: Cathodic Protection Design," DNV AS, 2021.

[142] ASTM G97-18, "Standard Test Method for Laboratory Evaluation of Magnesium Sacrificial Anode Test Specimens for Underground Applications," ASTM International, 2018.

[143] G. E. Totten, Friction, Lubrication, and Wear Technology, ASM International, 2017.

[144] S. Zahi, A. R. Daud, "Phase diagram, thermodynamics and microstructure of Al-Mg system," Proc. IEEE/CPMT Int. Electron. Manuf. Technol. (IEMT) Symp., 2010.

[145] ASM International, Alloy Phase Diagrams, Vol. 3, ASM Handbook, 1992.

[146] N. Birbilis, M. K. Cavanaugh, R. G. Buchheit, "Electrochemical Characterization and Surface Analysis of Intermetallic Phases in Aluminum Alloys," Corrosion, 62 (2006) 706–715.

[147] O. Lunder, J. C. Walmsley, P. Mack, K. Nisancioglu, "Formation and Characterisation of a Ti-Zr Based Conversion Coating on AA6060 Aluminium," Corros. Sci., 47 (2005) 1604–1624.

[148] J. R. Galvele, "Transport Processes and the Mechanism of Pitting of Metals," J. Electrochem. Soc., 123 (1976) 464.

[149] M. G. Fontana, N. D. Greene, Corrosion Engineering, 3rd ed., McGraw-Hill, New York, 1986.

[150] F. Mansfeld, "Electrochemical Impedance Spectroscopy (EIS) as a New Tool for Investigating Methods of Corrosion Protection," Electrochim. Acta, 35 (1990) 1533–1544.

[151] C. M. Afonso, "Microstructural Evolution of Al-Mg-Si Alloys During Artificial Aging," Mater. Sci. Forum, 514 (2006) 1301–1305.

[152] K. Nisancioglu, "Electrochemical Behavior of Aluminum-Magnesium-Silicon Alloys," J. Electrochem. Soc., 137 (1990) 69–77.

[153] J. H. Nordlien, S. Ono, N. Masuko, K. Nisancioglu, "A TEM Study of the Morphology of Naturally Formed Oxide Films on Pure Magnesium," Corros. Sci., 39 (1997) 379–388.

[154] G. Svenningsen, J. E. Lein, A. Bjørgum, J. H. Nordlien, K. Nisancioglu, "Effect of Grain Boundary Precipitation on Intergranular Corrosion of AlMgSi(Cu) Alloys," Corros. Sci., 48 (2006) 3969–3987.

[155] R. G. Buchheit, "A Compilation of Corrosion Potentials Representing Intermetallic Phases in Aluminum Alloys," J. Electrochem. Soc., 142 (1995) 3994–3996.

[156] P. L. Schaffer, "Solidification of Aluminum-Silicon Alloys: Influence of Magnesium Additions," Metall. Mater. Trans. A, 35 (2004) 2007–2015.

[157] E. McCafferty, "Validation of Corrosion Rates from Tafel Extrapolations to Charge-Transfer Controlled Reactions," Corros. Sci., 47 (2005) 3202–3215.

[158] D. G. Thomas, "The Use of Magnesium Anodes for the Protection of Pipelines," Corrosion, 10 (1954) 123–128.

[159] Y. W. Keuong, "Electrochemical Properties of Al-Zn-In Sacrificial Anodes in Tropical Seawater," Corrosion, 58 (2002) 234–240.

[160] S. P. Knight, "The Role of Intermetallic Phases in the Pitting Corrosion of AA2024-T3," Corros. Sci., 52 (2010) 3855–3860.

[161] M. Pourbaix, Atlas of Electrochemical Equilibria in Aqueous Solutions, NACE International, 1974.

[162] L. F. Mondolfo, Aluminum Alloys: Structure and Properties, Butterworths, London, 1976.

[163] H. P. Godard, "The Corrosion of Aluminum in Seawater," Corrosion, 16 (1960) 131–138.

[164] K. R. Cooper, "The Use of EIS for the Evaluation of Corrosion Inhibitors," J. Appl. Electrochem., 36 (2006) 123–130.

[165] X. G. Zhang, Corrosion and Electrochemistry of Zinc, Plenum Press, New York, 1996.

[166] A. W. Hassel, "The Use of Scanning Electrochemical Microscopy in Corrosion Research," Electrochim. Acta, 47 (2001) 163–170.

[167] M. J. Robinson, "The Influence of Microstructure on the Stress Corrosion Cracking of Al-Mg-Si Alloys," Corros. Sci., 22 (1982) 675–688.

[168] J. E. Hatch, Aluminum: Properties and Physical Metallurgy, ASM International, 1984.

[169] W. J. Placzankis, "The Performance of Aluminum Sacrificial Anodes in Various Marine Environments," Army Research Laboratory Report, 2008.

[170] O. R. Mattos, "The Use of Electrochemical Impedance Spectroscopy to Study the Corrosion of Aluminum Alloys," Corros. Sci., 33 (1992) 101–112.

[171] D. A. Little, "The Role of Cu-Rich Particles in the Localized Corrosion of Al-Mg-Si-Cu Alloys," Corrosion, 60 (2004) 1125–1135.

[172] N. D. Tomashov, Theory of Corrosion and Protection of Metals, Macmillan, New York, 1966.

[173] S. C. Dexter, "Role of Marine Bacteria in Localized Corrosion of Aluminum," Corrosion, 44 (1988) 710–718.

[174] J. R. Scully, "Metastable Pitting Corrosion," Science, 290 (2000) 1540–1541.

[175] T. J. Summerson, "Corrosion Resistance of Aluminum and Magnesium Alloys," Metals Handbook, 9th ed., Vol. 13, 1987.

[176] R. Winston Revie, Oil and Gas Pipelines: Integrity and Safety Handbook, Wiley, 2015.

LIST OF PUBLICATIONS

1) Kyada, T. K., Dave, I. B., & Patel, S. M. (2023). *An Extensive Overview of Al–Mg–Si Alloy's Electrochemical Behavior.* International Journal of Metallurgy and Alloys, 9(2).JournalsPub. ISSN: 2456-5113. https://doi.org/10.37628/ijma.v9i2.1078
2) Kyada, T. K., Dave, I. B., & Patel, S. M. (2024).*Microstructure and Corrosion Behavior of Al, Al–Mg, and Al–Mg–Si Alloy as a Sacrificial Anode.* Journal of the Maharaja Sayajirao University of Baroda: Science & Technology**,** 58, 44–48. The Maharaja Sayajirao University of Baroda, Vadodara, Gujarat, India.UGC CARE Listed. ISSN: 0025-0422.
3) Kyada, T. K., Dave, I. B., & Patel, S. M. (2024). *Study The Electrochemical Behaviour of al-mg-si Alloy - A Review.* Journal of the Maharaja Sayajirao University of Baroda: Science & Technology**,** 58, 35–43. The Maharaja Sayajirao University of Baroda, Vadodara, Gujarat, India. UGC CARE Listed. ISSN: 0025-0422.
4) Tushal Kalubhai Kyada, Indravadan B. Dave, Sonam M. Patel, Kunal Trivedi & Vandana J. Rao (03 Apr 2026): Evaluating the influence of silicon on phase formation, hardness and corrosion in Al–6.5% Mg alloy, Canadian Metallurgical Quarterly, DOI: 10.1080/00084433.2026.2650945
5) Kyada, T.K., Patel, S.M. & Dave, I.B. Influence of Silicon Content and T6 Heat Treatment on Microstructure and Sacrificial Anode Performance of Al–6.5Mg Alloys. Metallogr. Microstruct. Anal. (2026). https://doi.org/10.1007/s13632-026-01377-5

PUBLISHED PAPER-1

Journals Pub

International Journal of
Metallurgy and Alloys

ISSN: 2456-5113
Volume 9, Issue 2, 2023
July-December
DOI (Journal): 10.37628/IJMA

https://journalspub.com/journal/ijma/

Research IJMA

An Extensive Overview of Al-Mg-Si Alloy's Electrochemical Behavior

Tushal K. Kyada[1,2], Indravadan B. Dave[3,*], Sonam M. Patel[4]

Abstract

This review emphasizes on the effects of microstructure and alloying components on the electrochemical behavior of Al-Mg-Si alloys used as sacrificial anodes. The presence of alloying elements hinders surface film formation on aluminum, while microstructural factors such as grain size distribution and precipitate volume fraction influence alloy properties. The Al-Mg-Si phase diagram and the presence of the Mg_2Si phase are also discussed, highlighting the effects of Mg and Si solubility. Additionally, the addition of Mg and Si shifts anodic polarization curves and affects Mg_2Si morphology, impacting the alloys' electrochemical behavior. The paper also delves into the effects of heat treatment on precipitation sequence, aging time, cooling rate, and their role in intergranular corrosion susceptibility.

Keywords: Al-Mg-Si alloy, 6XXX, Electrochemical behavior, Mg_2Si, Sacrificial anode, Microstructure

INTRODUCTION

Aluminum can serve as a corrosion-resistant material or as an activated sacrificial anode in a cathodic protection system, depending on the appropriate alloying system. Aluminium as sacrificial anode has attained considerable merit as the basis for a galvanic anode mainly due to its low density, large electrochemical equivalent, availability, thermal and electrical conductivity, high current capacity, low specific weight, and reasonable cost.

However, if aluminum is utilized as a sacrificial anode, its passive film must be modified to undergo active dissolution. The metal's microstructure, the availability of an alloying element, and the volume quantity of second phase particles all have an impact on the film's continuity. Zn, Mg, Sn, Bi, Ti, In, and Ga are alloying elements that impede or prevent the formation of surface film on aluminum [1]. Aluminum anodes are usually alloyed with other elements to promote depassivation (breakdown of the oxide coating) and/or change the metal's working potential to a more electronegative direction in order to increase its efficiency. The alloying components that are employed to do this are known as modifiers and depassivators. The elements zinc (Zn), magnesium (Mg), barium (Ba), and cadmium (Cd) are among the modifiers that have been employed. This work uses both zinc and magnesium [2]. Magnesium, one of the most active metals in the galvanic series, can be added to aluminum to counteract its passivity [3].

***Author for Correspondence**
Indravadan B. Dave
E-mail: ibdave@gecg28.ac.in

[1]Research Scholar, Department of Metallurgy, Gujarat Technological University, Ahmedabad, Gujarat, India
[2]Lecturer, Department of Metallurgy, Dr. S & S.S. Ghandhy College of Engineering & Technology, Surat, Gujarat, India.
[3]Professor & Head, Department of Metallurgy, Government Engineering College Gandhinagar, Gujarat, India
[4]Lecturer, Department of Metallurgy, Dr. S & S.S. Ghandhy College of Engineering and Technology, Surat, Gujarat, India

Received Date: May 04, 2024
Accepted Date: July 02, 2024
Published Date: July 12, 2024

Citation: Tushal K. Kyada, Indravadan B. Dave, Sonam M. Patel. An Extensive Overview of Al-Mg-Si Alloy's Electrochemical Behavior. International Journal of Metallurgy and Alloys. 2023; 9(2): 1–11p.

6XXX ALLOY (AL-MG-SI ALLOY) SYSTEM

The composition of aluminum alloys in the 6xxx family is a significant factor in influencing both their mechanical and electrochemical properties.

PUBLISHED PAPER-2

Journal of the Maharaja Sayajirao University of Baroda: Science & Technology
Vol. 58, 2024, pp. 44-48

Microstructure and Corrosion Behavior of Al, Al-Mg, and Al-Mg-Si Alloy as a Sacrificial Anode

Tushal K. Kyada[1,2], Indravadan B. Dave[3*], Sonam M. Patel[2]

[1] Research Scholar, Gujarat Technological University, Ahmedabad, India

[2] Metallurgy Department, Dr. S. & S. S. Ghandhy College of Engineering & Technology, Surat-395001, Gujarat, India, tushalkyada21@gmail.com & smp22789@gmail.com

[3*] Metallurgy Engineering, Government Engineering College, Sector-28, Gandhinagar -382028, Gujarat, India, ibdave@gecg28.ac.in

Aluminium, alloyed with elements such as magnesium and silicon, is the preferred sacrificial anode for protecting carbon steel, demonstrating heightened efficiency in depassivation and shifting the operating potential in a more electronegative direction. Consequently, this study focuses on a comparative examination of the microstructure, hardness, and corrosion behavior of Al, Al-Mg, and Al-Mg-Si alloys. Microstructural analysis of the developed alloys was conducted using an optical microscope, revealing that the grain structure of pure aluminum is refined in the presence of Mg and Si. The study assesses hardness test results to provide insights into the mechanical characteristics of the materials, with hardness values increasing due to the presence of Mg and Si. Subsequently, the developed alloys were immersed in a 3.5 wt.% NaCl solution, and their corrosion behavior was scrutinized using the weight loss method. The findings enhance our understanding of Al, Al-Mg, and Al-Mg-Si sacrificial anode materials, emphasizing their potential for corrosion protection applications.

Keywords: *Al, Al-Mg, Al-Mg-Si, sacrificial anode materials, microstructure, corrosion, weight loss method, hardness test*

INTRODUCTION

Nowadays, the most common metals used as sacrificial anodes in cathodic protection systems, especially in oil and gas environments, are aluminum (Al) alloys, magnesium (Mg), and zinc (Zn). [1] Due to its many beneficial qualities, including its low density, significant electrochemical equivalent, accessibility, high current-carrying capacity, high electrical and thermal conductivity, low specific weight, and affordable price, aluminum has become increasingly well-known. [2] However, because γ-Al_2O_3 forms a thin, continuous, adherent, and passive layer on the surface of pure and unalloyed aluminum, it cannot be used as a sacrificial anode. The quick polarization that happens when aluminum is exposed to a corrosion load in a cathodic protection circuit is caused by this γ-Al_2O_3 compound. [3]

If aluminum is utilized as a sacrificial anode, its passive film must be modified to undergo active dissolution. The continuity of the film is affected by the microstructure of the metal, presence of alloying element and volume fraction of second phase particles. To enhance the effectiveness of aluminum anodes, they are often alloyed with other elements to promote the depassivation process, which involves breaking down the oxide film, and to shift the operating potential of the metal towards a more electronegative direction. [3–5]

Aluminum, alloyed with elements such as magnesium (Mg) and silicon (Si), has gained significant attention as a sacrificial anode for protecting carbon steel due to its superior depassivation efficiency and ability to shift the operating potential in a more electronegative direction. Mg has maximum solid solubility in an aluminium matrix which is 16.26 atomic weight percentage around 450°C and Si has maximum solid solubility in an aluminium matrix which is 1.59 atomic weight percentage around 1080°C. [6] Mg, having more negative potential than pure aluminum, are added, the corrosion potential typically increases to more noble values. For example, pure aluminum has a corrosion potential of -920 mV, which decreases to a more

* Corresponding author.
Email: ibdave@gecg28.ac.in

PUBLISHED PAPER-3

Journal of The Maharaja Sayajirao University of Baroda: Science & Technology
Vol. 58, 2024, pp. 35-43

Study The Electrochemical Behaviour of al-mg-si Alloy - A Review

Tushal K. Kyada[1,2], Indravadan B. Dave[3*], Sonam M. Patel[2]

[1] Research Scholar, Gujarat Technological University, Ahmedabad, India

[2] Metallurgy Department, Dr. S. & S. S. Ghandhy College of Engineering & Technology, Surat- 395001, Gujarat, India, tushalkyada21@gmail.com & smp22789@gmail.com

[3*] Metallurgy Engineering, Government Engineering College, Sector-28, Gandhinagar -382028, Gujarat, India, ibdave@gecg28.ac.in

This review comprehensively analyzes the electrochemical behavior of Al-Mg-Si alloys as sacrificial anodes, focusing on factors like microstructure, alloying elements, and second- phase particles. Alloying elements' presence can impede surface film formation on aluminum. Microstructure, grain size distribution, precipitate volume fraction, and crystallographic orientation affect aluminum alloy properties. The paper describes the Al- Mg-Si phase diagram, emphasizing Mg and Si solubility with the Mg2Si phase presence. Mg and Si addition shifts anodic polarization curves, impacting electrochemical behavior and Mg2Si morphology. Corrosion mechanisms consider varying Mg and Si content effects on mechanical properties and microstructure. Furthermore, the paper explores heat treatment effects, addressing precipitation sequence, aging time, cooling rate, and their influence on intergranular corrosion (IGC) susceptibility.

Keywords: *Al-Mg-Si alloy, 6XXX, electrochemical behavior, Mg_2Si, sacrificial anode*

INTRODUCTION

Aluminum can serve as a corrosion-resistant material or as an activated sacrificial anode in a cathodic protection system, depending on the appropriate alloying system. Aluminium as sacrificial anode has attained considerable merit as the basis for a galvanic anode mainly due to its low density, large electrochemical equivalent, availability, thermal and electrical conductivity, high current capacity, low specific weight, and reasonable cost.

However, if aluminum is utilized as a sacrificial anode, its passive film must be modified to undergo active dissolution. The continuity of the film is affected by the microstructure of the metal, presence of alloying element and volume fraction of second phase particles. The alloying element that hinder or prevent the formation of surface film on aluminum are Zn, Mg, Sn, Bi, Ti, In and Ga. [1] In order to improve the efficiency of aluminum anodes they are typically alloyed with other elements to encourage depassivation (breakdown of the oxide film) and/or shift the operating potential of the metal to a more electronegative direction. The alloying elements used to accomplish this are referred to as depassivators and modifiers. Modifiers that have been used include zinc (Zn), magnesium (Mg), barium (Ba), and cadmium (Cd). In this work, Zn and Mg are employed. The depassivators commonly used are indium (In), mercury (Hg), and tin (Sn) and also rarely used are gallium (Ga), titanium (Ti) and thallium (Tl). [2] To overcome the passivity of aluminum, magnesium, which is one of the most active metals in the galvanic series, can be added. [3]

6XXX ALLOY (AL-MG-SI ALLOY) SYSTEM

Composition of 6xxx series aluminum alloys plays an important role in determining its mechanical as well as electrochemical properties. Properties of aluminium alloys also depend on its microstructure, average grain size and its distribution, volume fraction of precipitate and the crystallographic orientation. [4]

6XXX series alloy mainly alloyed with Mg and Si and they are heat-treatable alloys. The maximum solid solubility of Mg in an aluminum matrix is around 16.26 atomic weight percentage when the temperature is around 450°C. [5] Similarly, Si has maximum solid solubility in an aluminum matrix, which is 1.59

* Corresponding author.
Email: ibdave@gecg28.ac.in

PUBLISHED PAPER-4

CANADIAN METALLURGICAL QUARTERLY
https://doi.org/10.1080/00084433.2026.2650945

Evaluating the influence of silicon on phase formation, hardness and corrosion in Al–6.5% Mg alloy

Tushal Kalubhai Kyada [a,b], Indravadan B. Dave[c], Sonam M. Patel[b], Kunal Trivedi[d] and Vandana J. Rao[e]

[a]Research Scholar, Gujarat Technological University, Ahmedabad, India; [b]Metallurgy Department, Dr. S. & S. S. Ghandhy College of Engineering & Technology, Surat, India; [c]Department of Metallurgy Engineering, Government Engineering College, Gandhinagar, India; [d]Facilitation Centre for Industrial Plasma Technologies, IPR,Gandhinagar, India; [e]Metallury & Mathematics Engineering Department, Faculty of Tech. & Engineering, The M. S. U. Baroda, Vadodara, India

ABSTRACT

Al–Mg alloys are widely investigated as candidate materials for sacrificial anodes because of their favourable electrochemical activity and resistance to passivation in chloride environments. In cathodic protection systems, aluminium, zinc, and magnesium alloys are commonly used, with most commercial aluminium anodes based on Al–Zn–In or Al–Zn–Mg systems. However, the influence of silicon additions on the phase evolution, mechanical properties, and corrosion behaviour of Al–6.5%Mg alloys remains insufficiently understood. In this study, Al–6.5%Mg alloys containing 1.5%, 3%, 4.5%, and 6% Si were produced using conventional melting and casting. The alloys were characterised using optical microscopy, SEM/EDS, X-ray diffraction, hardness testing, potentiodynamic polarisation, and 8-week immersion tests in 3.5 wt.% NaCl solution. Results show that increasing Si content modifies the morphology and distribution of Mg_2Si phases from fine dispersed particles to semi-continuous networks, affecting both hardness and corrosion behaviour. Hardness ranged from 67 to 83 BHN, with the highest values at 1.5% and 6% Si. Corrosion resistance decreased when Si exceeded 1.5% owing to intensified micro-galvanic interactions. The Al–6.5%Mg–1.5%Si alloy exhibited the most favourable balance of corrosion resistance and controlled anodic dissolution for sacrificial anode applications in chloride environments.

Les alliages Al-Mg sont largement étudiés en tant que matériaux candidats pour les anodes sacrificielles en raison de leur activité électrochimique favorable et leur résistance à la passivation en milieux chlorurés. Dans les systèmes de protection cathodique, on utilise couramment les alliages d'aluminium, de zinc et de magnésium, la plupart des anodes commerciales en aluminium étant basées sur des systèmes Al-Zn-In ou Al-Zn-Mg. Cependant, l'influence d'ajouts de silicium sur l'évolution des phases, les propriétés mécaniques et le comportement à la corrosion des alliages Al-6.5%Mg demeure encore mal comprise. Dans cette étude, on a produit des alliages Al-6.5%Mg contenant 1.5%, 3%, 4.5% et 6% de Si par fusion et moulage conventionnels. On a caractérisé ces alliages par microscopie optique, MEB/EDS, diffraction des rayons X, essais de dureté, polarisation potentiodynamique et essais d'immersion de 8 semaines dans une solution de 3.5% en poids de NaCl. Les résultats montrent que l'augmentation de la teneur en Si modifie la morphologie et la distribution des phases Mg_2Si, passant de fines particules dispersées à des réseaux semi-continus, affectant à la fois la dureté et le comportement à la corrosion. La dureté variait de 67 à 83 BHN, les valeurs les plus élevées obtenues à 1.5% et 6% de Si. La résistance à la corrosion diminuait lorsque Si dépassait 1.5%, en raison de l'intensification des interactions micro-galvaniques. L'alliage Al-6.5%Mg-1.5%Si présentait l'équilibre le plus favorable entre la résistance à la corrosion et la dissolution anodique contrôlée pour les applications d'anodes sacrificielles en milieux chlorurés.

ARTICLE HISTORY
Received 19 January 2026
Accepted 11 March 2026

KEYWORDS
Al–Mg alloy; Al–Mg–Si system; sacrificial anode; microstructure; corrosion; hardness; immersion test; process innovation

PUBLISHED PAPER-5

Metallography, Microstructure, and Analysis
https://doi.org/10.1007/s13632-026-01377-5

ORIGINAL RESEARCH ARTICLE

Influence of Silicon Content and T6 Heat Treatment on Microstructure and Sacrificial Anode Performance of Al–6.5Mg Alloys

Tushal K. Kyada[1,2] · Sonam M. Patel[2] · Indravadan B. Dave[3]

Received: 21 January 2026 / Revised: 31 May 2026 / Accepted: 11 July 2026

Abstract

Aluminum-based sacrificial anodes are extensively utilized in marine cathodic protection systems due to their low density, favorable electrochemical activity, and high current efficiency. This study investigates the influence of silicon addition and T6 heat treatment on the microstructure, hardness, and sacrificial anode performance of Al–6.5Mg–xSi alloys containing 1.5, 3, and 6 wt% Si. Microstructural analysis confirmed an α-Al matrix with Mg_2Si as the predominant secondary phase, while increasing Si content transformed the Mg_2Si morphology from coarse flake-like structures to a refined Chinese-script eutectic network. T6 treatment promoted partial dissolution and redistribution of Mg_2Si phases, resulting in precipitation strengthening and enhanced hardness in the higher-Si alloys. Electrochemical polarization studies revealed that T6 treatment shifted the corrosion potential (Ecorr) toward more negative values, indicating enhanced anodic activation; however, the simultaneous increase in corrosion current density (Icorr) indicated increased self-corrosion activity. Among the investigated compositions, the as-cast Al–6.5Mg–6Si alloy exhibited the best sacrificial anode performance, achieving an anode capacity of approximately 2781 Ah/kg with uniform dissolution behavior. In contrast, T6 treatment increased anodic consumption and reduced current efficiency in the high-Si alloy. Post-corrosion SEM analysis further confirmed that the refined Chinese-script Mg_2Si morphology promoted relatively homogeneous dissolution, whereas the heat-treated alloys exhibited increased electrochemical heterogeneity. The results demonstrate that silicon addition strongly influences anodic performance, while T6 heat treatment primarily improves mechanical properties rather than sacrificial anode efficiency.

Keywords Al–Mg–Si alloy · Heat treatment · Microstructure · Mg_2Si · Anode capacity · Electrochemical performance

Introduction

Aluminum-based alloys have been widely studied for sacrificial anode applications owing to their low density, favorable electrochemical potential, and high current efficiency compared to zinc and magnesium alloys [1]. The mechanical performance of cast aluminum components can be enhanced through several approaches, including the incorporation of alloying elements [2], structural modification techniques [3, 4], and appropriate heat treatment processes [5]. Among these, precipitation hardening is one of the most widely employed methods, typically consisting of solution treatment, rapid quenching, and subsequent aging—either naturally (T4 condition) or artificially (T6 condition). Alloying additions such as magnesium and silicon are particularly effective in refining the microstructure and altering corrosion behavior, thereby improving the performance of Al-based sacrificial anodes. Heat treatment further enhances these characteristics by modifying phase transformations, precipitation kinetics, and dissolution uniformity—parameters that are critical for ensuring efficient anodic behavior [6]. Research on Al–Si–Mg casting alloys has demonstrated that the introduction of magnesium into Al–Si matrices modifies corrosion resistance by promoting the formation of intermetallic compounds [7, 8]. Among these phases, Mg_2Si is particularly significant because its highly negative corrosion potential (−1.54 VSCE) allows it to act sacrificially,

✉ Indravadan B. Dave
ibdave@gecg28.ac.in

Tushal K. Kyada
tushalkyada21@Gmail.com

[1] Gujarat Technological University, Ahmedabad, India

[2] Metallurgy Department, Dr. S. & S. S. Ghandhy College of Engineering & Technology, Surat, India

[3] Department of Metallurgy Engineering, Government Engineering College, Gandhinagar, India

Published online: 27 July 2026